The PHILOSOPHICAL MAGAZINE

FIRST PUBLISHED IN 1798

1 Eighth Series | No. 12 | December 1956

A Journal of Theoretical Experimental and Applied Physics

EDITOR
PROFESSOR N. F. MOTT, M.A., D.Sc., F.R.S.

EDITORIAL BOARD
SIR LAWRENCE BRAGG, O.B.E., M.C., M.A., D.Sc., F.R.S.
SIR GEORGE THOMSON, M.A., D.Sc., F.R.S.
PROFESSOR A. M. TYNDALL, C.B.E., D.Sc., F.R.S.

PRICE £1 0s. 0d.
Annual Subscription £10 10s. 0d. payable in advance

ALERE FLAMMAM.
Printed and Published by
TAYLOR & FRANCIS LTD.
RED LION COURT, FLEET STREET, LONDON, E.C.4

The Scientific Work of René Descartes

(1596–1650)

By

J. F. SCOTT, B.A., M.Sc., Ph.D.

With a foreword by H. W. TURNBULL, M.A., F.R.S.

This book puts the chief mathematical and physical discoveries of Descartes in an accessible form, and fills an outstanding gap upon the shelf devoted to the history of philosophy and science.

There is to be found in this volume the considerable contribution that Descartes made to the physical sciences, which involved much accurate work in geometrical optics and its bearing upon the practical problem of fashioning lenses, as also the deeper problems of light and sight and colour. The careful treatment that Dr. Scott has accorded to this work of Descartes is welcome, is well worth reading and will be an asset to all libraries. Publication is recommended and approved by the Publication Fund Committee of the University of London

212 *pages,* 7″ × 10″, *amply illustrated*

Price £1 - 0 - 0 net **First published July 1952**

Printed & Published by

TAYLOR & FRANCIS, LTD.

RED LION COURT, FLEET STREET, LONDON, E.C.4

CONTENTS OF No. 12.

Page

CXI. The Optical Effects of Radiation Induced Atomic Damage in Quartz. By E. W. J. MITCHELL and E. G. S. PAIGE, The University of Reading 1085

CXII. Radiative Capture of Protons of less than 1 MEV in Beryllium. By A. B. CLEGG, Cavendish Laboratory, Cambridge 1116

CXIII. On the Coupling between Two Cavities. By R. N. GOULD and A. CUNLIFFE, The University, Hull 1126

CXIV. The Onset of Friction in Helium II. By D. F. BREWER, D. O. EDWARDS and K. MENDELSSOHN, F.R.S., The Clarendon Laboratory, Oxford 1130

CXV. An Analysis of the Magnetization Processes in Iron Single Crystals by an Electrical Method. By R. PARKER, Department of Physics, University College of North Wales, Bangor........ 1133

CXVI. Angles Between Partial Magnetizations in Spinel Ferrites Containing Manganese Ions of more than One Valency. By W. P. OSMOND, Mullard Research Laboratories, Salfords, Surrey 1147

CXVII. The Height Variation of Upper Atmospheric Winds. By J. S. GREENHOW and E. L. NEUFELD, Jodrell Bank Experimental Station, University of Manchester 1157

Index to Volume........ 1172

With Title-page, Contents, etc.

***All communications for the Philosophical Magazine should be addressed, post-paid, to the Editors, c/o Messrs. TAYLOR AND FRANCIS, LTD., Red Lion Court, Fleet Street, London, England.

CXI. *The Optical Effects of Radiation Induced Atomic Damage in Quartz*

By E. W. J. Mitchell and E. G. S. Paige†
The University of Reading‡

[Received April 20, 1956]

Summary

Measurements of the optical absorption of neutron irradiated crystalline and fused quartz have been made in the wavelength range 1450–10 000 Å (8·5–1·2 ev). Two absorption bands associated with atomic displacements in crystalline quartz have been found—*C* at 5·7 ev and *E* at 7·6 ev. Optical bleaching of the *C* band, when illuminated with light of the wavelength absorbed, occurs even in the purest specimens. A preferential optical and thermal bleaching is observed at 5·4 ev during the early stages of the bleaching of neutron irradiated specimens. It is suggested that this effect is associated with electron release and capture, without intermediate retrapping, by a close complementary pair of traps. The model which seems to fit the results best is that the *C* and *E* defects are oxygen ion vacancies and interstitial oxygen ions, which produce absorption bands after trapping electrons and holes respectively. The *C* and *E* bands are also found in fused quartz.

Results obtained using thin specimens show that the absorption in the long wavelength tail of the absorption edge was enhanced during irradiation. The absorption limit in irradiated crystalline quartz is at 8·1 ev and is the same as that found in both unirradiated and irradiated fused quartz specimens. The extension of the tail is interpreted as arising from the formation of regions of amorphous material as a result of local melting. This is taken into account in estimating the concentration of point defects on the basis of collision theories. All the damage is annealed by heating at 950°c.

§ 1. Introduction

There is a wide transparent region in quartz between the beginning of the infra-red absorption (2·7 microns) and the characteristic electronic absorption edge (1450 Å). For this reason quartz is a favourable material for studying point defects by the measurement of their associated optical absorption.

In spite of being one of the most perfect crystalline materials quartz nevertheless contains defects in measurable concentrations. For example, the smoky colour which is induced in most specimens by ionizing radiation, and which occurs naturally in 'smoky quartz' has been shown by O'Brien and Pryce (1954), Griffiths *et al.* (1954), Ditchburn *et al.* (1954),† O'Brien (1955) and Mitchell and Paige (1955) to be due to substitutionally incorporated aluminium impurity.

---

† Now at Radar Research Establishment, Malvern.
‡ Communicated by the Authors.

The main interest of the work described in the present paper has been to determine those effects which are produced by particle irradiation, and which are associated with atomic displacements. This is the only practical way of introducing interstitial atoms and vacant sites into quartz. To utilize fully the wide transparent region our measurements of these effects have extended to the absorption edge.

The concentration of defects

Point defects in crystals, either existing from growth or induced by irradiation, may give rise to an observable absorption spectrum directly. Thus, many impurities in the alkali halides (e.g. Tl, Johnson and William 1953) give absorption bands, as also do anion vacancies in potassium chloride (α band, Seitz 1954) and vacancies in diamond (Clark *et al.* 1956). These defects do not need to capture or lose electrons before becoming observable so that the concentration of absorbing centres ($\mathcal{N}_A$) is equal to the concentration of defects (N_A), being related to the absorption by

$$\mu \Delta E \approx 10^{-16} \mathcal{N}_A f \quad . \quad . \quad . \quad . \quad . \quad . \quad . \quad . \quad . \quad . \quad (1)$$

where μ(cm^{-1}) is the absorption coefficient at the band maximum, ΔE(ev) the width of the band at half-absorption and f the oscillator strength for the transition involved.

Alternatively, the point defect may be observable only after capturing or losing an electron—for example, the aluminium defect in quartz gives rise to absorption after losing an electron. In this case the defects may become observable after irradiation with ionizing radiation. The saturation value of the concentration of centres will, in general, not be equal to the concentration of defects but will depend on the nature of the ionizing radiation, the cross-sections for the capture and release of electrons by the electron traps, and for the capture and release of electrons by the positive hole traps. The concentration of absorbing centres will be given by (1) but $\mathcal{N}_A = xN_A$, where x is some function of the various cross-sections.

If the particle radiation is producing defects of this kind then it is only because all particle irradiation produces ionization that the defects lead to observable absorption. Providing that the ionization is sufficient, so that at any stage of the irradiation 'saturation' of the electronic effects is achieved, the value of $\mathcal{N}_A$ may be used to follow the rate of formation of defects. This can apply to neutron irradiations since ionization processes will occur as a result of the movement of those knocked on atoms which are charged, and as a result of the γ-irradiation which accompanies all pile irradiations.

---

† This paper will be referred to as I.

Most absorbing centres in ionic and semi-ionic solids seem to be of this type. It is often implicitly assumed, however, that $x=1$, as in the calculations of defect concentrations in fused quartz by Yokota (1952) and Levy and Varley (1954), both of whom also assumed that $f=1$.

§ 2. MATERIALS AND METHOD

2.1. *The Quartz*

Crystalline quartz is normally transparent in thin sections from 0·46 ev (2·7 microns) to 8·3 ev (1500 Å) and our measurements indicate that the absorption edge, which we take for convenience as the photon energy at which the absorption coefficient is 400 cm^{-1}, is at 8·5 ev (1450 Å). At this energy the absorption coefficient is increasing at a rate of about 200 cm^{-1} per 0·1 ev. That the absorption edge defined in this way is a property of pure crystalline quartz is suggested by the fact that the same value was obtained for both synthetic and natural crystals. It is unlikely that this would have been the case had we been working in the tail of the absorption edge, whose form can be influenced by crystalline imperfections. In the fused quartz used in the present work the transparent region extended to 8·1 ev (1450 Å). The absorption below 8·5 ev in fused quartz can be regarded as an enhanced tail of the crystalline quartz absorption edge arising because of the absence of long range order.

The crystalline quartz used in the present work was either synthetic, grown by the G.E.C. Research Laboratories, Wembley, or naturally occurring Braxilian quartz. The fused quartz was of optical grade 1 obtained from the Thermal Syndicate.

2.2. *The Optical Measurements*

In the wavelength range 2100 to 10 000 Å transmission measurements were made using a Hilger UVISPEK spectrophotometer. From 1450 to 2200 Å the transmission was determined photographically using a fluorite vacuum spectrograph of the type described by Cario and Schmitt-Ott (1931). The arrangement of the apparatus is shown in fig. 1. Exposures were made on Ilford Q1 plates, the wavelength calibration being obtained from the hydrogen emission lines from the source, and the absorption lines of oxygen which was deliberately introduced for this purpose during one exposure. The hydrogen lamp was of the type described by Heddle (1952). The grids, which were inserted into the beam to determine the characteristic curve of each plate, were similar to those used by Ditchburn and Heddle (1953) but in the present case they could be calibrated in situ, using a crystal of irradiated quartz whose transmission between 2100 and 2200 Å had previously been determined in the spectrophotometer. Specimens were mounted in the holder illustrated in fig. 2. The crystal is held in the vice V which could be moved by the screw driver D, controlled from the outside through a Wilson seal, so that the specimen could be in, or out of, the beam. Low temperature measurements were made with the well (W) filled with liquid air,

Fig. 1

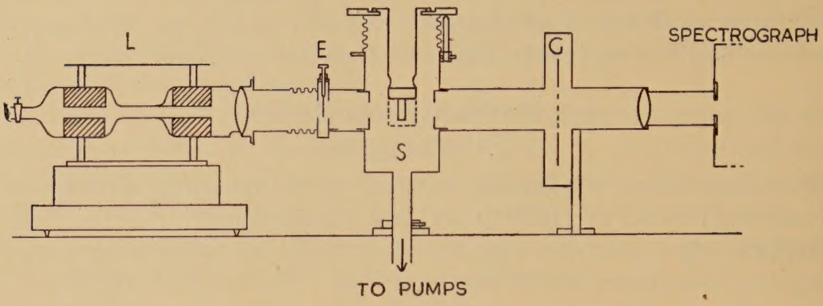

The arrangement of the apparatus for the vacuum ultra-violet measurements: L, water cooled, d.c. hydrogen discharge lamp ; E, exposure device ; S, specimen holder ; G, grids for the relative intensity calibration of the plates.

Fig. 2

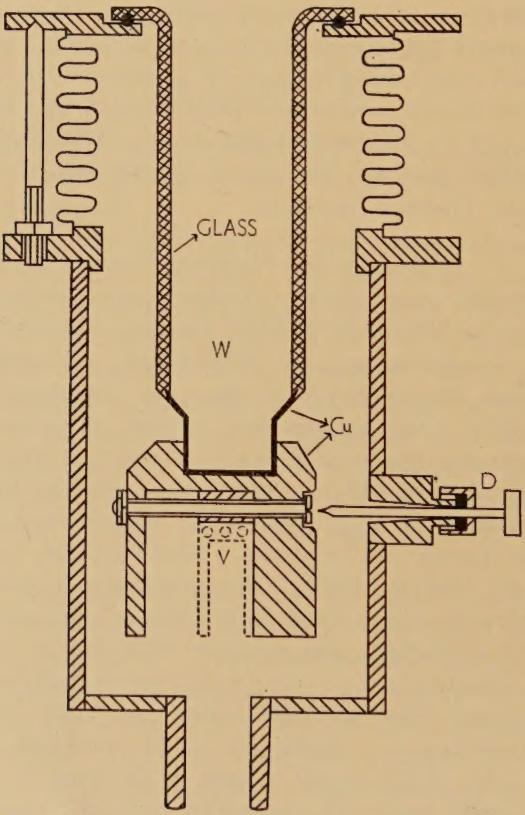

Diagram of specimen holder for use with the vacuum spectrograph in the liquid air to room temperature range.

By these two methods the percentage of incident light transmitted (T) by a thickness d cm of crystal has been determined from 1450 to 10 000 Å. The measurements were made under conditions of normal incidence so that the absorption coefficient (μ cm^{-1}) is defined by

$$T=T_0 \exp(-\mu d) \quad . \quad . \quad . \quad . \quad . \quad . \quad . \quad (2)$$

where T_0 is the percentage of incident light transmitted by a non-absorbing specimen having the same refractive index. If there is no scattering of light from the two surfaces and if, as in the present case, multiple reflections can be neglected, T_0 can be expressed in terms of the refractive index (n) by

$$T_0=(1-R)^2 \quad \text{where} \quad R=\left(\frac{n-1}{n+1}\right)^2 \quad . \quad . \quad . \quad (3)$$

Fig. 3

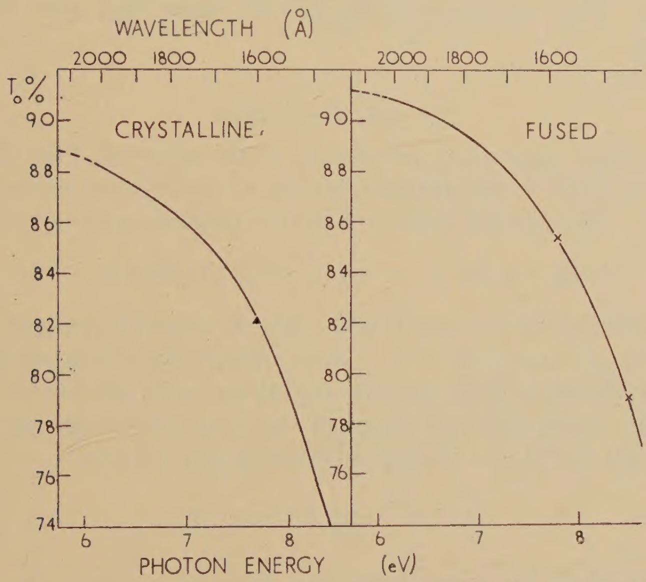

Values of T_0 (eqn. (2)) as a function of wavelength in the vacuum ultra-violet region for crystalline and fused quartz.

Between 2000 and 10 000 Å the values of n for crystalline and fused quartz were taken from the International Critical Tables (1933). In crystalline quartz the difference between T_0 calculated from n for the ordinary ray and n for the extraordinary ray was less than 0·2%. Such a difference is not significant in the present work so that values of T_0 calculated from n for the ordinary ray have been used. In the region 2000–1450 Å the reflection coefficients determined by Johnson (1941) have been used for fused quartz. For crystalline quartz we have determined T_0(=82%) at 1610 Å from transmission measurements on two unirradiated crystals of thickness 0·01 and 0·2 cm. We have extrapolated the data in the tables, which goes down to 1850 Å, through the 1610 Å point, giving the curve of T_0 as a function of wavelength as shown in fig. 3.

In using values of T_0 determined from unirradiated specimens to calculate the induced absorption coefficients it is assumed that: (*a*) the irradiation does not significantly affect n, (*b*) the surface topography is not changed sufficiently to cause significant scattering of light.

Some change of n must be expected to be associated with any absorbing centre, but for absorption coefficients up to the highest measured in the present work (500 cm^{-1}) the consequent change in reflectivity can be neglected. In order to check the second assumption the transmission in the visible was measured for a synthetic specimen which had received a large neutron dose ($10^{19}\ n^\circ\ \mathrm{cm}^{-2}$). The weak Al type band present in the crystal was completely radiation bleached and the measured transmission was within 1% of the value of T_0 (eqn. (2)) calculated from the index data. Thus no appreciable surface scattering was introduced by this dose.

2.3. *The Irradiation*

The specimens have been irradiated in the Harwell Pile (BEPO) in the centre of a cell of the graphite lattice at an ambient temperature of about 50°c. The neutron spectrum in this position is given by

$$n(\epsilon)d\epsilon = A\ (1/\epsilon_0{}^2 \,.\, \epsilon \,.\, \exp(-\epsilon/\epsilon_0) + 0\cdot05/\epsilon)\ d\epsilon. \quad . \quad . \quad . \quad . \quad (4)$$

where ϵ_0 is about 0·025 ev, $n(\epsilon)d\epsilon$ is the flux in neutrons per cm^2 per sec in the energy range ϵ to $\epsilon + d\epsilon$, and A is a constant depending on the power level of the pile and is given approximately for each irradiation.

The second term does not apply in the range of energy up to 0·1 ev so that we can write the integrated thermal flux (D_f) as

$$D_f = \int_0^{0\cdot1} n(\epsilon)\, d\epsilon = 0\cdot91\, A.$$

The flux of high energy neutrons is then given by

$$n(\epsilon)d\epsilon \approx 0\cdot055 D_f\, d\epsilon/\epsilon \quad . \quad . \quad . \quad . \quad . \quad . \quad . \quad . \quad . \quad (5)$$

provided that $\epsilon > 100$ ev.

Neutrons will not be expected to produce displacements of silicon or oxygen atoms when the neutron energy is less than about 100 ev so that (5) may be used to determine the energies of the primary knock on atoms. The neutron doses quoted in this paper are values of the product ($D_f \times$ exposure time in seconds)$=D$.

The induced radio activity was allowed to decay. In some cases measurements were made and they indicated that the activity was associated with traces of polishing powder which had adhered to the ground faces perpendicular to the polished surfaces. Autoradiographs confirmed this distribution.

§ 3. Experimental Results

3.1. *The C Band*

In good synthetic or natural crystals in which the concentration of aluminium impurity is of the order of, or less than, 0·01 atomic % the form of the damage induced *C* band (5·7 ev) can be seen. This is shown by curve I of fig. 4, which is the absorption curve of a synthetic crystal after a dose (*D*) of 7·4× $10^{17}n^\circ$ cm^{-2}. It will be noticed that even for this crystal there is some absorption in the region between 1 and 3 ev and the amount is consistent with the aluminium concentration found by Brown and Thomas (private communication) and Griffiths *et al.* (1954) in similar synthetic samples and also by Volger *et al.* (1955) in synthetic quartz from Bell Telephone Laboratories. Figure 4 also shows curves (II and III) for less pure specimens which had received the same dose.

Fig. 4

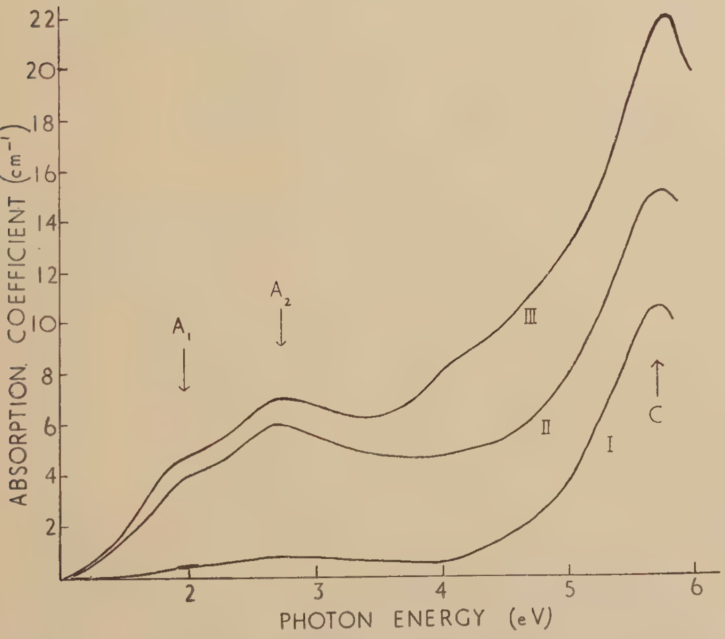

Absorption spectra of neutron irradiated crystalline quartz : dose, D, 7·4×10^{17} n° cm^{-2} ; curve I synthetic ; curves II and III natural Brazilian.

These curves indicate that some absorption in the *C* region, in addition to that induced by the damage, is present and that it is greater for specimens having greater A_1(2·0 ev) and A_2(2·7_5 ev) band absorption—i.e. greater aluminium concentration. We have found this to be true for all specimens.

Absorption in the *C* region can be induced by x-rays. It was shown in I that this absorption saturated, so that some of the defects which after ionization give rise to the *C* absorption must be present in the crystals initially. The level of *C* absorption due to trapping in existing defects seldom exceeds 20 cm^{-1} and is usually very much less than this. In a good synthetic or natural crystal it is about 5 cm^{-1}. Thus for the higher neutron doses the *C* band absorption is mainly due to displacements induced by the irradiation.

Figure 5 shows the neutron rate curve for the *C* band in different crystals for doses up to $10^{19}\, n^\circ\, \text{cm}^{-2}$. It is interesting to note that the points for all specimens eventually lie on the same curve which we call the Damage Rate Curve. For example, the results for the specimen whose rate curve is denoted by crosses lie on the Damage Rate Curve after a dose of $30 \times 10^{17}\, n^\circ\, \text{cm}^{-2}$. This specimen, judging by the A_2 absorption coefficient, was the least pure and it appears that the initial contribution to the *C* absorption has decayed with prolonged dose in a qualitatively similar manner to the A_1 A_2 bands, fig. 6.

Fig. 5

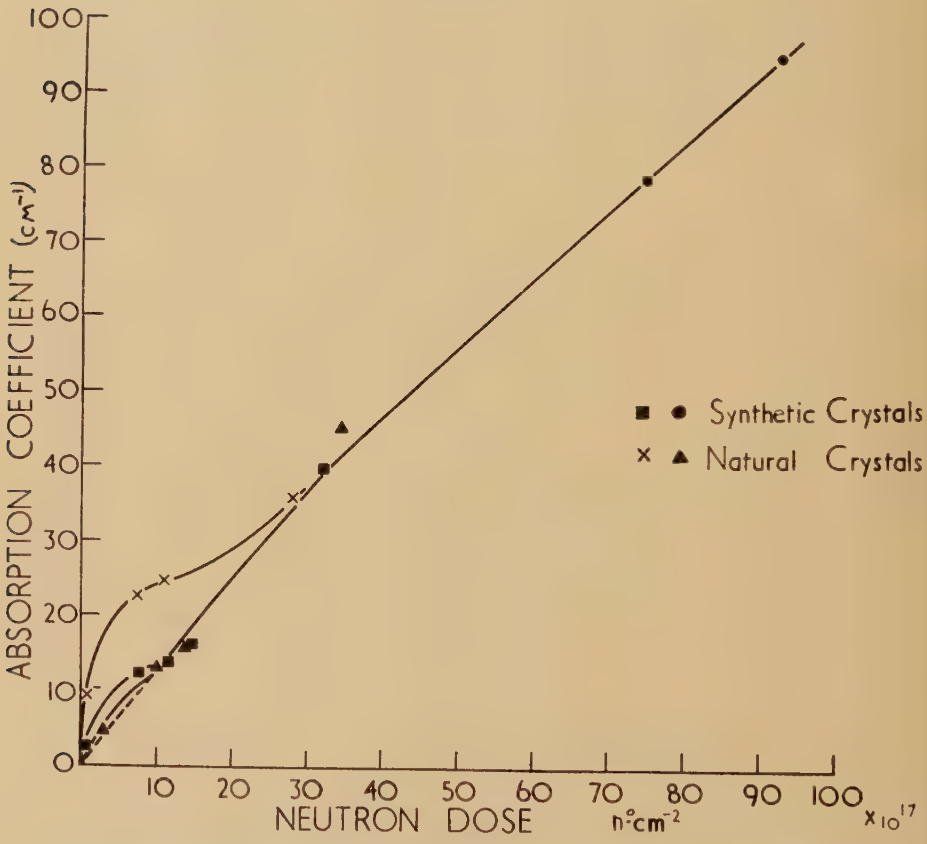

Rate curves for the *C* band induced by neutron irradiation.

The Damage Rate Curve is slightly curved but the absorption coefficient at the band maximum increases approximately as $10^{-17}\times D$. The half-width of the band is close to 1·4 ev so that

$$\mu_c\,.\,\Delta E_c \approx 1\cdot 4\times 10^{-17}\times D = 10^{-16}\mathcal{N}_c\,.\,f_c$$

or

$$\mathcal{N}_c = \frac{0\cdot 14}{f_c}D. \qquad (6)$$

Here $\mathcal{N}_c$ is the concentration of C centres and f_c the oscillator strength for the transition.

Fig. 6

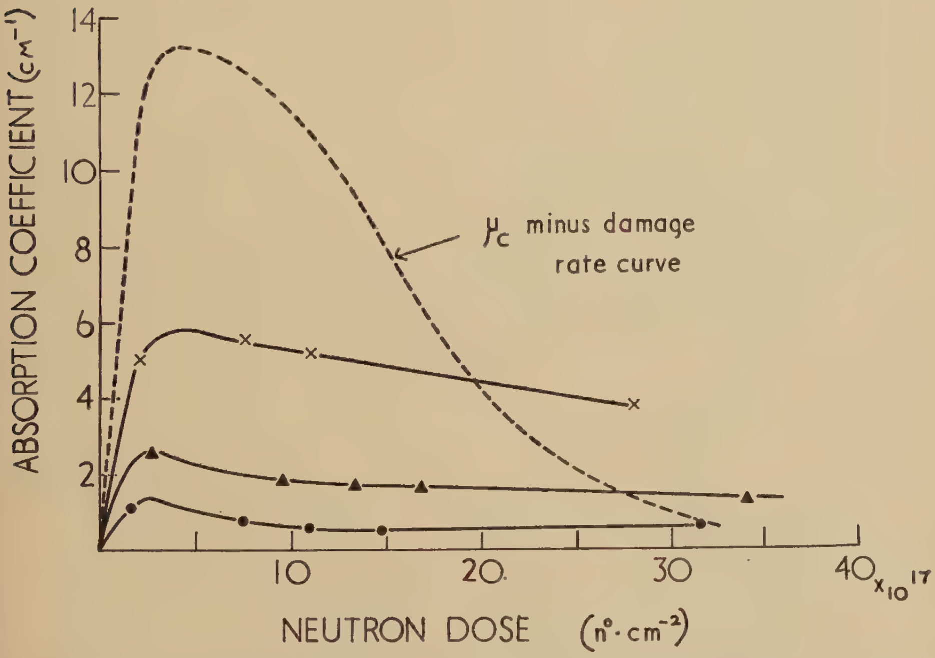

Rate curves for the A_2 band induced by neutron irradiation.

3.2. *Absorption at Photon Energies Greater than* 5·8 *eV*

The extent to which defects initially present in the crystals give rise to absorption in the vacuum ultraviolet after irradiation with ionizing radiation is shown in fig. 7. There is an additional band (D band) having a maximum absorption at $7\cdot 1_5$ ev of 7 cm^{-1} for this crystal after a 125 Mr dose of 50 kv x-rays. The values of absorption coefficient for energies greater than 7·4 ev are uncertain because of the subtraction of the absorption in the tail of the absorption edge which, owing to the thickness, was significant in this specimen.

The effects of neutron irradiation are illustrated in figs. 8 and 9. Curve 1 in fig. 8 refers to a synthetic specimen which had received a dose

Fig. 7

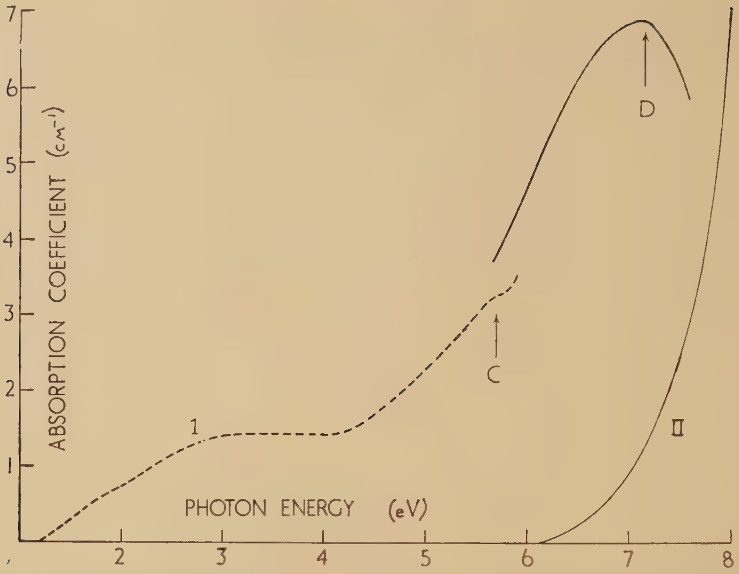

The absorption spectra of x-irradiated natural crystalline quartz : I, – – – – – UVISPEK measurements, ———— vacuum ultra-violet measurements. The absorption in the unirradiated crystal, curve II, has been subtracted from the measured absorption to give curve I.

Fig. 8

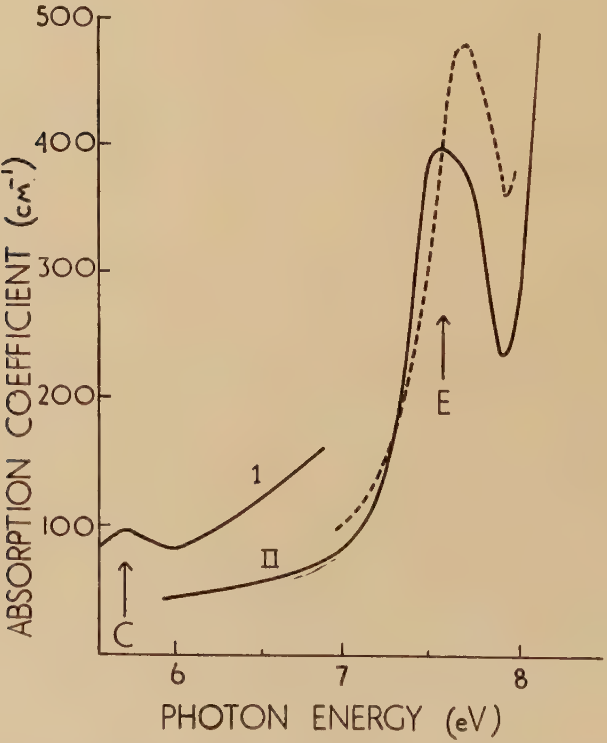

Vacuum ultra-violet measurements of neutron irradiated crystalline quartz : curve I for a dose of $75\times10^{17}\,n^{\circ}$ cm^{-2} ; curve II $17\times10^{17}\,n^{\circ}$ cm^{-2}, – – – – – at –195°c and ———— at 20°c.

of $75 \times 10^{17}\, n^{\circ}\ \mathrm{cm}^{-2}$. It will be seen that the *C* band peak is also found in the vacuum ultraviolet measurements. However, the transmission at 6·9 ev had fallen to less than 3% so that values of absorption coefficients were not obtained for higher photon energies with this specimen.

For a thinner specimen (0·011 cm) which had received a neutron dose of $17 \times 10^{17}\, n^{\circ}\ \mathrm{cm}^{-2}$, the spectrum shown in fig. 9 was obtained. The most prominent feature is the *E* band which has an absorption peak at about 7·6 ev and a half-width of 0·5 ev. After the decrease in absorption on the high energy side of 7·6 ev the absorption rises rapidly to immeasurably high values, the last measurable value being 300 cm^{-1} at 8·1 ev. No evidence has been found for a decrease in absorption between 8·1 and 8·5 ev, the induced absorption limit being similar to that found in both unirradiated and irradiated fused quartz at 8·1 ev. If the possible absorption tail denoted by the broken line in fig. 9 is subtracted from the measured curve the *E* band appears as a symmetrical band. At −195°c the *E* band is sharper and the peak has moved to a higher energy (fig. 8).

Fig. 9

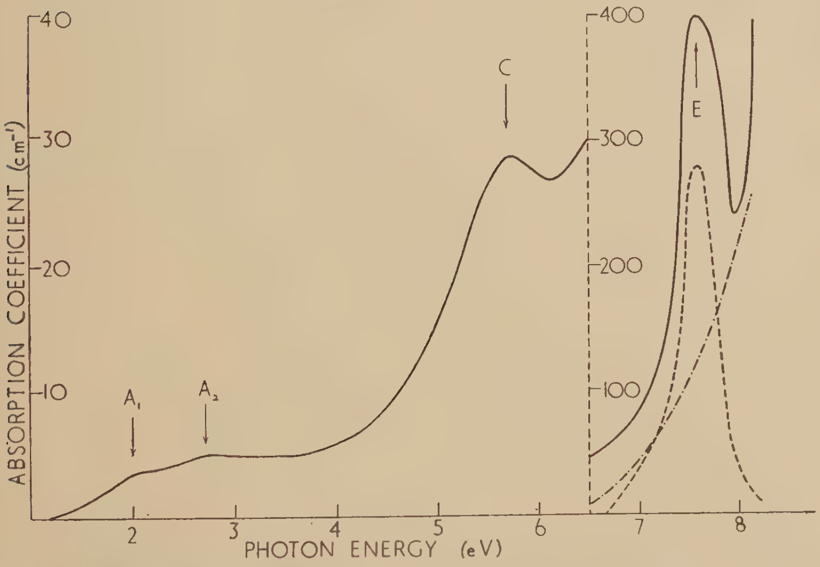

A complete absorption curve for neutron irradiated crystalline quartz.

Because of the low transmission at the *E* band peak the absorption coefficient is uncertain within ±20%. However, within these limits the absorption due to the *E* band has been found to vary linearly with neutron dose as

$$\mu_{\mathrm{E}} \,.\, \Delta E_{\mathrm{E}} \approx 8{\cdot}5 \times 10^{-17} \times D \approx 10^{-16} \,.\, \mathcal{N}_{\mathrm{E}} \cdot f_{\mathrm{E}}$$

or

$$\mathcal{N}_{\mathrm{E}} \approx \frac{0{\cdot}85}{f_{\mathrm{E}}} D \quad . \; . \; . \; . \; . \; . \; . \; . \; . \quad (7)$$

It has not been possible to discover whether the D band is enhanced by neutron irradiation because of the overlapping of the strong C and E bands in this region. If it is enhanced it is clear that the rate of increase is very much less than that of either the C or E bands.

3.3. *Optical Bleaching of the Induced Absorption*

Induced absorption bands which decrease in strength during illumination must be associated with defects which have trapped electrons or holes. The work of Choong (1945) and that reported in I has shown that in quartz both the A and C bands decrease upon illumination with light in the C band. The bleaching rates are, however, small so that it is not feasible to carry out the experiments using monochromatic light.

Illumination with light in the A bands leads only to a small optical bleaching effect (table 1) so that for experiments in which bleaching rates have been measured using light between 2100 Å and 10 000 Å the main effect is due to absorption in the C region.

Table 1. Effect of Illumination for 60 hr with Light of Photon Energy less than 3 ev

(High pressure Hg lamp and filters)

Transmission measured at	Before Illumination		After Illumination		Instrumental error in T
	$T\%$	μ cm^{-1}	$T\%$	μ cm^{-1}	
2·7 ev	23·3	14·6$_5$	23·8	14·4	±0·2
5·7 ev	5·8	29·3	6·0	28·9	±0·4

In a γ-ray (^{60}Co) irradiated specimen in which the dose was such (60 Mr) that only ionization effects were being studied the effect of optical bleaching is shown in fig. 10. The difference curve indicates that the spectrum bleaches uniformly. This is in contrast to the optical bleaching of neutron irradiated specimens reported in I. In this case, under the same conditions of illumination, preferential bleaching occurred in the region of 5·4 ev (fig. 15 of I). The preferential bleaching has now been shown to occur during the initial rapid bleaching of the C band shown in fig. 16 of I. This may be seen more clearly in fig. 11 where three difference curves are plotted for different parts of an optical bleaching rate curve. After 80 minutes bleaching there is a pronounced maximum at 5·4 ev which becomes less pronounced during the next 180 minutes, and is absent from the difference curve obtained after a further 320 minutes.

Experiments which have been carried out on a neutron irradiated ($92\times 10^{17}\, n^\circ$ cm^{-2}) synthetic crystal indicate that the presence of

Fig. 10

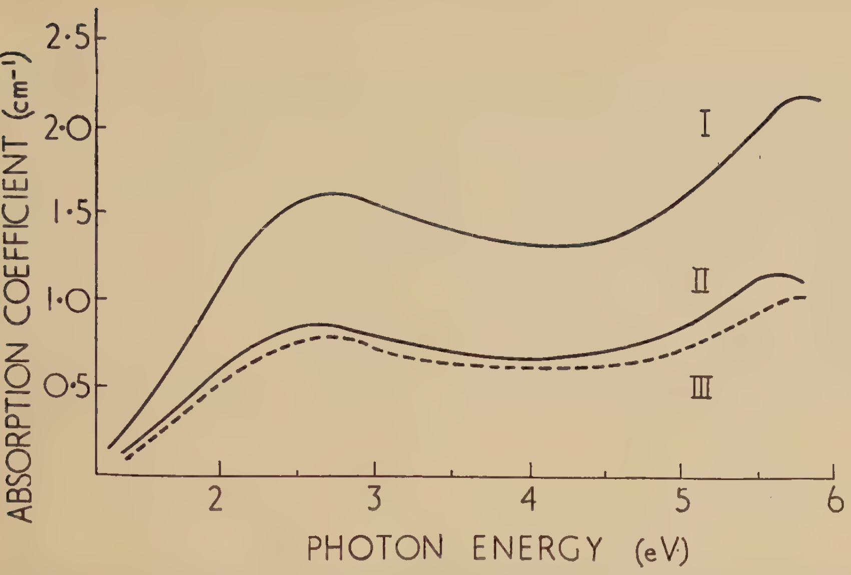

The absorption spectra of γ irradiated crystalline quartz: curve I after the irradiation; curve II after subsequent ultra-violet illumination for 22 hr; curve III the difference spectrum.

Fig. 11

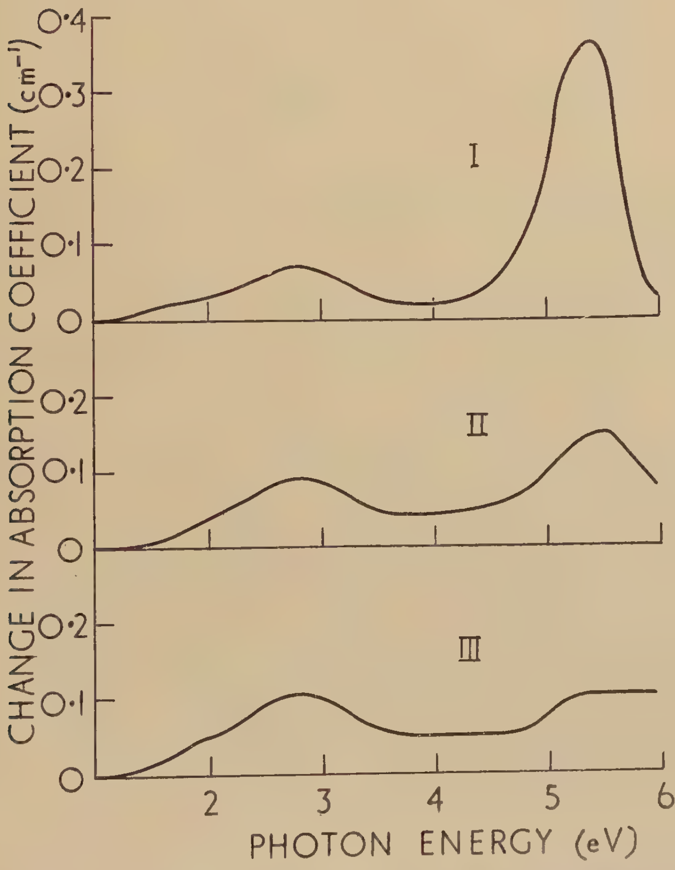

The optical bleaching of a neutron irradiated crystal by illumination with light in the *A* and *C* bands: curve I, the change after the first 80 min; curve II, after the next 160 min; curve III, after the next 320 min.

the A bands is not essential for optical bleaching. These curves (fig. 12) show that the C band is bleached and that during the first 30 hours there is preferential bleaching in the region of 5·4 ev. (In the specimen which had received the lower dose $2{\cdot}4\times10^{17}\,n^\circ\,\mathrm{cm}^{-2}$ above, the preferential bleaching effect was absent after 5 hours). During the following 80 hours bleaching is less rapid and the preferential bleaching is relatively much smaller. Presumably one of the vacuum ultra-violet bands is also being bleached but optical bleaching measurements on these bands have not yet been made.

If the illumination is with light of all wavelengths up to the absorption edge it is found that the C band is bleached much more rapidly in relation to the A band than if illuminated with light in the 2100–10 000 Å region. This experiment was carried out using a neutron irradiated natural crystal and is another indication that some of the vacuum ultra-violet absorption must be optically bleached.

Fig. 12

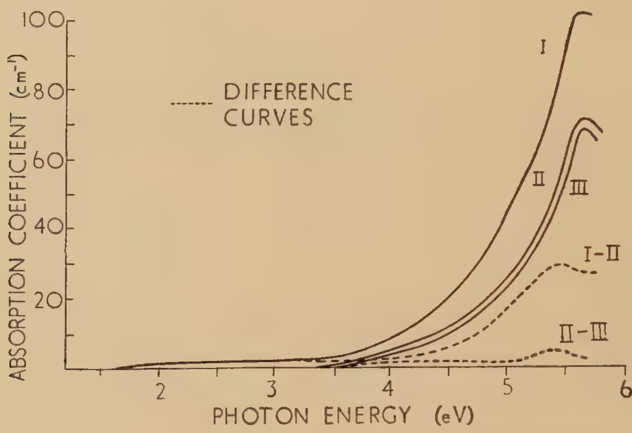

The optical bleaching of neutron irradiated synthetic quartz: dose $92\times10^{17}\,n^\circ\,\mathrm{cm}^{-2}$; curve I, no illumination; curve II, 30 hr; curve III, after a further 80 hr.

3.4. *The Effects of Heat Treatment*

It is necessary to distinguish two processes which can lead to decreases in absorption—the thermal activation of electrons, and the thermal activation of atoms or vacancies. For convenience we refer to the former as ‘ bleaching ’ and the latter as ‘ annealing ’.

The A and C bands may be bleached at temperatures less than 500°c and it will be shown later that at this temperature there is little annealing taking place. The isothermal bleaching curves do not follow a simple rate law but there are two interesting features. Firstly, in neutron irradiated specimens there is preferential thermal bleaching in the region of 5·4 ev which is not found for γ- or x-ray irradiated specimens. This is shown by the curves of fig. 13. Secondly, it is possible to deduce activation energies for the electron excitation from successive isothermal bleaching curves on the same specimen. This procedure, e.g. Overhauser (1953), is independent of the rate kinetics. The energy ϵ' is given by

$$\ln\left\{\left(\frac{d\mu}{dt}\right)_{t_1T_1} \Big/ \left(\frac{d\mu}{dt}\right)_{t_1T_2}\right\} = \frac{\epsilon'}{(2)\mathrm{k}}\left(\frac{1}{T_2}-\frac{1}{T_1}\right) \quad . \quad . \quad . \quad . \quad (8)$$

Fig. 13

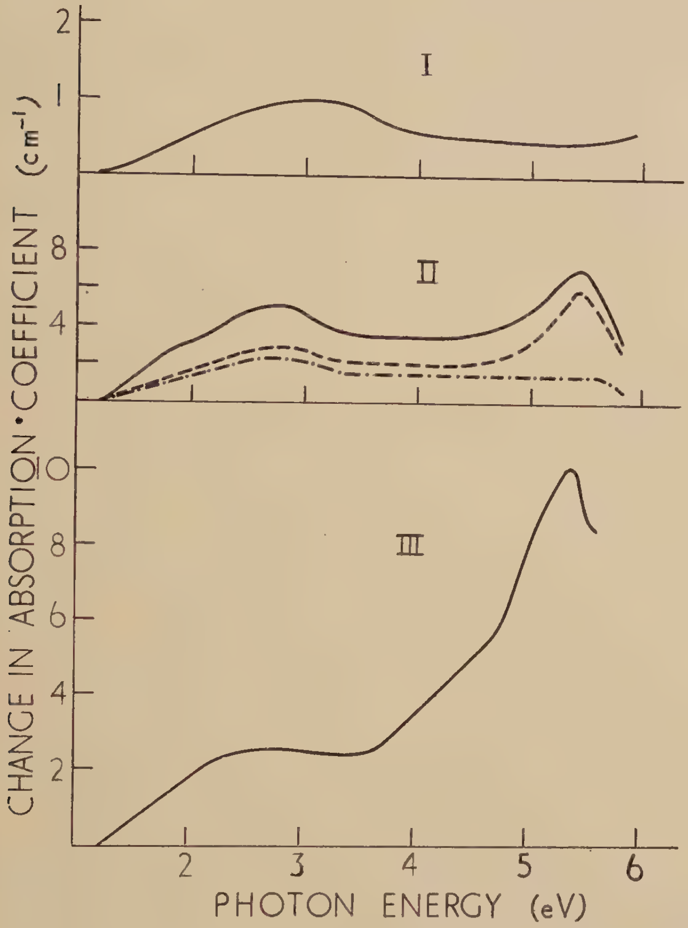

The thermal bleaching of radiation induced absorption in crystalline quartz. The curves show the change in absorption after heating for 9 hr at 240°c for: I, x-irradiated crystal; II, neutron irradiated crystal (small dose), – – – – – – after the first 10 min and · – · – · – · – after the next 8 hr 50 min; III, neutron irradiated crystal (large dose).

For crystalline quartz, measurements at 215 and 335°C on one specimen and also at 220 and 260°C on another both gave $\epsilon'/(2)$ equal to 0·75 ev.

Annealing Experiments

High temperature heat treatments were carried out in either air or vacuum, the crystal being contained in either a platinum crucible or wrapped in platinum gauze. From 950°C it was necessary to cool the crystal slowly to prevent cracking and in these experiments specimens were cooled at a controlled rate (approx. 40°C/hour) for 24 hours. To decide the extent to which the atomic defects are annealed at any given temperature it is necessary to re-irradiate the specimen after the heat treatment. Ideally x-ray irradiations to saturation are desirable for this purpose but in many cases this process is so long as to make the experiment impossibly slow. The alternative of a standard x-ray dose for the second irradiation cannot be relied upon since Forman (1951) has shown that heating at even 400°C can affect the rate of visible colouring although the saturation value appears unaltered. In the present experiments we have used a second pile irradiation to determine the effect of the heat treatment, this being done in conjunction with an irradiated, but unheated, control specimen.

Fig. 14

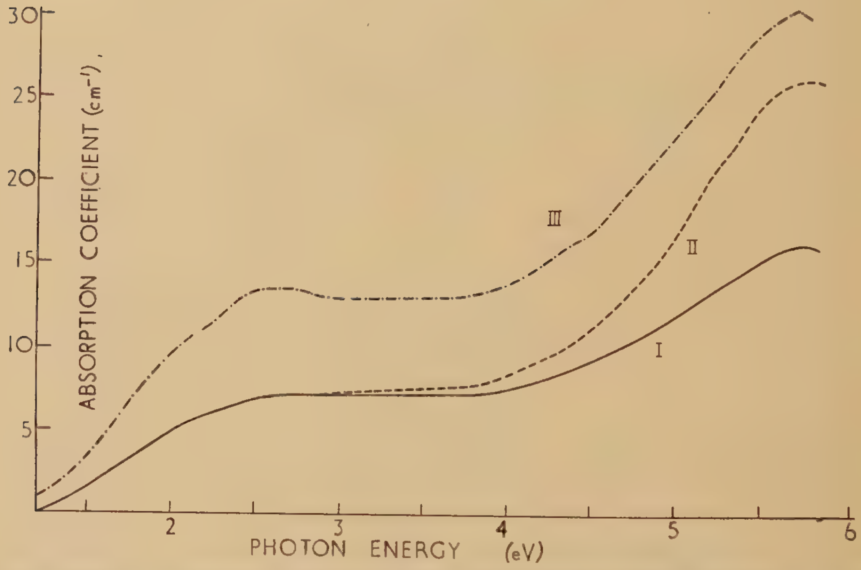

The effect of a neutron irradiation-heat treatment-neutron irradiation cycle on the absorption spectra of natural crystalline quartz: curve I, after the first irradiation; curve II, after the second irradiation; curve III, after the same irradiations but with heat treatment at 950°C for 24 hr in air between irradiations.

Three specimens were cut from the same crystal, all with the *c*-axis perpendicular to the polished surfaces. These specimens were placed in the same container and received a dose of $2{\cdot}4\times10^{17}\,n^\circ\,\mathrm{cm}^{-2}$. After measuring the absorption spectra between 1·2 and 5·8 ev, one specimen (N32) was heated for 45 minutes at 500°c in air, another (N34) was heated in air for 24 hours at 950°c and the third specimen (N33) was untreated. All specimens were re-irradiated (the C absorption of the control increasing by $8{\cdot}8\,\mathrm{cm}^{-1}$) and the absorption spectra redetermined. Curve I of fig. 14 is the absorption spectrum of one of the crystals after the first irradiation. This was typical of all three specimens, the differences being $\pm0{\cdot}05\,\mathrm{cm}^{-1}$ for μ_{A} and $\pm2\,\mathrm{cm}^{-1}$ for μ_c. Curve II is the absorption spectrum of N32 after the second irradiation and the absorption spectrum of N33 was similar. The major change shown by the second irradiation was the increase in the absorption of the *A* bands of N34 after the high temperature heat treatment (curve III). The same large increase in *A* band absorption was found for N33 following an irradiation after high temperature heat treatment in vacuum. Thus the effect is not significantly sensitive to the ambient atmosphere. Finally, heating N34 for a further 24 hours in air after the second irradiation produced a further enhancement of the *A* bands, which was less, however, than the original increase.

In view of the evidence that the *A* bands are associated with substitutional Al, the first conclusion to be drawn from these experiments is that heating to 950°c after neutron irradiation leads to a higher concentration of substitutional Al. This in turn indicates that normally some of the Al impurity is present in interstitial positions.† Then during heat treatment the interstitial Al atoms diffuse at a similar rate to the interstitial Si atoms produced by displacements, so that some of the Si vacancies are filled by Al atoms.

It has already been pointed out that the *C* band absorption due to defects initially present in the crystal seems to be related to the *A* band absorption, that is to the substituted Al concentration. The heat treatment results lead to a similar conclusion, for an increase in *C* absorption always accompanied the *A* band enhancement in spite of whatever annealing processes were taking place (cf. curve III, fig. 14).

To examine this quantitatively the heat treatment results have been analysed using the two alternative relations:

$$(a)\ \mu_C=\alpha\mu_{\mathrm{A}}+\beta D \qquad \text{(9)}$$

$$(b)\ \mu_C=\alpha'\mu_{\mathrm{A}}+\beta D+D_0 \qquad \text{(10)}$$

where α, α' and β are constants, D is the neutron dose and D_0 is a contribution to the absorption from defects in the crystal prior to irradiation, for example, the tail of the *D* band. It is clear that using (9) α and β cannot both be constants applying to all three specimens for after the first irradiation μ_C was not constant. We assume that β, the damage component per unit dose, was constant. In the comparison of results in table 2 we consider the extremes of no annealing and complete annealing for each temperature.

---

† The non-linear increase in μ_{A} with Al concentration reported by Ditchburn *et al*. (1954) is a further indication of the presence of interstitial Al.

There is not a great deal to choose numerically between the two analyses, what difference there is being in favour of (10) in which α' is constant for all quartz crystals. In either case the results lead to the conclusions that there is very little annealing at 500°c and that annealing is complete at 950°c. These conclusions are also supported by the observations on the absorption edge. The same result has been found by Wittels (1953) for the annealing of the density changes, while Berman (1951) has found that the irradiation induced thermal resistance was not completely annealed at 700°c.

Table 2. Analysis of Heat Treatment Results

Specimen	Heat treatment	μ_c cm^{-1} observed	Assumption	μ_c cm^{-1} calc. 9	μ_c cm^{-1} calc. 10
N 32 $\alpha=2{\cdot}2$ $\alpha'=1{\cdot}3_5$ $D_0=5{\cdot}8$	500°c in air	30±1	No annealing	30	30
			Complete annealing	25	25
N 34 $\alpha=1{\cdot}5_5$ $\alpha'=1{\cdot}3_5$ $D_0=1{\cdot}4$	950°c in air	30·5±1	No annealing	35	33
			Complete annealing	30	28
	950°c in air	32±1	No annealing	47	46
			Complete annealing	34	32
N 33 $\alpha=1{\cdot}7$ $\alpha'=1{\cdot}3_5$ $D_0=2{\cdot}6$	950°c in vacuum	34±1	No annealing	51	48
			Complete annealing	38	34

Measurements in the vacuum ultra-violet were also made on the specimens N 33/34. It was found that after heating at 500°c for $\frac{3}{4}$ hr the E band was still present, although reduced in strength (from $\approx$100 to 35 cm^{-1}). After heating at 950°c the E band was completely bleached and the absorption in the region of the edge was identical with an unirradiated crystal.

While the above heating results refer to high temperature heat treatments carried out *after* neutron irradiations, it has been found that the amount of A band absorption induced may also be altered by heat treatment *before* irradiation. Two specimens cut from the same block were irradiated, one of them having been previously heated in air at 950°c for 24 hr while the other was untreated. The value of the absorption coefficient at the A_2 band peak was 17% higher in the heated specimen. This is much larger than the variations in the A_2 band absorption amongst non-banded specimens cut from the same block (±2%), although much smaller than when the specimen has undergone an irradiation-heat-irradiation cycle. We conclude that it is possible by heat treatment to increase the concentration of substituted Al in an unirradiated crystal. It must be assumed that there is a variable concentration of Si vacancies existing from growth in unirradiated crystals, for it is improbable that sufficient vacancies can be created by heat treatment at 950°c.

3.5. *Observations on Fused Quartz*

As reported previously in paper I for the spectral range 2100 to 10 000 Å, the behaviour of fused quartz is similar to that of crystalline quartz and this similarity of the shape, positions and properties of the bands has now been found to extend into the vacuum ultra-violet region. The local environment of such centres must be similar in the two solids, a view which is consistent with the model of fused quartz as a solid lacking the long range order of the crystalline form. Recently Weeks (1956) has shown that similar magnetic resonance lines are associated with the radiation induced damage in the two solids. The optical effects are summarized below and some of them are illustrated in fig. 15.

(*a*) Corresponding to the A_1 and A_2 bands in crystalline quartz there is a band (A) with a peak at 2·3 ev. This absorption also decreases with prolonged neutron irradiation.

(*b*) There is a band at 4·1 ev (B_1) which is strong after x-irradiation, although in some specimens the absorption passes through a maximum before reaching a steady value. With neutron irradiation it is bleached, in all specimens, more rapidly than the A band.

(*c*) There is a band induced at 5·1 ev (B_2) in neutron irradiated, but not in x-irradiated specimens. The same result was found by Levy (1955) but the band was not observed by Levy and Varley (1954).

(*d*) A band (C) occurs at 5·8 ev and increases with neutron dose, but more rapidly than the C band in crystalline quartz.

(*e*) In x-ray irradiated fused quartz a band is found at 7·2 ev (D) as in x-ray irradiated crystalline quartz. It is similarly not known whether the band is present in neutron irradiated specimens because of the rapid growth of the C and E bands.

(*f*) The E band occurs at 7·6 ev. In fused quartz, however, the E band has been found in a specimen which was irradiated with x-rays with a dose 7× that required for the A band saturation. It was not observed at saturation. This suggests that in unirradiated fused quartz

E defects either exist or can be produced with a small probability by x-ray photo electrons. The latter alternative may arise since in fused quartz, because of the irregular packing of the SiO$_4$ groups, there will exist atoms having binding energies less than in crystalline quartz. The band has also been found in $\gamma(1\times10^{9}\mathrm{r})$ irradiated specimens.

(*g*) The absorption limit is found at about 8·1 ev in unirradiated and irradiated fused quartz, and is not affected by heat treatment.

Fig. 15

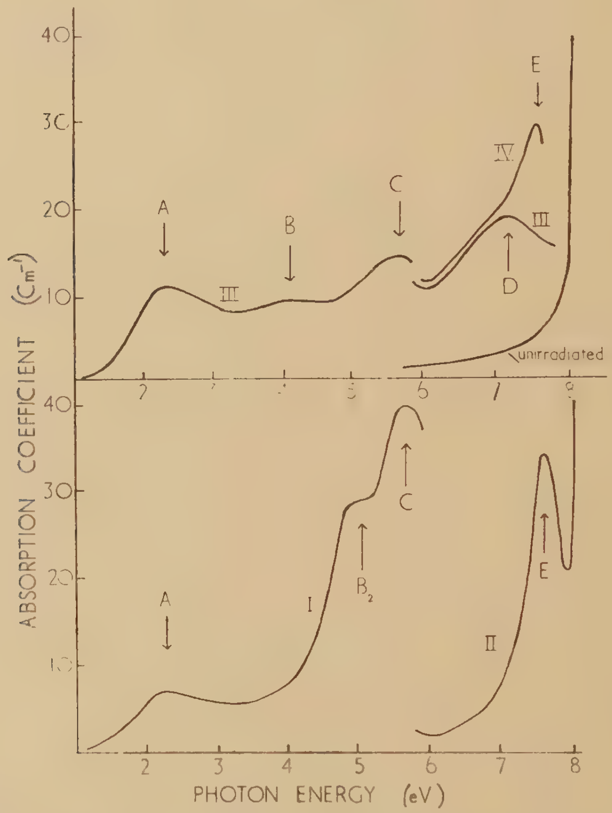

The radiation induced absorption spectra in fused quartz: curve I, after neutron irradiation; curve II, the same specimen after heating at 520°c showing the presence of the *E* band; curve III, an x-ray dose corresponding to saturation of the *A* band; curve IV, the same specimen after ×7 the saturation dose.

Since the visible absorption does not increase with neutron dose the *A* band is probably associated with impurity. It has been reported by Levy (1955) and also Cohen (1955), that specially purified fused silica manufactured by the Corning Co. does not colour with x-irradiation, and shows only a small visible colour after neutron irradiation. The effect may not be due simply to purification, however, as Yokota (1952) has shown that in fused quartz prepared under strongly oxidizing conditions the *A* band is absent. Similarly we have found that the strength of the *A* band induced by a small neutron bombardment, while practically unaffected by prior heat treatment at 950°c for 24 hr in vacuum, is less if the treatment is in air (table 3). Levy and Varley (1954) have suggested that boron is the relevant impurity and that it exists in amorphous quartz as sodium tetraborate, the *A* and *C* centres being induced by hole and electron trapping in the borate. The general similarity with crystalline quartz suggests that boron may play a role in fused quartz similar to aluminium in crystalline specimens and exist in place of silicon in the SiO_4 network rather than occur as sodium tetraborate. In six of our specimens which were analysed, however, the boron concentration was less than 0·0001% by weight, too small to give an observable absorption band by the same mechanism as aluminium, while the aluminium concentrations were all around 0·05%.

Table 3. The Effect of Previous Heat Treatment on the Absorption Induced in Fused Quartz by a Neutron Dose of $4{\cdot}2\times10^{17}\ n^\circ\ \mathrm{cm}^{-2}$

Specimen	Treatment	Absorption coefficient (cm^{-1})			
		A	B_1	B_2	C
F7	—	8·5	7·1	16·8	20·0
F8	950°c 24 hr in vacuum	8·2	7·0	17·3	20·0
F9	950°c 24 hr in air	5·7	6·5	17·3	19·4

As in crystalline quartz, all the defects introduced by neutron irradiation may be annealed by heating at 950°c. Thermal bleaching of the *A* and *C* bands takes place with an activation energy $\epsilon'_t(2)$ of 1·6 ev. A detailed account of the results on fused quartz will be published separately.

§ 4. Discussion of Results

The three primary optical effects of the neutron irradiation of quartz with doses up to $10^{19}\ n^\circ\ \mathrm{cm}^{-2}$ are: (i) the growth of the *C* band, (ii) the formation and growth of the *E* band and (iii) the edge shift. The first two of these occur at practically the same energies in both fused and crystalline quartz, while the edge shift is only found in crystalline specimens. All three types of defect are completely annealed by heating at 950°c but are hardly affected at 500°c. Neutron irradiation also decreases the strength of the visible absorption (A_1, A_2) bands associated with Al impurity—the effect which we have referred to as radiation bleaching.

4.1. *Radiation Bleaching*

Continuous radiation bleaching of the *A* bands occurs only with neutron irradiation and we examine first the rates to be expected for the destruction of the defect. There seems to be two possibilities : (*a*) transmutation of Al by thermal neutrons, and (*b*) displacement of the Al or some of its neighbouring atoms. Both these processes, however, give rates which are too low to account for the observed changes. In the case of (*a*) this may be seen immediately from the low cross section for the transmutation of Al (0·008 barns) while the calculations in (iii) below show that a given Si (or Al) atom has a chance of *ca.* 1/1000 of being displaced after a dose of 10^{18} n° cm^{-2}. Experimentally the decrease is by about 1/5 after this dose. Even if it is supposed that the displacement of any one of 10 surrounding atoms destroys the defect the rate of destruction is still too small.

Fig. 16

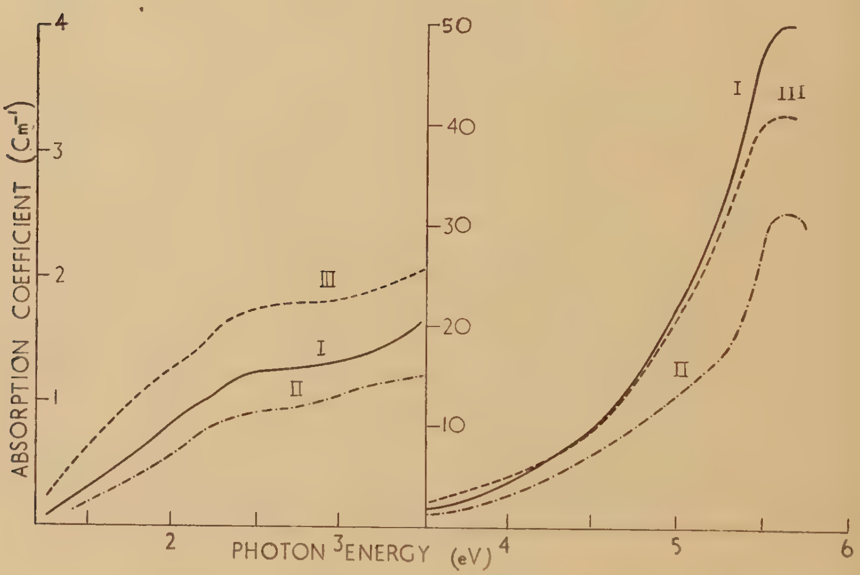

The absorption spectrum of neutron irradiated crystalline quartz, curve I ; after optical bleaching, curve II ; after optical bleaching and subsequent x-irradiation, curve III.

It is more probable that the effect is electronic. There is no evidence of any new centre being formed at the same time as the *A* bands decrease, The following experiment, however, indicates that the ratio ($\mathscr{N}_A/N_A$) for a given type of radiation depends on the relative occupancy of the other trapping centres. Such a dependence could provide a basis for a mechanism of radiation bleaching.

A specimen which had been partially radiation bleached ($3{\cdot}0\times10^{18}$ n° cm^{-2}) was irradiated with x-rays and no increase of the A_1,A_2 band absorption was found. The absorption curve of a similarly radiation bleached specimen is shown in fig. 16 (I). This specimen was further bleached by illumination with C (and A) band light, giving the absorption curve II. An x-irradiation of the same dose as for the other specimen led to the absorption curve III. Since the action of the light cannot be to anneal atomic defects the increase of A_1, A_2 band absorption above the original level must be due to change in the ratio $\mathcal{N}_A/N_A$.

4.2. *The Edge Shift*

On the high energy side of the E band the absorption rises rapidly at 8·1 ev, compared with the corresponding rise at 8·5 ev in unirradiated quartz. The increase at 8·1 ev is similar to the increase found in unirradiated fused quartz.

In fused quartz the SiO_4 groups are not regularly arranged. The variations in Si—O distances presumably lead to allowed energy levels occurring below the energy at which the conduction band is found in crystalline quartz, and above the valence band. The absorption spectra indicate that the neutron irradiation of crystalline quartz produces levels in the same energy range. We infer that some regions of the crystal have been converted to a phase analogous to fused quartz.

It is not possible to estimate the total volume occupied (after a given irradiation) by these regions from the present measurements since this involves knowing the whole absorption curve up to values of 10^5–10^6 cm^{-1} for both the irradiated and unirradiated specimens. Single crystal specimens have to be used and for reliable measurements thicknesses of 10^{-5} and 10^{-6} cm are required. As a method of detection of a disordered structure, however, the sensitivity is large. The present results could correspond to the conversion of only 10^{-3} of the total volume of the crystal, equivalent to a density change of 0·015%.

The occurrence of disordered regions (M regions) for the doses used in our measurements (up to $10^{19}\ n^\circ$ cm^{-2}) is of some interest following the work of Wittels and Sherril (1954), and the discussion of this work by Kinchin and Pease (1955). Wittels and Sherril found that after doses of about $10^{20}\ n^\circ$ cm^{-2}, an amorphous, optically isotropic material was obtained having a density 15% less than α-quartz and 3% greater than a typical value for fused quartz. For doses up to $7\times10^{19}\ n^\circ$ cm^{-2} the damage, as indicated by density and x-ray measurements, could be annealed by heating at 930°c, but beyond this dose the heat treatment gave polycrystalline α-quartz. The simplest explanation of the transformation to the amorphous state is that near the ends of the tracks of the knocked on atoms collisions are so frequent that we may consider a small region being heated momentarily to a high temperature. This is the ‘displacement spike’ discussed by Brinkman (1954). In the case of quartz it is suggested that the rapid heating and cooling leads to the formation of a volume v of amorphous solid. This process would lead to a saturation according to a rate

$$V_a = V[1-\exp(-D\alpha v)] \quad \ldots\ldots\ldots \quad (11)$$

where V_a is the total volume of amorphous solid, V is the volume of the crystal, v the average volume of an amorphous region and α is the number of knocked on atoms, per unit dose, which produce such regions. However, the variation of density with neutron dose observed by Wittels and Sherril was not of this form. The relation (11) predicts that the slope should decrease with dose over the whole range, contrary to what was observed.

Kinchin and Pease (1955) have suggested that the quartz structure becomes unstable when the crystal contains a sufficient concentration of point defects and that this is the reason for the rapid increase observed by Wittels and Sherril for doses *ca.* $10^{20}\,n^{\circ}\,\mathrm{cm}^{-2}$. The smaller decrease in density at lower doses is then assumed to be due to the expansion produced by interstitial atoms, and not to a smaller number of regions of amorphous solid. This is in contradiction to the observed edge shift.

The experimental results require that regions of amorphous quartz are formed at all doses. At the boundaries of such regions there must be large stresses, arising because the amorphous material normally occupies a volume about 15% greater than the crystalline material from which it is formed. Fry (private communication) has suggested that as the concentration of amorphous regions increases an intermediate volume can become sufficiently stressed for the next displacement spike to lead to a larger volume of amorphous solid than would be produced at lower doses, the additional thermal energy arising because of the release of strain energy.

Suppose $v=v_0+cD^n$, where c and n are constants, then the rate law becomes

$$V_a=V\left\{1-\exp\left[-\alpha D\,v_0+\frac{c}{n+1}\cdot D^n\right]\right\} \quad . \quad . \quad . \quad : \quad (12)$$

To obtain a curve resembling that obtained by Wittels and Sherril we have to assume further than when $V_a=V$ expansion can take place by the continued production of point defects. Equation (12) can be made to fit the three points given by Wittels in the range $(5\text{–}6{\cdot}6)\times 10^{19}\,n^{\circ}\,\mathrm{cm}^{-2}$, but there are no points in the most sensitive range immediately above $6{\cdot}6\times 10^{19}\,n^{\circ}\,\mathrm{cm}^{-2}$.

4.3. *Collision Theory Estimates of the Concentration of Point Defects*

The M regions are not considered to contain significant concentrations of point defects, as discussed by Brinkman (1954). Calculations of point defect concentrations, therefore, have to allow for the loss of energy of the primary knock-on atoms by this process.

In the case of quartz the primary knock-ons have energies up to $2{\cdot}6\times 10^5$ ev for silicon and $4{\cdot}4\times 10^5$ ev for oxygen corresponding to the highest energy (2 MEV) of the pile neutrons. We have to consider the energy loss by four processes: (*a*) excitation of the electron system of the solid, (*b*) elastic collisions in which the recoil energy is insufficient to produce displacements, (*c*) elastic collisions which produce displacements and, (*d*) the formation of M regions. The loss of energy of primary knock-ons by processes (*b*), (*c*) and (*d*) has been discussed by Brinkman (1954) and by processes (*a*), (*b*) and (*c*) by Kinchin and Pease (1955). We have to apply their results to the spectrum of primary knock-ons produced during the pile irradiation.

The method used is to calculate the upper limit of the concentration of defects assuming that no energy is lost by processes (*a*) and (*d*). We then estimate the maximum effects of (*a*) and (*d*) which enables an estimate to be made of the lower limit to the concentration of defects.

The maximum concentration can readily be determined. Neutrons in the energy range ϵ to $\epsilon+d\epsilon$, $n(\epsilon)d\epsilon$, produce primaries having energies E in the range 0 to $F_{MX}\epsilon$, where F_{MX} is the largest fraction of neutron energy which can be transferred in an elastic collision. Since the cross sections for neutron collisions with oxygen and silicon atoms are isotropic and independent of energy in the present energy range, the energy density of primaries is independent of energy up to $E_{MX}(=F_{MX}\cdot\epsilon_{MX})$ and is given by

$$N_E\,dE=\frac{(N_a\sigma_a)\,n(\epsilon)d\epsilon}{F_{MX}\epsilon}\,dE \quad . \quad . \quad . \quad . \quad . \quad . \quad . \qquad (13)$$

where N_a is the concentration of atoms a and σ_a the cross section for n° collisions with a. Following the discussion by Kinchin and Pease (1955) a primary produces $E/2E_d$ displacements in slowing down to rest, as long as $E<L_B$ (in their nomenclature). This condition is satisfied for all the knock-on energies occurring in the present work. Thus the maximum concentration of defects will be given by the sum of two terms, representing the effects of oxygen and silicon primaries, of the form

$$N_{MX}=\int_{2E_d/F_{MX}}^{\epsilon_{MX}}\int_{2E_d}^{F_{MX}\epsilon}\frac{E}{2E_d}\,N_E\,dE+\int_{E_d/F_{MX}}^{\epsilon_{MX}}\int_{E_d}^{F_{MX}\epsilon}N_E\,dE$$

which, using eqn. (1) and since $F_{MX}\epsilon_{MX}\gg 2E_d$ gives

$$N_{MX}=(N_a\sigma_a)\,\frac{0\cdot055D}{2E_d}\,\frac{E_{MX}}{2} \quad . \quad . \quad . \quad . \quad . \quad . \quad . \qquad (14)$$

We suppose that the knocked on atoms will cease to lose energy by ionization when their energy has fallen to E_I, the value of which is discussed below. The maximum reduction in N_{MX} will occur when it is assumed that above E_I all the energy is lost by ionization. Thus taking ionization losses into account, the lower limit to the concentration of defects is

$$N_I=\int_{2E_d/F_{MX}}^{\epsilon_{MX}}\int_{2E_d}^{E_I}\frac{E}{2E_d}\,N_E\,dE+\frac{E_I}{2E_d}\int_{E_I/F_{MX}}^{\epsilon_{MX}}\int_{E_I}^{F_{MX}\epsilon}N_E\,dE \quad . \qquad (15)$$

which gives

$$N_I=\phi_I N_{MX} \text{ when } \phi_I=\frac{E_I}{F_{MX}}\left\{\frac{E_I}{E_{MX}}+\ln\left(\frac{E_{MX}}{E_I}\right)^2\right\}.$$

When the energy of knocked on atoms falls to E_M, the upper limit for the formation of M regions as discussed below, we assume that no permanent point defects are produced. Thus, considering processes (*b*), (*c*) and (*d*) we obtain a lower limit

$$N_M = \int_{E_M/F_{MX}}^{\varepsilon_{MX}} \int_{E_M}^{F_{MX}\varepsilon} \frac{E}{2E_d} N_E \, dE - \frac{E_m}{2E_d} \int_{E_M/F_{MX}}^{\varepsilon_{MX}} \int_{2E_d}^{E_M} N_E \, dE \quad . \quad . \quad (16)$$

giving

$$N_M = \phi_M N_{MX} \quad \text{when} \quad \phi_M = \left\{1 - \left(\frac{E_M}{E_{MX}}\right)^2 \left[1 + \frac{E_{MX}}{E_M} \ln\left(\frac{E_{MX}}{E_M}\right)\right]^2\right\}.$$

Taking all processes into account we have the minimum value given by

$$N_M^I = N_{MX} - (1-\phi_I)N_{MX} - (1-\phi_M)N_{MX}$$

as long as $E_I > E_M$.

The limiting conditions are satisfied by the above relations: $E_I = E_{MX}$, $E_M = 0$, $N_M^I = N_{MX}$; $E_I = E_M$, $N_M^I = 0$; $E_M = 0$, $N_M^I = \phi_I N_{MX}$.

The value of E_I.

We are assuming that neutral particles do not lose energy by electronic excitation. It is known that electronic energy transfer can occur between neutral particles, for example the loss of energy of excited Hg atoms in the presence of Na atoms, but the cross section is small except when the energy transfer is small (Mott and Massey 1949).

The rate of energy loss by electronic excitation for particles moving with velocity v greater than the velocities u of the valence electrons in the solid, is much greater than the rate due to elastic collisions for the corresponding velocities, Kinchin and Pease (1955). We shall assume that as long as the particle is charged all the energy is lost by inelastic processes. However, as the energy decreases the net charge decreases and, if E_I is the energy at which an atom moving through matter can be considered neutral, we assume that all the energy in excess of E_I is lost by electronic excitation.

The work of Stephens and Walker (1955) on fast (6–20 MEV) N, O and Fl ions has shown that the average charge for a given velocity is in reasonable agreement with the criterion proposed by Lamb (1940). According to this the moving particle of mass M exchanges electrons with the atoms of the solid such that the particle loses those electrons whose ionization potential is less than $\mathscr{E}(=mE/M)$. If I_1 is the first ionization potential we regard atoms for which $E < E_I'$ as, on the average, neutral ($E_I' = MI_1/m$). Although in doing this we shall have over-estimated the number of charged particles for $E > E_I'$, we shall also have underestimated the number of charged particles for $E < E_I'$.

Bohr (1948) has also considered the value of the average charge on an atom which is moving through matter. He gives the average charge q as: $q = (Z^{1/3}/E_R)m/M$ where E_R is the Rydberg energy and Z the atomic number of the moving particles. We define a second value of $E_I(E_I'')$ below which the average charge is less than $+1$. The values of E_I'' are within a factor of 2 of those of E_I' as shown in table 4, and as also shown in the table this uncertainty does not critically affect the values of N_M^I.

Table 4. The Results of the Damage Calculations

Primary	E_{MX} ev	E_M	E_I'	E_I''	N_{MX} cm^{-3}
Si O	$2{\cdot}6\times10^5$ $4{\cdot}4\times10^5$	$2{\cdot}9\times10^4$ $1{\cdot}1\times10^4$	$4{\cdot}2\times10^5$ $4{\cdot}0\times10^5$	$3{\cdot}0\times10^5$ $2{\cdot}0\times10^5$	$9{\cdot}_5$ D 36 D
					45 D
	ϕ_M	ϕ_I'	ϕ_I''	$N_M^{I'}$	$N_M^{I''}$
Si O	0·51 0·81	1·0 0·99	1·0 0·91	$4{\cdot}_8$ D 29 D	$4{\cdot}_8$ D 26 D
				34 D	31 D

Both E_I' and E_I'' are greater than the limit suggested by Seitz (1949) below which a charged particle ceased to lose energy by electronic excitation—$E_I'''=E_g/x$ where E_g for an insulator is the forbidden energy gap and x was taken arbitrarily to be 8.

The value of E_M.

In his calculations Brinkman (1954) took E_M to be the energy at which the mean distance between non-displacement collisions was equal to the interatomic spacing. This value was not put forward as an upper limit which, owing to the uncertainties of the details of the process, is the value required in the present calculations.

The criteria for the formation of M regions are that there should be non-displacement collisions and that they should occur sufficiently frequently so that the energy cannot be dissipated by the lattice. We have taken E_M as the energy below which the elastic collisions can be described by the rigid atomic sphere approximation (L_A of Kinchin and Pease 1955). This is a convenient upper limit because Snyder and Neufeld (1954) have shown that for $E>L_A$ the predominant elastic collision energy loss is in displacement collisions. Below L_A non-displacement collisions occur with increasing probability. The mean distance between collisions at L_A is $l=N_a^{-1}[\pi a_0^2(Z_1^{-2/3}+Z_2^{-2/3})]^{-1}$ giving an upper limit $l=30$ Å. The results of the calculations are shown in table 4.

The results in the table are not seriously affected by the uncertainties in E_d and a value of 40 ev has been used for the displacement of either atom in quartz. The extreme values are, for all displacements in quartz, $31D$ to $45D$. Of the total concentration on the average $2/3$ will be oxygen displacements, giving

displaced oxygen atoms : 30 to $21D$

displaced silicon atoms : 15 to $10D$.

The results apply to the low dose region where the rate of replacement collisions is negligible. The most serious error is probably the specification of the neutron dose which may lead to an uncertainty of 50% in the above values. For the given spectrum, however, the maximum and minimum estimates of defect concentrations are unexpectedly close.

4.4. *Remarks on the Nature of the C and E Bands*

Both the C and E bands increase with neutron dose, indicating that these bands are associated with atomic defects since an increase is not observed with x-irradiation. The C band can be optically bleached so that the observed transition must be due to a trapped electron or hole, and not to electrons normally in the neighbourhood of the defect. It is assumed that the trapped charge originates from the E defect, which then gives rise to the E band. The optical bleaching of the C band, which occurs even in synthetic crystals, is attributed to the release of charge trapped at C and the recombination of this charge with that trapped at E.

The initial rapid and preferential optical and thermal bleaching of the C band was found only in neutron irradiated crystals. This bleaching probably occurs when the recombination can take place without intermediate retrapping, such as would be expected when C and E centres are close enough together. It is also required that the mean separation for which this process is possible should lead to a modification of the energy levels of the C centre so as to give an absorption maximum at 5·4 ev. If this explanation is correct a larger effect would be expected, and possibly a 5·4 ev peak would be observed, in specimens irradiated with electrons of energy near to the threshold for atomic displacements, thus favouring the production of close pairs.

In specimens in which A bands are present, illuminating with C light leads to bleaching of both C and A bands. Charge is therefore being released from the C centres, being recaptured by the A centres thereby neutralizing both. Since, following the O'Brien–Pryce model, an electron is required to bleach the A centre we assume that the C defect gives rise to the C band after trapping an electron. (There is always some absorption in the C region arising from the low energy tail of the D band. However, the possibility that the D centre is complementary to A is ruled out by the fact that increasing the D band wavelength range content of the bleaching light does not increase the bleaching rate of A.)

The conclusion is that the C defect gives rise to the C band after trapping an electron and that the E defect leads to the E band after trapping a hole.

Following the results of heat treatment before irradiation, which indicated the presence of silicon vacancies in unirradiated crystals, we consider that the E defect is not a silicon vacancy since the E band is not induced in crystalline quartz by ionizing radiation alone. Further, on the grounds that the close complementary defects, suggested for the explanation of the rapid preferential bleaching, probably correspond to either oxygen interstitial–vacancy pairs or silicon interstitial–vacancy pairs we reject the possibility that the C defect is an interstitial silicon atom.

Whether a given defect traps an electron or a hole depends to some extent on the nature of the binding in quartz. If it were ionic the simplest electron traps are O^{-2} vacancies or interstitial Si^{+4}. Having already rejected the latter this leads to the conclusion that the C centre is an electron trapped at an O^{-2} vacancy, and the E centre an electron missing from an interstitial O^{-2}. The properties of quartz—for example, the high infra-red absorption and the large magneto-optic anomaly, suggest that the binding is mainly ionic. Although the net charge on each ion may not be $+4$ or -2, the traps will trap the same sign of charge carrier as above, in which case the C and E defects are associated with displaced oxygen ions.

Taking the concentrations of these displacements as $\gtrsim 25D$ we then find for the C and E defects using (6) and (7) —$f_c x_c \gtrapprox 0{\cdot}05$, $f_E x_E \gtrsim 0{\cdot}2$ Since x_c and x_E cannot be greater than 1 the lower limits to the f values are 0·05 and 0·2 respectively.

4.5. *Defects in Unirradiated Crystals*

The relation between the C and A absorption is still not certain. One possibility is that in the unirradiated crystal the charge on two aluminium centres is balanced by an oxygen ion vacancy. This would provide an explanation of the observation in I (1954) that, for low neutron doses, the absorption in both C and A bands varied with Al concentration. In addition, since this mechanism gives a concentration of oxygen vacancies related to the substitutional Al content and taking into account the overlap of the D band in the C band region, a relation of the form (10) above may be obtained. Against the explanation, however, is the fact that if true it has to be assumed that oxygen vacancies can be generated at 950°c in order to account for $\mu_c\,\mathrm{III} > \mu_c\,\mathrm{II}$ in fig. 14—an assumption which is unlikely in view of the insulating properties of quartz. Further work is required.

Both the A_2 and C bands are broad and they do not become narrower on cooling to the temperature of liquid air which suggests that in both cases the transitions are between localized levels and one of the energy bands of the solid. Concerning the A_2 band it is probable that only the non-bonding orbitals of the oxygen ions of the aluminium defect are in the forbidden energy gap. If the valence band corresponds to electrons spending most of their time on oxygen ions the upper valence band will correspond to non-bonding electrons having orbitals of the type p_x and sp_z. There will be an allowed transition from this band to the p_x level of the aluminium centre thereby giving a wide absorption band (A_2) having the s–p_x anisotropy found by Mitchell and Paige (1955).

The small optical bleaching in the A_2 band (table 1) suggests that the rate at which holes can move through the upper valence band is low. On the other hand the rapid bleaching associated with absorption in the *C* band indicates, independently of the conclusion in § 4.1, that this absorption corresponds to excitation of an electron from the centre—the excitation being to the conduction band thereby giving the wide and temperature independent absorption which is observed.

§ 5. CONCLUSIONS

Two of the types of point defect produced by the neutron irradiation of quartz have been found to give optical absorption bands in the spectral range 1·2 to 8·5 ev. One of the bands (*C*—5·7 ev) has been shown to be associated with an electron trapped at the defect, while indirect experiments suggest that the other (*E*—7·6 ev) arises when a positive hole is trapped at the second defect. The bands occur at about the same energies in fused quartz indicating that the energy of the transition is determined by the short range atomic arrangement.

The existence of more extensive regions of damage following neutron irradiation is suggested by the shift of the absorption edge in crystalline quartz to the absorption limit which is found in unirradiated fused quartz. The latter limit is not changed by irradiation. In these regions the structure is considered to be amorphous, the phase change occurring as a result of local melting.

There is some evidence that the defects responsible for the *C* and *E* bands are oxygen vacancies and interstitial oxygen ions respectively.

An attempt has been made to put upper and lower limits on the concentration of point defects by a collision theory calculation and from the results the lower limits to the *f* values have been found to be 0·05 (*C*) and 0·2 (*E*).

It is found that all the neutron induced damage may be annealed by heating at 950°c.

ACKNOWLEDGMENTS

The authors wish to thank Professor R. W. Ditchburn for placing a vacuum spectrograph at their disposal and Mr. L. A. Thomas and Mr. C. S. Brown of the G.E.C. Research Laboratories, Wembley, for discussions about quartz and for providing some specimens. They are also grateful to Professor Ditchburn, Dr. R. J. Elliot and Dr. K. Robinson for their comments on the paper. One of us (E. G. S. P.) wishes to acknowledge the receipt of a D.S.I.R. maintenance grant.

References

BERMAN, R., 1951, *Proc. Roy. Soc.* A, **208,** 90.
BOHR, N., 1948, *Dan. Mat. Fys. Medd.*, **18,** No. 8.
BRINKMAN, J. A., 1954, *J. Appl. Phys.*, **25,** 961.
CARIO, G., and SCHMIDT-OTT, H. D., 1931, *Z. Phys.*, **69,** 719.
CHOONG, S. P., 1945, *Proc. Phys. Soc.*, **57,** 49.
CLARK, C. D., DITCHBURN, R. W., and DYER, H. B., 1956, *Proc. Roy. Soc.* A, **234,** 363.
COHEN, A. J., 1955, *Amer. Phys. Soc. Bull.*, **30,** No. 4, 8; *J. Chem. Phys.*, **23,** 765.
DITCHBURN, R. W., and HEDDLE, D. W. O., 1953, *Proc. Roy. Soc.* A, **220,** 61.
DITCHBURN, R. W., MITCHELL, E. W. J., PAIGE, E. G. S., CUSTERS, J. F. H., DYER, H. B., and CLARK, C. D., 1954, *Report of Bristol Conference on Defects in Crystalline Solids* (London: Physical Society).
FORMAN, C., 1951, *J. Opt. Soc. Amer.*, **41,** 377.
GRIFFITHS, J. H. E., OWEN, J., and WARD, J. M., 1954, *Report of Bristol Conference on the Defects in Crystalline Solids* (London: Physical Society).
HEDDLE, D. W. O., 1952, *Ph.D. Thesis*, University of Reading.
JOHNSON, B. K., 1941, *Proc. Phys. Soc.*, **53,** 258.
JOHNSON, P. D., and WILLIAMS, F. E., 1953, *J. Chem. Phys.*, **21,** 125.
KINCHIN, G. H., and PEASE, R. S., 1955, *Rep. Prog. Phys.*, **18,** 1.
LAMB, W. E., 1940, *Phys. Rev.*, **58,** 696.
LEVY, M., and VARLEY, J. H. O., 1955, *Proc. Phys. Soc.* B, **68,** 223.
LEVY, P. W., 1955, *J. Chem. Phys.*, **23,** 764.
MITCHELL, E. W. J., and PAIGE, E. G. S., 1955, *Phil. Mag.*, **46,** 1353.
MOTT, N. F., and MASSEY, H. S. W., 1949 *The Theory of Atomic Collisions*, 2nd ed. (Oxford: University Press).
O'BRIEN, M. C. M., 1955, *Proc. Roy. Soc.* A, **231,** 404.
O'BRIEN, M. C. M., and PRYCE, M. H. L., 1954, *Report of Bristol Conference on Defects in Crystalline Solids* (London: Physical Society).
OVERHAUSER, A. W., 1953, *Phys. Rev.*, **90,** 393.
SEITZ, F., 1949, *Disc. Faraday Soc.*, **5,** 271; 1954, *Rev. Mod. Phys.*, **26,** 7.
SNYDER, W. S., and NEUFELD, J., 1954, *Phys. Rev.*, **94,** 760.
STEPHENS, K. G., and WALKER, D., 1955, *Proc. Roy. Soc.* A, **229,** 376.
VOLGER, J., STEVELS, J. M., and VAN AMERONGEN, C., 1955, *Phil. Res. Rep.*, **10,** 260.
WEEKS, R. A., 1956, *Amer. Phys. Soc. Bull.*, Ser. II, **1,** No. 1, 12.
WITTELS, M., 1953, *Phys. Rev.*, **89,** 656.
WITTELS, M., and SHERRILL, F. A., 1954, *Phys. Rev.*, **93,** 1117.
YOKOTA, R., 1952, *J. Phys. Soc. Japan*, **7,** 316.

CXII. *Radiative Capture of Protons of less than* 1 MEV *in Beryllium*

By A. B. CLEGG †
Cavendish Laboratory, Cambridge ‡

[Received March 19, 1956]

§ 1. INTRODUCTION

THE radiative capture of protons of less than 1 MEV in beryllium has been studied by a number of authors (see Ajzenberg and Lauritsen 1955, Lönsjö *et al.* 1955, Carlson and Nelson 1955); there is some disagreement on the number of resonances involved. This paper describes some investigations of the gamma-rays produced by the radiative capture of protons in beryllium, which show that their yield for protons of less than 1 MEV is due to two broad resonances; any other resonances are weak. One of these resonances, at 995 kev, is well known (Fowler *et al.* 1948, Hornyak and Coor 1953); the gamma-radiation from the other, at 330 kev, has been investigated in detail in the present work.

§ 2. EXCITATION FUNCTIONS

The excitation function of the gamma-rays produced has been investigated at different times in the course of this work. The detector has usually been a $1\frac{1}{2}$ in. long × $1\frac{1}{2}$ in. diameter sodium iodide crystal attached to an EMI photomultiplier type 6262. The target, of beryllium metal evaporated onto a copper backing, was bombarded with protons from the Cavendish Laboratory two million volt H.T. set. With the detector bias set so that pulses corresponding to electron energies of greater than 3 MEV in the crystal were counted, the only resonances that were seen were the well known broad resonance at 995 kev, the well known narrow resonance at 1086 kev and a resonance at 330 kev with a width of approximately 160 kev, corresponding to a state of ^{10}B at 6·88 MEV, together with weak resonances of variable yield due to the ^{19}F(p, α, γ) reaction, produced in fluorine contamination in the beryllium and on beam-collimating stops. A typical excitation function over the lower resonance is shown in fig. 1, taken with a target of thickness 10 kev (for protons of 1 MEV). (The high points at 340, 480 kev are due to the ^{19}F(p, α, γ) reaction.) This shows well the resonance at 330 kev, while at higher proton energies the yield is rising towards the 995 kev resonance. This and similar excitation functions are quite comparable with the results of Tangen (Tangen 1946, Lönsjö *et al.* 1955) but disagree with Hunt (1952).

---

† Communicated by Dr. D. H. Wilkinson, F.R.S.
‡ Present address: California Institute of Technology.

§ 3. GAMMA-RADIATION FROM THE 330 KEV RESONANCE

The gamma-radiation from the 330 kev resonance has been examined in detail, using a sodium iodide crystal spectrometer described in § 2. A typical pulse-height spectrum produced by the high energy gamma-rays is shown in fig. 2. Marked on it are the positions of the peaks that would be produced by gamma-rays emitted to each of the first few states of ^{10}B. Six distinct peaks are definitely seen in the spectrum. Peaks A and B are the total energy peaks of gamma-rays of 1·7, 2·15 MEV which were examined in more detail in the low energy spectra. The simplest assignment of peaks C, D, E, F is to assume that they are the two- and one-quantum escape peaks due to gamma-ray transitions to states of ^{10}B at 0·72, 1·74 MEV. This was checked by observing the pulse-height spectra with two different crystals: (i) the $1\frac{1}{2}$ in. long × $1\frac{1}{2}$ in. diameter cylinder already referred to and (ii) a 1 in. cube (both systems having similar resolutions). As was expected, peaks C and E were relatively higher with the smaller crystal, confirming the assignment of these peaks. This spectrum also gives evidence for two more gamma-rays. The bump at G appears consistently and could be due to the two-quantum escape peak of a gamma-ray emitted to the 2·15 MEV state of ^{10}B; this gamma-ray is confirmed by the observation of low energy gamma-rays de-exciting this state. The high energy tail can be compared with the high energy tail of a 6·14 MEV gamma-ray produced by the 340 kev resonance in the reaction $^{19}F(p, \alpha, \gamma)$. It is certain that there are more high energy pulses present than can be due to a 6·14 MEV gamma-ray; they are quite consistent with a weak transition to the ground state of ^{10}B. These results are consistent with those of Carlson and Nelson (1955).

Fig. 1

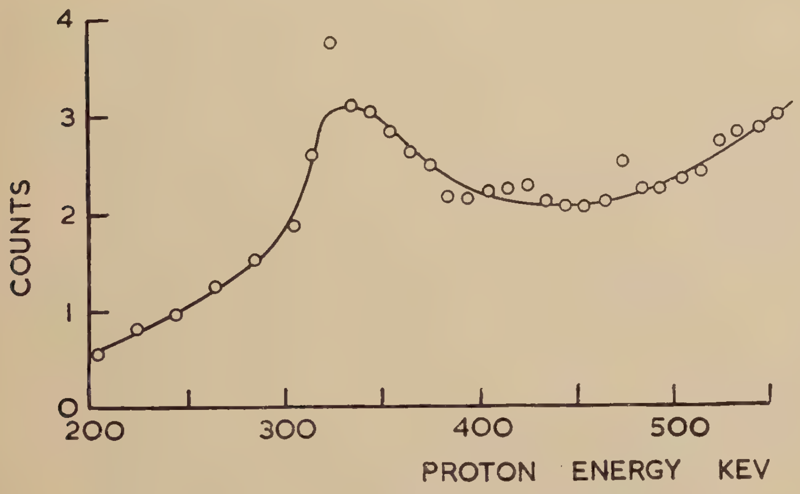

Gamma-ray excitation function in the reaction $^{9}Be(p, \gamma)^{10}B$.

A general pulse-height spectrum showing the low energy gamma-rays is shown in fig. 3 ; it contains evidence for gamma-rays of 0·72, 1·02, 1·43, 1·7, 2·15 MeV. Different parts of this spectrum have been examined in detail and all these gamma-rays have been seen consistently, together with a weak gamma-ray of 0·42 MeV which is not resolved in fig. 3. Using results from the ^{9}Be(d, n, γ) reaction (Rasmussen *et al.* 1949, Shafroth and Hanna 1954) all these gamma-rays can be fitted in as transitions between low states of ^{10}B (except for the 1·7 MeV gamma-rays which are discussed in § 4) as shown here :

Gamma-ray energy (MeV)		0·420 ±0·004	0·731 ±0·008	1·018 ±0·007	1·426 ±0·021	2·176 ±0·020
Assignment	from state (MeV)	2·15	0·72	1·74	2·15	2·15
	to state (MeV)	1·74	0	0·72	0·72	0
Relative intensity		0·045	1·00	0·76	0·043	0·062

The energies and relative intensities are obtained by comparison with pulse-height spectra from known gamma-rays, interleaved with the ^{9}Be(p, γ) runs, knowing the stopping cross section of sodium iodide. The relative intensities are thought to be accurate to ±25%.

Two experiments were done to check that the transitions to the first three excited states of ^{10}B come from the same resonance (evidence is given in § 5 for thinking that the ground state transition is not resonant at 330 kev but is due to the tail of the 995 kev resonance). First the high energy gamma-rays were examined at four different proton energies ranging from 225 kev to 320 kev. No difference could be seen in the pulse-height spectra, implying that if there was a change in the relative intensity of the 5·1 and 6·1 MeV gamma-rays it was distinctly less than 10%. Similarly six runs were done at four proton energies ranging from 245 kev to 330 kev with the total energy peaks of the 0·42 and 0·72 MeV gamma-rays displayed on the kicksorter. By comparing the areas of the total energy peaks it was shown that any change in their relative intensity was distinctly less than 10%. These two measurements show that there is no large change in the relative intensities of the 4·7, 5·1 and 6·1 MeV gamma-rays over quite a large range of proton energy, implying that all these three transitions come from the same state of ^{10}B.

The high energy gamma-rays were also examined at proton energies at approximately 20–30 kev intervals between 250 and 550 kev. It was found that each pulse-height spectrum was made up of the addition of two pulse-height spectra in varying amounts ; (*a*) the pulse-height spectrum shown in fig. 2, (*b*) the pulse height spectrum from a nearly pure transition to the ground state of ^{10}B. As the proton energy is increased, spectrum (*a*) decreases in intensity while spectrum (*b*) increases. We can estimate what proportion of the pulses in each spectrum corresponds to spectrum (*a*) and so correct the observed total excitation function to obtain the excitation function of the gamma-rays corresponding to spectrum (*a*). Such a corrected excitation function is shown in fig. 4, where the continuous line gives the observed total excitation function while the points are the estimates of the excitation function of the gamma-rays corresponding to spectrum (*a*).

Thus it seems definite that the transitions to the first three excited states of ^{10}B are all due to the same resonance of the ^{9}Be(p, γ) reaction.

Fig. 2

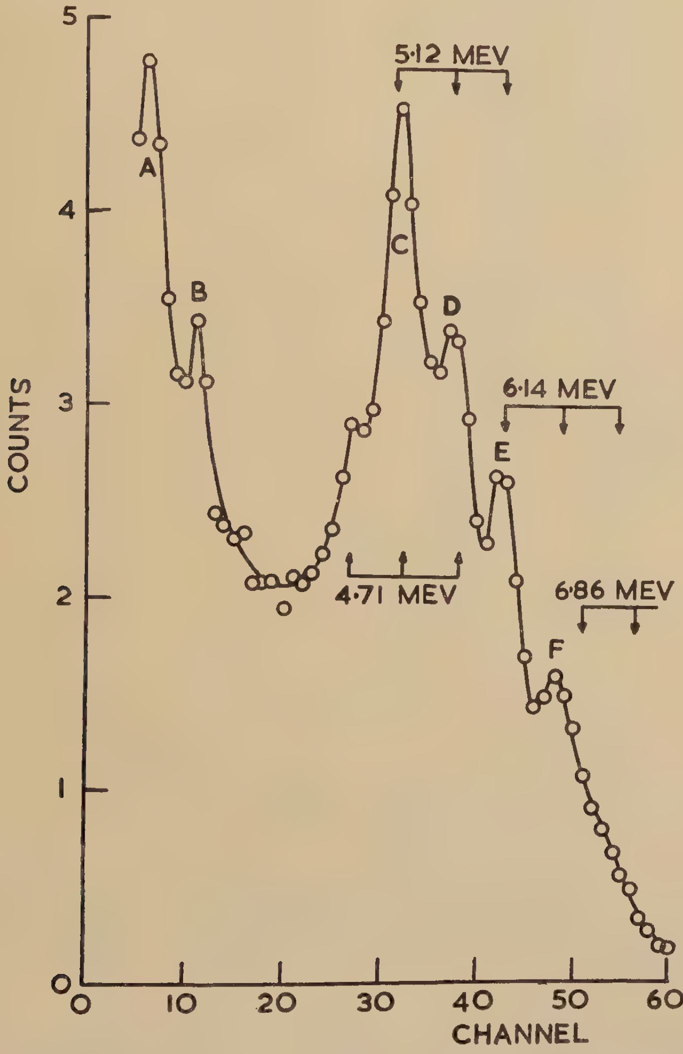

Pulse-height spectrum of high energy gamma-rays from the reaction ^{9}Be(p, γ)^{10}B at a proton bombarding energy of 310 kev.

§ 4. The 1·7 Mev Gamma-Ray

It remains to fit the 1·74 Mev gamma-ray (which has an intensity of 0·15 of the intensity of the 0·72 Mev gamma-ray) into the decay scheme. It cannot be fitted in as a transition from the 1·74 Mev state to the ground state of ^{10}Be as this would imply a magnetic octupole transition, which has definitely not been seen in the reaction ^{9}Be(d, n, γ) (Rasmussen *et al.* 1949, Shafroth and Hanna 1954). So we consider that it is a transition from the capture state to one of the states of ^{10}B at 5·11, 5·16 Mev, checking this by measuring its energy for different proton bombarding

Fig. 3

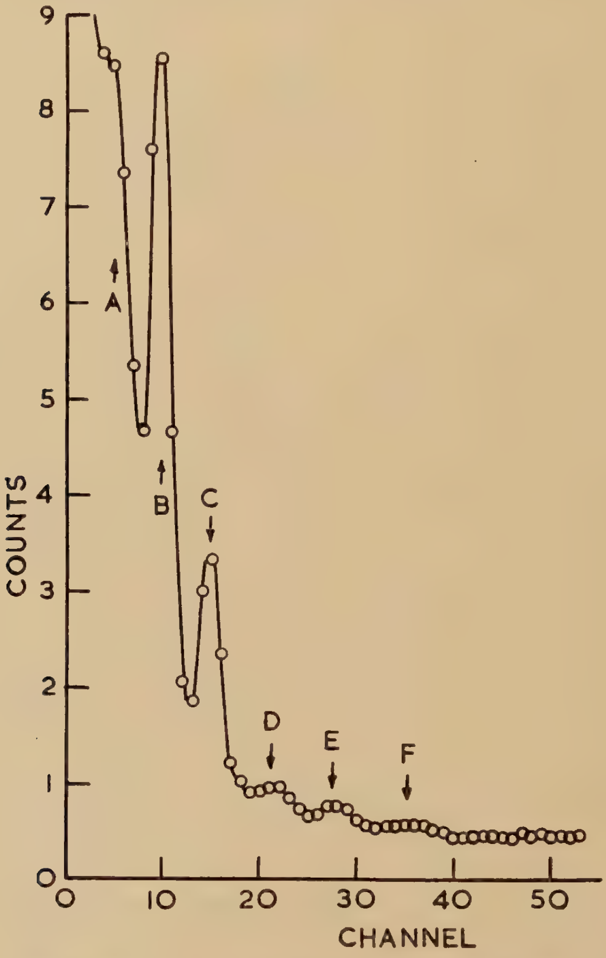

Pulse-height spectrum of low energy gamma-rays from the reaction ^{9}Be(p, γ)^{10}B at a proton bombarding energy of 310 kev. The arrows A, B, C, D, E, F show the expected positions of photopeaks corresponding to gamma-rays of 0·41, 0·72, 1·02, 1·43, 1·74 and 2·15 Mev respectively.

energies. Seven runs were made, with the total energy peaks of the 1·43 1·7, 2·15 MeV gamma-rays displayed on the kicksorter, at proton energies ranging from 245 kev to 374 kev, the runs being interleaved with radiothorium calibration runs. It was obvious that, as the proton energy changed, the 1·7 MeV peak moved with respect to the 1·43, 2·15 MeV peaks so this was checked quantitatively by calculating the gamma-ray energy from each run by comparison with the 1·592 MeV two-quantum escape peak of the 2·614 MeV gamma-ray in the decay of ^{208}Tl. A least squares analysis, assuming $E\gamma = a + bE_p$, gave :

Fig. 4

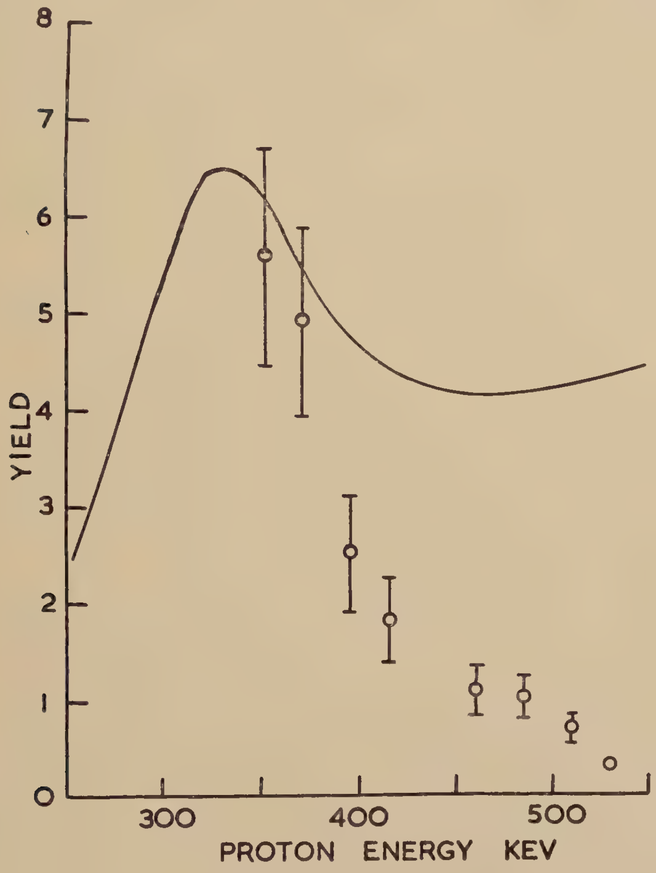

Excitation function of 4·7, 5·1 and 6·1 MeV gamma-rays in the reaction ^{9}Be(p, γ)^{10}B. The full line is the excitation function for gamma-rays of all energy in the same reaction.

$$E\gamma = (1{\cdot}486 \pm 0{\cdot}054) + (0{\cdot}893 \pm 0{\cdot}174) E_p \text{ MeV}$$

confirming that this gamma-ray is emitted by the capture state. Then assuming $E\gamma = A + 0{\cdot}9E_p$ MeV, from all measurements on this energy of this gamma-ray we find :

$$A = 1{\cdot}473 \pm 0{\cdot}010 \text{ MeV.}$$

Then from the Q-values of the reactions ^{9}Be(p, α)^{6}Li, ^{10}B(n, α)^{7}Li, ^{6}Li(d, p)^{7}Li and the binding energy of the deuteron (taken from Li *et al.* 1951, Ajzenberg and Lauritsen 1955) we find :

$$(^{9}\text{Be}+\text{p}-{}^{10}\text{B})=6{\cdot}587\pm0{\cdot}012 \text{ MeV}$$

so that the 1·7 MeV gamma-ray corresponds to a transition to a state of ^{10}B at 5·114±0·016 MeV which agrees very well with the state reported at 5·111±0·005 MeV and is in definite disagreement with the next state at an energy of 5·163±0·005 MeV (Jones and Wilkinson 1954).

It was also noted that the intensity of the 1·7 MeV gamma-ray relative to the intensities of the 1·43, 2·15 MeV gamma-rays did not change with proton energy, showing that it came from the same state of ^{10}B as the 4·7, 5·1, 6·1 MeV gamma-rays.

Both from the high energy and low energy spectra it was possible to obtain the relative intensities of the gamma-rays emitted by the 6·88 MeV state :

Transition to state of ^{10}B at (MeV)	0·72	1·74	2·15	5·11
Relative intensity	40	100	20	25

§ 5. GROUND STATE TRANSITION

As mentioned above the ground state transition observed at 310 kev is believed to be due to the tail of the 995 kev resonance, which is well known to emit gamma-rays mainly to the ground state of ^{10}B, and not due to the 330 kev resonance. This is based on three pieces of evidence :

(i) The excitation functions and the spectra in the proton energy region 350–550 kev reported in § 3 which show that the tail of the 993 kev resonance merges into the 330 kev resonance.

(ii) The observations of Lönsjö *et al.* (1955) that an excitation function, with the bias cut out to correspond to 5·6 MeV excitation energy in the crystal so that very few pulses due to 4·7, 5·1, 6·1 MeV gamma-rays would be recorded, shows very little indeed of the 330 kev resonance.

(iii) It is possible to calculate the yield of the ground state transition that would be expected at 330 kev due to the 995 kev resonance. This was done using both a simple resonance denominator and the full single level Breit–Wigner formula, taking the penetrabilities for a standard interaction radius of 1·45 $(A_1^{1/3}+A_2^{1/3})\times10^{13}$ cm from tables of Coulomb wave functions. These two estimates only differ by a factor of two at 330 kev and give roughly the intensity of the ground state transition observed ; this was found using the excitation functions described in § 6, knowing the relative intensity of the ground state transition at 330 kev.

§ 6. RADIATIVE WIDTH

The radiative width was found by a comparison of the yield of the 330 kev resonance with that of the 995 kev resonance. To do this we used a thick walled brass Geiger counter of the type described by Barnes *et al.*

(1952) with a sensitivity proportional to gamma-ray energy. Using this as detector excitation functions were run over both resonances so obtaining the relative yield of the two resonances. Then, assuming for the 995 kev resonance $\Gamma\gamma=23$ ev (Hornyak and Coor 1953) we get for the 330 kev resonance :

assuming small value of proton width : $\Gamma\gamma=4\cdot8$ ev
assuming large value of proton width : $\Gamma\gamma=1\cdot0$ ev.

We favour the value $\Gamma\gamma=4\cdot8$ ev as this gives better agreement with the theoretical value of the radiative width for the transition to the 1·74 MEV state. (Then the radiative width is uncertain to a factor of two, principally due to uncertainties in the proton width.) This gives for the partial radiative widths :

Transition to state of ^{10}B at (MEV)	0·72	1·74	2·15	5·11
$\Gamma\gamma$ (ev)	1·0	2·6	0·52	0·65

§ 7. ANGULAR DISTRIBUTIONS

The angular distributions of the transitions to the 0·72 and 1·74 MEV states were studied. The theoretical angular distributions considered are (capture states 0, 2, 3+ are ignored because of the strength of the transition to the 0+ state at 1·74 MEV) :

Angular momentum of protons	Capture state (spin, parity)	To state of spin	Angular distribution
s–wave	1, 2–	0, 1	isotropic
p–wave	1+	0	$1+1/10\times\frac{5-a}{1+a}P_2(\cos\theta)$
p–wave	1+	1	$1+1/20\times\frac{a-5}{a+1}P_2(\cos\theta)$

a is the proportion of the compound nucleus formed by channel spin=2 to that formed by channel spin=1. Writing the p-wave angular distributions $1+AP_2\cos\theta$ we see that A has opposite signs for the gamma-rays to the 0·72, 1·74 MEV states so that there is a possibility of seeing a change in the relative intensity of these two gamma-rays with angle.

The crystal and photomultiplier were mounted with the front face of the crystal 4 in. from the beryllium target so that it could be rotated to different angles with respect to the proton beam. Another crystal, $2\frac{1}{2}$ in. long × $1\frac{3}{4}$ in. diameter, was mounted with its front face 1 in. from the target to monitor the gamma-ray yield. The isotropy of this set up was checked by observing the angular distribution of the gamma-rays from the 340 kev resonance of the ^{19}F(p, α, γ) reaction, a fluorine target replacing the beryllium target. When measuring the angular distribution of the ^{10}B gamma-rays the pulses from the movable detector corresponding to electron energies in the crystal from 1·3 to 6·8 MeV were displayed on a kicksorter. Eight runs were made spread over five angles : 0°, 30°, 45°, 60°, 90° ; in each case the pulse-height spectrum and the number of counts were recorded. The spectra showed no obvious variation in the relative intensity of the gamma-rays with angle so a more careful comparison was made. Each spectrum was split into six regions of pulse-height : four being equally spaced about peaks C, D, E, F in fig. 2, the fifth covering the high energy pulses, and the sixth covering the trough between peaks B and C. The angular distribution of the number of counts in each region divided by the corresponding number of monitor counts was then studied and they were all found to be individually isotropic. From these results it was possible to say that if the angular distributions of the 5·1, 6·1 MeV gamma-rays were of the form $1+a\cos^2\theta$, then for each of them :

$$|a|\leqslant 0{\cdot}025.$$

Also no departure from isotropy was seen for the 1·7, 4·7 MeV gamma-rays but no good limit could be put on their departures from isotropy.

From these results either of two conclusions is possible for the 6·88 MeV state of ^{10}B :

either (i) s-wave protons forming a state of 1, 2−
or (ii) p-wave protons forming a state of 1+, $4{\cdot}2\leqslant a\leqslant 6{\cdot}3$.

§ 8. Conclusions

If we assume that the 330 kev resonance in the ^{9}Be(p, γ) reaction is the same as the 330 kev resonance in the ^{9}Be(p, α) and ^{9}Be(p, d) reactions (Thomas *et al.* 1949) which is probable as the widths are the same, then the first of the two conclusions at the end of § 7 is the more probable as the second conclusion seems to lead to a value of the reduced proton width which is too large. If s-wave protons are assumed the comparatively large radiative width for the transition to the 0+ state makes an assignment of 1− for the 6·88 MeV state necessary. Then the large deuteron reduced width makes a $T=0$ assignment to the 6·88 MeV state follow. If this is so the transitions to the 1+, $T=0$ states at 0·72, 1·74 MeV should be forbidden by the isotopic spin selection rules on electric dipole transitions in self conjugate nuclei, contrary to what is observed. This failure of these rules implies a $T=1$ impurity in the 6·88 MeV state of approximately 20% in intensity, which is distinctly larger than any other such impurity in a light nucleus. This is discussed in detail in a further paper (Wilkinson and Clegg 1956).

Acknowledgment

I should like to thank Dr. D. H. Wilkinson for his encouragement of this investigation.

REFERENCES

AJZENBERG, F., and LAURITSEN, T., 1955, *Rev. Mod. Phys.*, **27,** 77.

BARNES, C. A., CARVER, J. H., STAFFORD, G. H., and WILKINSON, D. H., 1952, *Phys. Rev.*, **86,** 359.

CARLSON, R. R., and NELSON, E. B., 1955, *Phys. Rev.*, **98,** 1310.

FOWLER, W. A., LAURITSEN, C. C., and LAURITSEN, T., 1948, *Rev. Mod. Phys.*, **92,** 675.

HORNYAK, W. F., and COOR, T., 1953, *Phys. Rev.*, **92,** 675.

HUNT, S. E., 1952, *Phys. Rev.*, **87,** 902.

JONES, G. A., and WILKINSON, D. H., 1954, *Phil. Mag.*, **45,** 703.

LI, C. W., WHALING, W., FOWLER, W. A., and LAURITSEN, C. C., 1951, *Phys. Rev.*, **83,** 512.

LÖNSJÖ, O., OS, O., and TANGEN, R., 1955, *Phys. Rev.*, **98,** 727.

RASMUSSEN, V. K., HORNYAK, W. F., and LAURITSEN, T., 1949, *Phys. Rev.*, **76,** 581.

SHAFROTH, S. M., and HANNA, S. S., 1954, *Phys. Rev.*, **95,** 86.

TANGEN, R., 1946, *K. norske vidensk. Selsk. Aarsberetn.*, Skr. No. 1.

THOMAS, R. G., RUBIN, S., FOWLER, W. A., and LAURITSEN, C. C., 1949, *Phys. Rev.*, **75,** 1012.

WILKINSON, D. H., and CLEGG, A. B., 1956, *Phil. Mag.* (in the press).

CXIII. *On the Coupling between Two Cavities*

By R. N. Gould and A. Cunliffe
The University, Hull†

[Received January 22, 1956]

Summary

C and C′ are two electromagnetic cavity resonators which communicate with each other through an iris. The present note describes a general method of calculating the electric and magnetic field configurations and the associated eigenvalues of this compound system, in terms of certain orthogonal functions of the separate cavities C and C′ formed when the iris is closed by a thin partition.

§ 1. Introduction

A problem which frequently arises with cavity resonators is the calculation of the effect on the resonant frequency and Q value of the operating mode caused by subsidiary cavities which connect with the main resonator. Recesses may be introduced into the cavity walls for the purpose of reducing the effects of unwanted modes, or the method of introducing or extracting energy from the cavity may require the addition of side tubes to accommodate the coupling elements ; such recesses or side tubes may be regarded as small cavities which are coupled to the main cavity. Another example is the case of a cavity coupled through a slot or iris to a waveguide circuit of low loss which effectively acts as a second cavity. Some of these cases have been treated by a boundary perturbation method (Slater 1950), or by the method of Hahn (Hahn

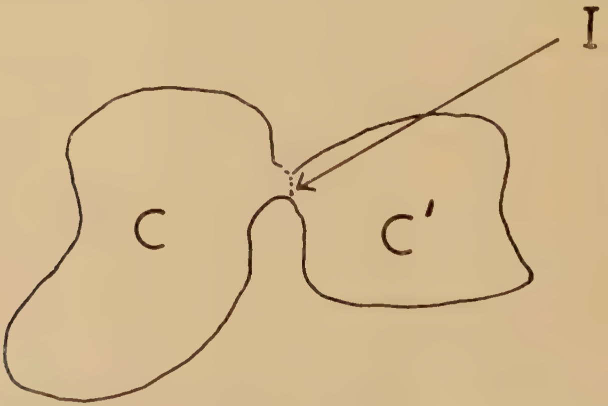

---

† Communicated by the Authors.

1941). This note describes a method for treating the general problem of two cavities coupled by an iris as in the figure.

§ 2. THEORY

Consider the separate cavity C formed when the iris I of the figure is closed by a thin perfectly conducting partition. The cavity then has completely enclosing walls which will be assumed to be perfectly conducting. It will further be assumed that it is filled with a uniform isotropic medium of permittivity ϵ and permeability μ. If the electric field is written as $e/\sqrt{\epsilon}\sin\sqrt{(k/\epsilon\mu)}t$ and the magnetic field as

$$h/\sqrt{\mu}\cos\sqrt{(k/\epsilon\mu)}t,$$

where t denotes time, then the electromagnetic field equations and the boundary conditions require that

$$\nabla\times e=\sqrt{(k)}h, \qquad \nabla\times h=\sqrt{(k)}e \quad . \quad . \quad . \quad . \quad . \quad . \quad (1)$$

within the cavity and,

$$e\times ds=0=h\;.\;ds \quad . \quad . \quad . \quad . \quad . \quad . \quad . \quad . \quad (2)$$

at the cavity wall S. The solution of these equations gives rise to an infinite set of eigenfunctions e_i, h_i, and eigenvalues k_i. e_i and h_i determine the electric and magnetic field configurations, and can be chosen so that

$$\int_C e_i\;.\;e_j\,d\tau=\delta_{ij}=\int_C h_i\;.\;h_i\,d\tau \quad . \quad . \quad . \quad . \quad . \quad . \quad (3)$$

where $d\tau$ is an element of volume and the integrals are taken throughout the whole volume C of the cavity. The frequency of oscillation f_i of the i'th mode is given by

$$f_i=\frac{\sqrt{(k_i/\epsilon\mu)}}{2\pi} \quad . \quad . \quad . \quad . \quad . \quad . \quad . \quad . \quad . \quad . \quad (4)$$

Let e_i', h_i', and k_i', similarly be eigenfunctions and eigenvalues for cavity C′. Let E, H and K similarly refer to the compound cavity formed when the partition is removed. The compound cavity is assumed to be filled with a uniform isotropic medium of permittivity ϵ and permeability μ. Everywhere within the compound cavity

$$\nabla\times E=\sqrt{(K)}H, \qquad \nabla\times H=\sqrt{(K)}E \quad . \quad . \quad . \quad . \quad (5)$$

and at the walls

$$E\times ds=0=H\;.\;ds. \quad . \quad . \quad . \quad . \quad . \quad . \quad . \quad . \quad (6)$$

Suppose that throughout the volume of cavity C, ψ_i satisfies the wave equation $\nabla^2\psi_i=\lambda_i\psi_i$ and the condition $\nabla\psi_i\;.\;ds=0$ on its boundary. The ψ_i's are assumed to form a complete set of scalar functions in terms of which an arbitrary function of position throughout C may be expanded. If it is further assumed that such an expansion represents the function on the boundary of the cavity C as well as throughout its volume, then it can be shown that the gradient of a scalar function of position throughout C may be expanded in terms of the gradients of the functions ψ_i. The ψ_i's may be chosen to satisfy orthonormal relations $\int_C\psi_i\psi_j\,d\tau=\delta_{ij}$, in which case the functions $g_i=\sqrt{-1}/\sqrt{\lambda_i}\,.\,\nabla\psi_i$ satisfy similar relations ${}_{\mathrm{C}}\, g_i \,.\, g_j\, d\tau=\delta_{ij}$. The set ψ_i includes a constant term for which the corresponding g is to be taken to be zero. It can be shown (Slater 1950) that the g_i's are orthogonal to the h_i's. That is, $\int_{\mathrm{C}} h_i \,.\, g_j\, d\tau=0$. Let ψ_i' and g_i' be defined for cavity C′ in a similar way to ψ_i and g_i for cavity C. It can be shown (Teichmann 1953) that within the region C of the compound cavity, H can be expressed in the form

$$H=\sum_i \alpha_i h_i+\nabla u \quad . \quad . \quad . \quad . \quad . \quad . \quad . \quad . \quad (7)$$

where u is a scalar function of position. Expanding ∇u in terms of the functions g_i, eqn. (7) becomes

$$H=\sum_i \alpha_i h_i+\sum_i \beta_i g_i \quad . \quad . \quad . \quad . \quad . \quad . \quad . \quad . \quad (8)$$

where, as the functions h_i, g_j are orthonormal, $\beta_i=\int_{\mathrm{C}} g_i \,.\, H\, d\tau$ which can be put in the form $\int_S E\times g_i \,.\, ds/\sqrt{K}$, the final integration being carried out over the surface of the cavity C. Since $E\times ds$ vanishes on the walls of the compound cavity the integral need only be taken over the iris I, and thus $\beta_i=\int_{\mathrm{I}} E\times g_i \,.\, ds/\sqrt{K}$. The α_i's can be expressed

$$\alpha_i=\sqrt{(K)}\int_{\mathrm{I}} E\times h_i \,.\, ds/K-k_i$$

(Slater 1950). Equation (8) now becomes

$$H=\sum_i\left\{\left(\sqrt{(K)}\int_{\mathrm{I}}\frac{E\times h_i \,.\, ds}{K-k_i}\right)h_i+\left(\int_{\mathrm{I}}\frac{E\times g_i \,.\, ds}{\sqrt{K}}\right)g_i\right\} \quad . \quad . \quad (9)$$

ds is in the direction of the outward normal to cavity C. A similar expression for H can be derived in terms of the functions h_i' and g_i', namely

$$H=-\sum_i\left\{\left(\sqrt{(K)}\int_{\mathrm{I}}\frac{E\times h_i' \,.\, ds}{K-k_i'}\right)h_i'+\left(\int_{\mathrm{I}}\frac{E\times g_i' \,.\, ds}{\sqrt{K}}\right)g_i'\right\} \quad . \quad (10)$$

where the negative sign appears because ds is in the direction of the inward normal to cavity C′. Equations (9) and (10) are assumed to give the correct tangential component of H on I. To find the perturbed eigenvalues, it is now necessary to match the tangential components of E and H over I. Everywhere on I,

$$\sum_i\left\{\left(\sqrt{(K)}\int_{\mathrm{I}}\frac{E\times h_i' \,.\, ds}{K-k_i'}\right)h_i'+\left(\sqrt{(K)}\int_{\mathrm{I}}\frac{E\times h_i \,.\, ds}{K-k_i}\right)h_i\right.$$
$$\left.+\left(\int_{\mathrm{I}}\frac{E\times g_i' \,.\, ds}{\sqrt{K}}\right)g_i'+\left(\int_{\mathrm{I}}\frac{E\times g_i \,.\, ds}{\sqrt{K}}\right)g_i\right\}=0. \quad . \quad . \quad . \quad (11)$$

Let η_i form a set of two dimensional orthonormal vector functions of position over the surface of the iris I in terms of which any vector tangential to I can be expanded. Then

$$h_i=\sum_s\left(\int_{\mathrm{I}} h_i \,.\, \eta_s\, ds\right)\eta_s, \quad h_i'=\sum_s\left(\int_{\mathrm{I}} h_i' \,.\, \eta_s\, ds\right)\eta_s \quad . \quad . \quad (12)$$

and

$$g_i=\sum_s\left(\int_{\mathrm{I}} g_i \,.\, \eta_s\, ds\right)\eta_s, \quad g_i'=\sum_s\left(\int_{\mathrm{I}} g_i' \,.\, \eta_s\, ds\right)\eta_s$$

on I. If $\int_{\mathrm{I}} E\times\eta_s \,.\, ds=\gamma_s$ eqn. (11) becomes

$$\sum_s\gamma_s\sum_i\sum_t\Bigg\{\left(\frac{\sqrt{(K)}\int_{\mathrm{I}} h_i' \,.\, \eta_s\, ds\int_{\mathrm{I}} h_i' \,.\, \eta_t\, ds}{K-k_i'}\right)\eta_t + \left(\frac{\sqrt{(K)}\int_{\mathrm{I}} h_i \,.\, \eta_s\, ds\int_{\mathrm{I}} h_i \,.\, \eta_t\, ds}{K-k_i}\right)\eta_t\times\left(\frac{\int_{\mathrm{I}} g_i' \,.\, \eta_s\, ds\int_{\mathrm{I}} g_i' \,.\, \eta_t\, ds}{\sqrt{K}}\right)\eta_t + \left(\frac{\int_{\mathrm{I}} g_i \,.\, \eta_s\, ds\int_{\mathrm{I}} g_i \,.\, \eta_t\, ds}{\sqrt{K}}\right)\eta_t\Bigg\}=0. \quad . \quad . \quad . \quad . \quad . \quad (13)$$

If eqn. (13) is multiplied scalarly by each of the η_t in turn and integrated over the iris I, an infinite set of equations will be obtained. By eliminating the unknown γ_s's from these equations a secular equation is obtained.

$$\left|\sum_i\left\{\frac{\sqrt{(K)}\int_{\mathrm{I}} h_i' \,.\, \eta_s\, ds\int_{\mathrm{I}} h_i' \,.\, \eta_t\, ds}{K-k_i'}+\frac{\sqrt{(K)}\int_1 h_i \,.\, \eta_s\, ds\int_{\mathrm{I}} h_i \,.\, \eta_t\, ds}{K-k_i'} + \frac{\int_{\mathrm{I}} g_i'\,\eta_s\, ds\int_{\mathrm{I}} g_i' \,.\, \eta_t\, ds}{\sqrt{K}}+\frac{\int_{\mathrm{I}} g_i \,.\, \eta_s\, ds\int_{\mathrm{I}} g_i \,.\, \eta_t\, ds}{\sqrt{K}}\right\}\right|=0. \quad . \quad . \quad (14)$$

The roots of this equation give the various eigenvalues of the compound system. When one of these has been determined, the ratio's of the γ_s's may be found from the infinite set of equations derived from (13). Knowing the γ_s's, the α_i's, β_i's, α_i''s and β_i''s can be calculated. This enables H to be determined. E can also be found from the α_i's and α_i''s (Slater 1950).

ACKNOWLEDGMENTS

The authors would like to express their thanks to Professor M. H. L. Pryce, F.R.S., and Dr. A. F. Devonshire of the University of Bristol for some very valuable discussions.

REFERENCES

SLATER, J. C., 1950, *Microwave Electronics* (New York: D. van Nostrand Co. Inc.).
HAHN, W. C., 1941, *J. Appl. Phys.*, **12**, 62.
TEICHMANN, T., and WIGNER, E. P., 1953, *J .Appl. Phys.*, **24**, 262.

CXIV. *The Onset of Friction in Helium II*

By D. F. Brewer, D. O. Edwards and K. Mendelssohn, F.R.S.
The Clarendon Laboratory, Oxford †

[Received June 11, 1956]

Experiments have been carried out on the heat conduction in a tube of 5×10^{-3} cm diameter filled with liquid helium II. The tube whose closed end was fitted with a thermometer and a heater was thermally insulated, and its open end communicated with a bath of liquid helium the temperature of which could be kept constant automatically within $\sim 2\times10^{-5}$ deg. Applying the two-fluid model and assuming that the superfluid moving towards the heater suffers no dissipation, it can easily be shown that for a tube of length l and radius a, the heat resistance should be

$$\frac{\triangle T}{Q}=\eta_n\left(\frac{8l}{\pi a^4}\right)\frac{1}{\rho^2S^2T} \quad . \quad . \quad . \quad . \quad . \quad . \quad . \quad (1)$$

where η_n is the viscosity of the normal fluid, ρ the density and S the entropy, the bracketed term being the Poiseuille constant. The aim of the work was a determination, using eqn. (1), of the temperature and pressure dependence of η_n, which will be described elsewhere. The object of the present note is to report observations of the onset of friction made with this apparatus.

According to the suggestion of Gorter and Mellink (1949) there is a mutual friction between the normal fluid and superfluid with a force per unit volume

$$F=A\rho_s\rho_n(v_s-v_n)^N \quad . \quad . \quad . \quad . \quad . \quad . \quad . \quad (2)$$

where v_s and v_n are the superfluid and normal velocities, A a constant and N is supposed to have the value 3. This would lead to a total heat resistance of the form

$$\frac{\triangle T}{Q}=\eta_n\left(\frac{8l}{\pi a^4}\right)\frac{1}{\rho^2S^2T}+BQ^{N-1} \quad . \quad . \quad . \quad . \quad . \quad . \quad (3)$$

where B is a function of the temperature and of the dimensions of the tube. It is obvious that if (2) were correct for all velocities, (1) would only be valid for vanishing values of Q. On the other hand, experiments have shown (Bowers and Mendelssohn 1952, Winkel *et al.* 1955) that, at least in narrow channels, no dissipation of this kind occurs until a critical velocity v_c is reached. Accordingly

$$F=A\rho_s\rho_n[(v_s-v_n)-v_c]^N, \quad (v_s-v_n>v_c) \quad . \quad . \quad . \quad . \quad (4)$$

has been proposed (see Daunt and Smith 1954) as a refinement of (2).

---

† Communicated by the Authors.

A typical result for $\Delta T/Q$ against Q is given in the figure. Taking A and N from the data at high velocities, the curve for eqn. (4) is plotted as a dotted line. Neither this curve, nor eqn. (3), shown by the broken line, represent the data for all values of Q. Instead, two states of thermal resistance appear to be possible. For heat inputs up to a critical value, no non-linear friction takes place, and eqn. (1) is followed. At the critical heat input, the thermal resistance rises at first almost discontinuously, and from then onward increases in agreement with eqns. (2) and (3) if N is taken as 4. In the terms of the two-fluid model this means that dissipation involving the superfluid, possibly by mutual friction with the normal component, appears suddenly and at a finite value. This dissipation is velocity dependent and extrapolates back to zero for zero flow velocity. The actual dependence of the friction on velocity, which in the figure and in a number of other observations requires the value 4 for N in eqn. (2), becomes more complicated close to the lambda-point.

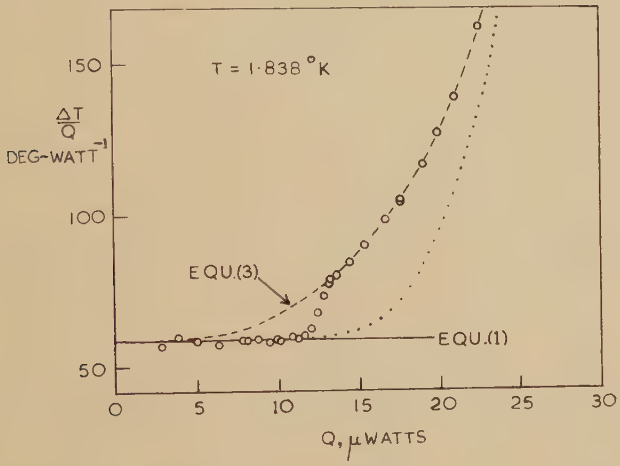

Thus, instead of the non-linear resistance appearing gradually beyond a certain velocity, the onset of friction in the superfluid resembles the case of a superconductor. There, too, the resistance remains zero up to the critical current and then changes over discontinuously to the finite value characteristic of the normal state. This similarity is further underlined by observations on a tube which was slightly obstructed. There the onset of friction was found at a higher value of Q than the disappearance of friction on decreasing the heat current. A number of such hysteresis loops in the thermal resistance were observed at different temperatures. Instability in the hysteresis loop could be demonstrated by tapping the cryostat, in which case the low heat resistance would suddenly change over to the high one or vice versa. While no true hysteresis occurred in the unobstructed tube, there was a marked instability in the transition region which may be of interest in connection with a recent suggestion of Feynman (1955).

Note added in proof.—Very large hysteresis effects have since been observed in apparently unobstructed tubes of larger diameter. These effects, which under some conditions were time-dependent, were also sensitive to vibration, and may possibly account for the inconsistencies in the reported values of critical velocity.

REFERENCES

BOWERS, R., and MENDELSSOHN, K., 1952, *Proc. Roy. Soc.* A, **213,** 158.
DAUNT, J. G., and SMITH, R. S., 1954, *Rev. Mod. Phys.*, **26,** 172.
FEYNMAN, R. P., 1955, *Prog. in L.T. Phys.* (Amsterdam: North-Holland Publ. Co.), **1,** 17.
GORTER, C. J., and MELLINK, J. H., 1949, *Physica*, **15,** 285.
WINKEL, P., DELSING, A. M. G., and POLL, J. D., 1955, *Physica*, **21,** 331.

CXV. *An Analysis of the Magnetization Processes in Iron Single Crystals by an Electrical Method*

By R. Parker
Department of Physics, University College of North Wales, Bangor†

[Received May 13, 1956]

Abstract

Döring's theory of the anisotropy of electrical resistivity of ferromagnetics is applied to the published magnetoresistance data of single crystals of iron. The theory is shown to be in good agreement with experiment and the five anisotropy coefficients for iron are evaluated. It is suggested that a study of the magnetoresistance as a function of magnetization may be used to obtain information concerning the magnetization processes in ferromagnetic crystals of cubic symmetry. An analysis has been made of the measurements reported by Kuwahara on single crystal strips of iron. In certain favourable cases the actual magnetization process can be inferred from a number of plausible alternatives by a consideration of the electrical data. For other specimens an estimate of the domain vector orientation in the demagnetized state is obtained. The relative advantages of the electrical method are discussed.

§ 1. Introduction

It is well known that the electrical resistivity of a single crystal of a ferromagnetic metal depends upon its state of technical magnetization in a complex manner. In order to describe this phenomenon quantitatively it is convenient to define magnetoresistance coefficients, $\Delta\rho/\rho$, where $\Delta\rho$ represents the change in the resistivity ρ, which results from the magnetization. Döring (1938) has suggested that the magnetoresistance coefficients may be explained by assuming that the resistivity is a function of the direction cosines of the magnetization and current vectors with respect to the crystal axes. On assuming this function to be a power series expanded as far as the fourth power, and upon taking into consideration the requirements of Ohm's Law and of cubic crystal symmetry, an equation can be derived for $\Delta\rho/\rho$ in terms of five independent anisotropy constants. These constants have been evaluated for the case of nickel and the calculated values are in close accord with experimental observations. In comparing theory with experiment Döring has confined himself to differences in $\Delta\rho/\rho$ of specimens magnetized to saturation along different directions. This has the advantage of avoiding assumptions concerning the distribution of domains in the demagnetized state.

---

† Communicated by the Author.

The only other material for which sufficient experimental data are available to test Döring's hypothesis is 99·5% pure iron ; measurements were made by Webster (1926, 1927) on single crystal rod specimens cut along the three principal crystal directions with magnetic fields applied along (longitudinal) and perpendicular to (transverse) the direction of current flow. In § 2 the five magnetoresistance anisotropy constants for iron are evaluated and the experimental results found to be in good agreement with Döring's hypothesis. The extension of the latter to initially demagnetized specimens is briefly considered in the light of recent developments of our knowledge of ferromagnetic domains.

In subsequent sections it is shown that Döring's theory may be applied to magnetoresistance data below technical saturation ; in some cases an analysis of the electrical data can yield information concerning the mechanism of the magnetization processes. In certain favourable cases the same information cannot be obtained by any other experimental method.

The magnetoresistance of single crystal strips of iron as a function of magnetization has been studied in detail by Kuwahara (1954) and Kuwahara and Tatsumoto (1955). The conclusions which may be drawn from an analysis of the results of these investigators are discussed in § 4.

§ 2. THE MAGNETORESISTANCE ANISOTROPY CONSTANTS OF IRON

When a single crystal of iron is brought from the ideally demagnetized state to technical saturation the magnetoresistance coefficient is given by :

$$
\begin{aligned}
(\Delta\rho/\rho)_{\mathrm{sat}} = {} & k_1\Big(\sum_i \alpha_i^2\beta_i^2-\tfrac{1}{3}\Big)+2k_2\sum_{i,j\neq i}\alpha_i\alpha_j\beta_i\beta_j+k_3\sum_{i,j\neq i}\alpha_i^2\alpha_j^2 \\
& +k_4\Big(\sum_i{}_i\alpha_i^4\beta_i^2+\tfrac{2}{3}\sum_{i,j\neq i}\alpha_i^2\alpha_j^2-\tfrac{1}{3}\Big)+2k_5\sum_{i,j\neq i}\alpha_i\alpha_j(1-\alpha_i^2-\alpha_j^2)\beta_i\beta_j \qquad \text{. . . (1)}
\end{aligned}
$$

where α_i and β_i are the direction cosines of the magnetization and current vector, respectively, with reference to the ith cubic crystals axis, and where $k_1 \ldots k_5$ are constants to be determined from experiment. Equation (1) differs slightly from the corresponding equation for nickel because of the differences in the easy direction of magnetization in the two metals in the demagnetized state.

Equation (1) is now applied in turn to specimens cut along the three principal crystal directions for which measurements have been reported by Webster. When a demagnetized specimen with a long axis coincident with a [100] crystal direction is brought to saturation in a longitudinal field the resulting magnetoresistance coefficient is given by

$$(\Delta\rho/\rho)_{\parallel\ \mathrm{sat}}=\tfrac{2}{3}(k_1+k_2). \qquad \text{. . . . . (2)}$$

For the case of transverse magnetization one obtains from eqn. (1)

$$(\Delta\rho/\rho)_{\perp\ \mathrm{sat}}=-\tfrac{1}{3}\,k_1+\tfrac{1}{8}\,k_3-\tfrac{1}{4}\,k_4-(\tfrac{1}{8}\,k_3+\tfrac{1}{12}k_4)\cos 4\theta_1 \qquad \text{. . (3)}$$

where θ_1 is the angle between the magnetization vector and one of the cubic axes perpendicular to the direction of current flow. The corresponding equations for a specimen cut along a [110] crystal direction are :

$$(\Delta\rho/\rho)_{\parallel\,\mathrm{sat}}=\tfrac{1}{6}\,k_1+\tfrac{1}{2}\,k_2+\tfrac{1}{4}\,k_3+\tfrac{1}{12}k_4 \quad . \quad . \quad . \quad . \quad . \quad (4)$$

and

$$(\Delta\rho/\rho)_{\perp\,\mathrm{sat}}=a_1+a_2\cos 2\theta_2+a_3\cos 4\theta_2 \quad . \quad . \quad . \quad . \quad (5)$$

where θ_2 is the angle between the magnetization vector and the cubic axis perpendicular to the direction of current flow and where

$$a_1= -\tfrac{1}{4}(\tfrac{1}{3}\,k_1+k_2-\tfrac{7}{8}\,k_3+\tfrac{3}{8}\,k_4+\tfrac{1}{4}\,k_5)$$
$$a_2= -\tfrac{1}{4}(k_1-k_2+\tfrac{1}{2}\,k_3+\tfrac{5}{6}\,k_4)$$
$$a_3= -\tfrac{1}{16}(\tfrac{3}{2}\,k_3+\tfrac{1}{4}\,k_4-k_5).$$

For a specimen cut along a [111] crystal direction eqn. (1) yields

$$(\Delta\rho/\rho)_{\parallel\,\mathrm{sat}}=\tfrac{2}{3}\,k_2+\tfrac{1}{3}\,k_3+\tfrac{2}{9}\,k_5 \quad . \quad . \quad . \quad . \quad . \quad . \quad (6)$$

and

$$(\Delta\rho/\rho)_{\perp\,\mathrm{sat}}=-\tfrac{1}{3}\,k_2+\tfrac{1}{4}\,k_3. \quad . \quad . \quad . \quad . \quad . \quad . \quad . \quad (7)$$

Unfortunately, values for $(\Delta\rho/\rho)_{\parallel\,\mathrm{sat}}-(\Delta\rho/\rho)_{\perp\,\mathrm{sat}}$ for individual specimens have not been reported by Webster. However, the reproducibility of separate saturation magnetoresistance constants on crystallographically similar specimens from Webster's own results as well as those of other investigators (Gondo and Funatogawa 1952) is sufficiently close to establish the coefficients to 1×10^{-4} in most cases. An exception is the value of $(\Delta\rho/\rho)_{\parallel\,\mathrm{sat}}$ for specimens with an easy direction of magnetization parallel to the specimen axis. This is undoubtedly due to the variation of domain structure in the demagnetized state from one specimen to the next and will be considered in greater detail at the end of the section. In the meantime no use is made in determining $k_1 \ldots k_5$ of any data which involve assumptions concerning the demagnetized state of these specimens. This still leaves seven independent equations for the evaluation of only five constants, namely three equations from (5) and one each from (4), (6), (7) and one equation from the periodic term in (3).

After the usual linear extrapolation of the experimental results to correct for the changes in spontaneous magnetization (see, for example, Bates 1946) one obtains from Webster's results :

$$k_1=-8\times10^{-4},\ \ k_2+57\times10^{-4},\ \ k_3=+14\times10^{-4},$$
$$k_4=+12\times10^{-4},\ \ k_5=-16\times10^{-4}. \quad . \quad . \quad . \quad . \quad . \quad . \quad . \quad . \quad (8)$$

Saturation magnetoresistance coefficients calculated with the above constants and with eqns. (4), (6) and (7) are compared with experimental results in the table. A similar comparison is made for eqns. (3) and (5) in fig. 1 (*a*) and 1 (*b*). It will be noted that the agreement is remarkably good, both with regard to numerical values as well as functional dependence upon the angles θ_1 and θ_2[†]. It may be concluded that Döring's theory of resistivity anisotropy describes the saturation magnetoresistance coefficients of iron crystals so far discussed to well within the uncertainties of extrapolation and of probable errors of measurement.

[†] Constants differing substantially from these in eqn. (8) are quoted by Bozorth (1951) ; these constants are not in good agreement with some of the experimental results described above.

In the determination of the anisotropy constants it has been assumed implicitly that in the demagnetized state the volume of domains are distributed equally over the [100], [010] and [001] directions. This

Fig. 1 (*a*)

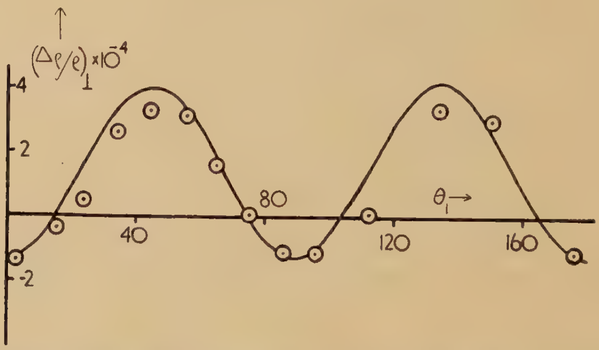

Saturation magnetoresistance coefficient of [100] specimen. Curve calculated from eqns. (3) and (8); points from experiment.

Fig. 1 (*b*)

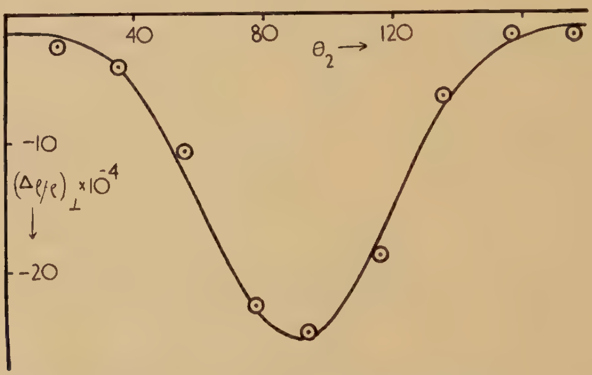

Saturation magnetoresistance of [110] specimen. Curve calculated from eqns. (5) and (8); points from experiment.

Comparison of saturation magnetoresistance coefficients calculated from eqns. (4) to (8) with experiment

Specimen	Field	Calculated coefficient ($\times 10^{-4}$)	Range of experimental results $\times 10^{-4}$
[110]	longitudinal	32	30 to 34
[111]	longitudinal	39	39 to 41
[111]	transverse	−15·5	−14 to −17

assumption is certainly reasonable for well annealed cylindrical specimens with their long axes along [110] and [111] directions. For the case of a strain and inclusion free specimen cut along a [100] direction however, one would expect that in the absence of an external magnetic field the magnetostatic free energy is reduced by an almost complete alignment of domain vectors parallel and antiparallel to the specimen axis. If a field is now applied, magnetization proceeds by 180° Bloch wall movements and no change in resistivity takes place. If, however, an electric current is flowing, a transverse magnetic field is set up, whose value at the surface of the specimens investigated by Webster, is several oersteds. There is now a tendency for domains to be aligned parallel and antiparallel to the [010] and [001] axes. It is, therefore, not possible to predict the domain distribution (and hence the saturation magnetoresistance) in the demagnetized state without detailed information with regard to coercivity, current density and the ratio of length to diameter of the specimens.

In general, those domains which are initially aligned perpendicularly to the specimen axis contribute a term to the saturation magnetoresistance coefficient. This according to eqn. (1) is given by

$$(\Delta\rho/\rho)_{\parallel\,\mathrm{sat}}=k_1+\tfrac{2}{3}\,k_3+\tfrac{1}{3}\,k_4. \qquad (9)$$

Thus from (8) and (9) the longitudinal saturation magnetoresistance is given by the small term

$$(\Delta\rho/\rho)_{\parallel\,\mathrm{sat}}=c\times 5{\cdot}3\times 10^{-4} \qquad (10)$$

where c is the fraction of the volume of [010] and [001] type domains between the potential leads of the specimen in the demagnetized state. On comparison with experiment the results for all specimens can be accounted for by values of c between 0 and 1.

It is significant that c estimated from the results of Gondo and Funatogawa (1952) and Shirakawa (1940) is considerably less than 0·1, whereas that from Webster's results range from 0·3 to 0·9. The former workers used specimens of length to diameter ratio in excess of 50, whereas that in Webster's case is about 15. The electrical measurements thus support the view that magnetic domains have a preference for those easy directions of magnetization which correspond to the smallest demagnetizing factor of the specimen.

The magnetoresistance of single crystal strips of iron as a function of magnetization has been studied recently by Kuwahara (1954) and Kuwahara and Tatsumoto (1955). The specimens used had approximate dimensions 150 mm × 2 mm × 0·5 mm. The remainder of this paper is devoted to discussion of the conclusions which may be drawn from our analysis of the results of these investigators.

§ 3. MAGNETORESISTANCE AND THE IMPURITY OF SPECIMENS

The specimens used by Kuwahara and Tatsumoto were made from a block which contained a certain amount of impurity. The effects of impurity upon the magnetoresistance of polycrystalline iron has been discussed in some detail by the author (Parker 1952). It was shown that the saturation magnetoresistance coefficient of a dilute solid solution in iron differs from that of the pure metal by an amount which is principally determined by the increase in the specific resistivity that results from the presence of the impurity atoms. The impurities listed by Webster have a negligible influence upon the resistivity of iron at room temperature. It may therefore be concluded that the magnetoresistance coefficients reported by Webster differ from those of ideally pure iron by only a very small amount. In the case of the alloy used by Kuwahara however, the relevant impurities are 0·66% aluminium and 0·46% silicon by weight. The effect of these elements upon $(\Delta\rho/\rho)_{\parallel\,\mathrm{sat}}$ of polycrystalline iron is predicted explicitly by eqns. (2) and (3) in the paper by Parker (1952). The predicted values are consistent with the measured values of Kuwahara and Tatsumoto over the temperature range −95°c to +100°c. At room temperature both the theoretical and experimental value of $(\Delta\rho/\rho)_{\parallel\,\mathrm{sat}}$ is 0·60 times that of pure iron. It will be assumed that the value of each of the anisotropy constants of eqn. (2) must be multiplied by the same factor. This procedure may be justified by the fact that the value of $\Delta\rho/\rho$ for every single crystal specimen at any state of magnetization shows exactly the same temperature dependence as the value for the polycrystalline alloy. The impurity contribution to $\Delta\rho/\rho$ is strongly temperature dependent; it is concluded therefore, that the reduction of the polycrystalline magnetoresistance as a result of impurity is due to a proportionate reduction in each constituent crystallite. Consequently in the subsequent calculations each anisotropy constant in eqn. (8) is separately reduced by a factor 0·60.

§ 4. ANALYSIS OF THE MAGNETIZATION PROCESS OF SINGLE CRYSTAL STRIPS

Of the results to be discussed in this section there is only one case for which a detailed knowledge of magnetization processes is already available. For this reason it will be considered first.

4.1. *Specimen plane* (100), *long axis* [011]

The distribution of magnetic domains for this specimen has been predicted by Néel (1944) and demonstrated with the aid of the Bitter figure technique by Bates (1946), Bates and Neale (1950), Bates and Mee (1952) and Williams *et al.* (1949). In the demagnetized state almost the whole specimen volume is occupied by domains with their vectors equally distributed along the [001], [00$\bar{1}$], [010] and [0$\bar{1}$0] directions. In addition very small closure domains at the edge of the specimen are directed along the [100] and [$\bar{1}$00] directions. In a small longitudinal magnetic field the volume of [00$\bar{1}$] and [0$\bar{1}$0] domains diminishes by 180° boundary wall movements until the bulk of the specimen volume consists of alternating [001] and [010] domains. An increase in the applied field then causes a rotation of these domains into the direction of the applied field. According to eqn. (1) the saturation magnetoresistance coefficient is given by

$$(\varDelta\rho/\rho)_{\parallel\,\mathrm{sat}}=(1-v/V)\,(\tfrac{1}{2}\,k_2+\tfrac{1}{4}\,k_3-\tfrac{1}{12}\,k_4)+(v/2V)\,(k_1+k_2+\tfrac{1}{2}\,k_3+\tfrac{5}{6}\,k_4) \quad . \quad . \quad . \quad (11)$$

where v is the volume initially occupied by closure domains and V the total specimen volumes, respectively, between the attached potential leads. The ratio v/V is of the order of magnitude $d/2L$, where L is the width of the specimen and d the width of [001] domains. For the specimen under consideration the ratio v/V is so small (Lee 1953) that the second term in eqn. (11) contributes a quantity too small to be detected with the present sensitivity of electrical measurements. It can therefore be ignored in the subsequent discussion.

The magnetoresistance coefficient below magnetic saturation can also be determined. While the magnetization proceeds by 180° domain wall movements, $(\varDelta\rho/\rho)_{\parallel}$ is zero. In the higher applied field range each domain separately is inclined at angles θ, $(90°-\theta)$, and 90° with respect to the cubic crystal axes (fig. 2). Thus according to eqn. (1) the magnetoresistance coefficient of the specimen is given by

Fig. 2

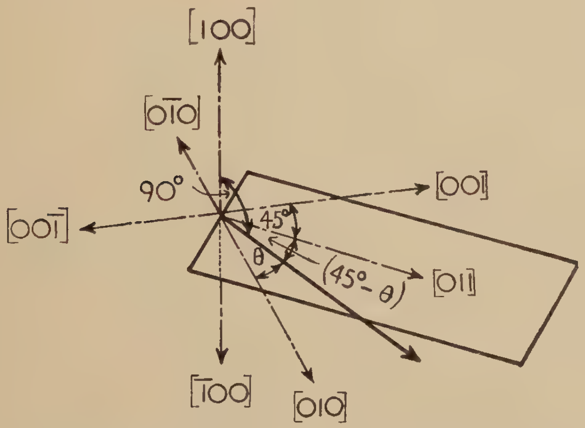

Crystal axes and domain vector of (100) [011] specimen.

$$(\varDelta\rho/\rho)_{\parallel}=\tfrac{1}{2}\,k_2\sin 2\theta+(\tfrac{1}{4}\,k_3-\tfrac{1}{12}\,k_4)\sin^2 2\theta. \quad . \quad . \quad . \quad (12)$$

If I is the intensity of magnetization of the whole specimen and I_s its saturation value then

$$I=I_s\,(\sin\theta+\cos\theta)\times 1\sqrt{2} \quad . \quad . \quad . \quad . \quad . \quad . \quad (13)$$

and therefore from (12) and (13)

$$(\varDelta\rho/\rho)_{\parallel}=k_2\,[(2I^2-I_s^{\,2})/2I_s^{\,2}]+(k_3-\tfrac{1}{3}\,k_4)\,[(2I^2-I_s^{\,2})/2I_s^{\,2}]^2. \quad . \quad (14)$$

Values of $(\Delta\rho/\rho)_{\parallel}$ calculated from eqn. (14) are now compared with those obtained by experiment in fig. 3. It will be noted that excellent agreement is obtained.

Fig. 3

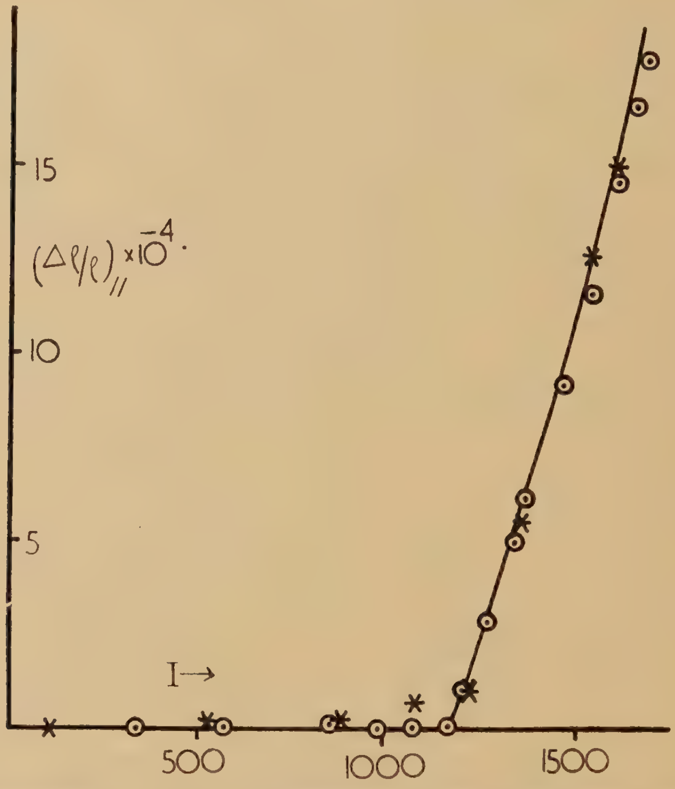

Magnetoresistance of (100) [011] specimen. Curve calculated according to eqn. (14).

Experimental results : ⊙ increasing field ; * decreasing field.

4.2. *Specimen plane* $(\bar{1}10)$, *long axis* [110]

This specimen is of some interest since there are a number of plausible alternative modes of magnetization. These will now be described in turn and it will be seen that only one mode is consistent with the electrical data.

(*a*) The domain vectors in the demagnetized state are all directed along the only directions of easy magnetization contained in the plane of the specimen, i.e. [001] and $[00\bar{1}]$. If an increasing longitudinal field is applied the vectors remain parallel to the $(\bar{1}10)$ plane and rotate towards the [110] direction. In this case one obtains separately for each domain (fig. 4) :

$$\alpha_1=\alpha_2=1/\sqrt{2}\cos\gamma_1,\ \alpha_3=\sin\gamma_1,\ \beta_1=\beta_2=1/\sqrt{2},\ \beta_3=0, \quad . \quad . \quad (15)$$

Fig. 4

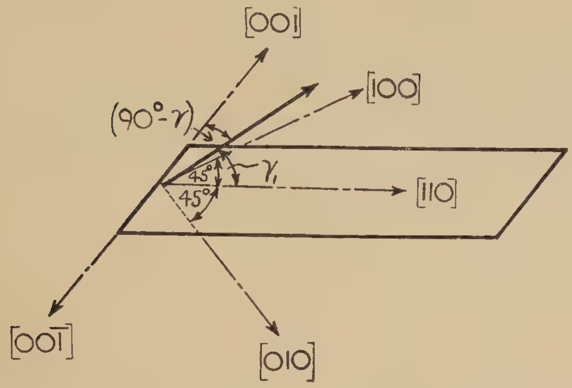

Crystal axes and domain vector $(\bar{1}10)$ [110] specimen.

where $\gamma_1 = \cos^{-1} I/I_s$. On substituting (15) into (1) one obtains after simplification

$$(\Delta\rho/\rho)_{\parallel} = a_0 + a_1 \cos\gamma_1 + a_2 \cos^2\gamma_1 \quad . \quad . \quad . \quad . \quad . \qquad (16)$$

with

$$a_0 = \tfrac{1}{4}(k_1 + k_2 + \tfrac{5}{4}\,k_3 + \tfrac{13}{12}\,k_4 + \tfrac{1}{2}\,k_5)$$
$$a_1 = \tfrac{1}{4}(k_1 + k_2 + \tfrac{1}{2}\,k_3 + \tfrac{5}{6}\,k_4)$$
$$a_2 = -\tfrac{1}{16}(3\,k_3 + k_4 + 2\,k_5).$$

This value of $(\Delta\rho/\rho)_{\parallel}$ is plotted against I in fig. 5, curve A.

(*b*) The demagnetized state is characterized by an equal distribution of domain volumes over the [010], $[0\bar{1}0]$, [100] and $[\bar{1}00]$ directions. A small applied longitudinal field then causes the disappearance of $[0\bar{1}0]$ and $[\bar{1}00]$ domains by 90° or 180° boundary wall movements. There is thus no change in electrical resistivity from crystal symmetry considerations until I has reached the value $I_s/\sqrt{2}$. In larger applied fields a rotation of the [010] and [100] domains towards the [110] direction takes place in the (001) plane. Let the angle between a domain vector and the [110] direction be γ_2. Then from considerations of crystal symmetry one finds separately for each domain that

$$\alpha_1 = \cos(45° - \gamma_2),\ \alpha_2 = \cos(45° + \gamma_2),\ \alpha_3 = 0. \quad . \quad . \quad . \quad . \qquad (17)$$

On substituting (17) into (1) one obtains

$$(\Delta\rho/\rho)_{\parallel} = \tfrac{1}{2}k_2 \cos 2\gamma_2 + (\tfrac{1}{4}\,k_3 - \tfrac{1}{12}\,k_4)\cos^2 2\gamma_2. \quad . \quad . \quad . \quad . \qquad (18)$$

Since $I = I_s \cos\gamma_2$ a relationship is obtained between $(\Delta\rho/\rho)_{\parallel}$ and I, and this has been plotted in fig. 5, curve B.

(*c*) The domain vectors in the demagnetized state are along the $[00\bar{1}]$ and [001] directions as described in case (*a*) but a small applied field causes a redistribution in favour of the two easy directions of magnetization nearest to the specimen axis, namely [100] and [010]. In larger fields the magnetization proceeds exactly as described in (*b*). The magnetoresistance coefficient is thus similar to that derived from eqn. (18); there is however an additional term $\frac{1}{2}(k_1+k_2)$ arising from the 90° boundary wall movements which predominate in the initial part of the magnetization process. The predicted values of $(\Delta\rho/\rho)_{\|}$ as a function of I have been plotted in fig. 5, curve C. It will be seen that this is indeed the mode which is consistent with the electrical measurements.

Fig. 5

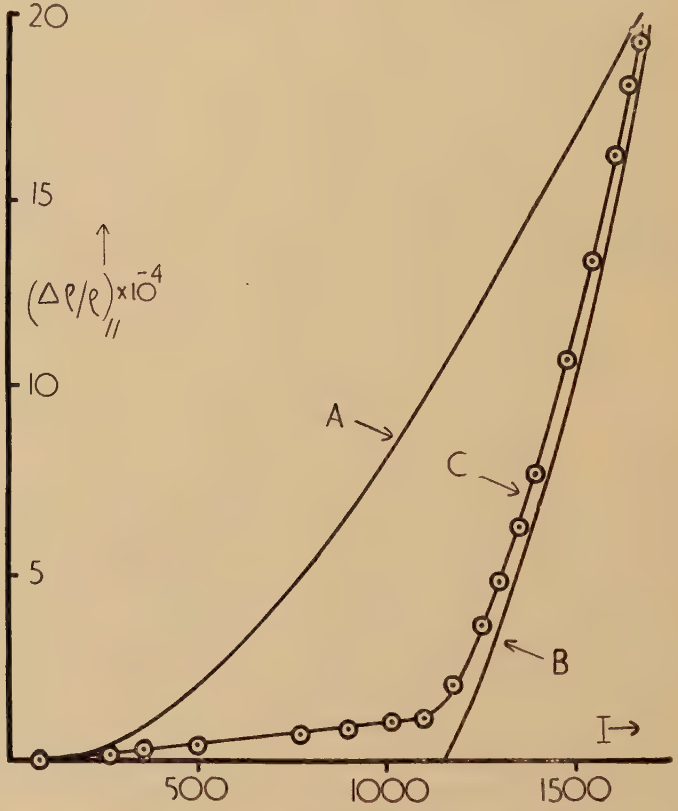

Magnetoresistance of $(\bar{1}10)$ [110] specimen. For explanation of curve see accompanying text. ⊙ Experimental results.

4.3. *Specimen plane* (011), *long axis* [100]

In this case the long axis coincides with the only easy direction of magnetization in the plane of the specimen. The magnetization process would then be expected to proceed entirely by 180° Bloch wall movements within the specimen volume contained between the potential probes. The longitudinal magnetoresistance coefficient must therefore be zero for all values of I. This is indeed found to be the case by experiment. A very small departure from zero magnetoresistance for $I > 0{\cdot}95\,I_s$ is readily explained by a disalignment of the crystal axes with the applied field of approximately 2°.

4.4. *Specimen plane* (001), *long axis* [100]

The directions of easy magnetization of this specimen are both along (i.e. [100] and [$\bar{1}$00]) and perpendicular (i.e. [010], [0$\bar{1}$0], [001] and [00$\bar{1}$]) to the specimen axis. From a consideration of shape and magnetocrystalline anisotropy only, the domain vector distribution would be entirely along the [100] and [$\bar{1}$00] directions in the demagnetized state. As an applied longitudinal field causes 180° boundary wall movements only, there can be no change of resistivity according to eqn. (1).

On the other hand, the [010] and [0$\bar{1}$0] directions also lie in the plane of the specimen and are almost as favourable directions in the demagnetized state, if the length to width ratio of the specimen is not excessive. Moreover, the specimen current sets up a magnetic field perpendicular to its direction of flow. This field has an estimated intensity of 0·3 oersted at the surface of the specimen under discussion. If this field intensity should exceed the transverse demagnetizing field appreciably, the domain vectors would be aligned perpendicularly to the direction of current flow in the demagnetized state. In this case $(\Delta\rho/\rho)_{\parallel\,\mathrm{sat}}$ would be given according to eqn. (9) as $(\Delta\rho/\rho)_{\parallel\,\mathrm{sat}}=k_1+\frac{2}{3}\,k_3+\frac{1}{3}\,k_4$.

If the field due to the specimen current is comparable with the transverse demagnetizing field, the possibility of coexistence of longitudinal and transverse domains in the demagnetized state must be considered. The relative volume occupied by these two types of domains is then expected to be sensitive to small elastic stresses and to the magnetic history of the specimen. This appears to be the case in the results reported by Kuwahara. The latter are shown in fig. 6 together with the value calculated from eqn. (9). In the general case

$$(\Delta\rho/\rho)_{\parallel\mathrm{sat}}=c(k_1+\tfrac{2}{3}\,k_2+\tfrac{1}{3}\,k_4) \quad . \quad . \quad . \quad . \quad . \quad . \quad (19)$$

where c is the fractional volume of transverse domains in the demagnetized state. The experimentally determined values of $(\Delta\rho/\rho)_{\parallel}$ should then follow a curve contained within the area OAB in fig. 6. The slope of curve can be shown to be

$$\frac{d(\Delta\rho/\rho)_{\parallel}}{dI}=c'(k_1+\tfrac{2}{3}k_3+\tfrac{1}{3}\,k_4)/(2-c')I_s \quad . \quad . \quad . \quad . \quad (20)$$

where c' represents the ratio of the reduction of volume of transverse to antiparallel domains at any point on the magnetization curve. Equations (19) and (20) are not independent since the relationship

$$c=1/I_s\int_0^{I_s} c'\,dI$$

must be satisfied.

With the aid of eqns. (19) and (20) the reported magnetoresistance data allow the following inference of the magnetization processes. After cooling from the Curie temperature almost the whole specimen volume between the potential probes is occupied by domains whose vectors coincide with the specimen axis. Magnetization in an applied longitudinal field then proceeds by the disappearance of antiparallel domains by 180° Bloch wall movements. If on the other hand the specimen is demagnetized in a diminishing a.c. field, over 90% of the volume is occupied by domains with their vectors perpendicular to the specimen axis. An increasing longitudinal field in the [100] direction will first cause the disappearance of all [$\bar{1}$00] (antiparallel) domains and then a growth of [100] domains at the expense of the 'transverse' domains which had their vectors originally orientated along the [010] and [0$\bar{1}$0] axes.

The small additional increase in magnetoresistance coefficient just below technical saturation is undoubtedly due to a slight departure of the crystal axes from correct alignment with respect to the applied field direction.

Fig. 6

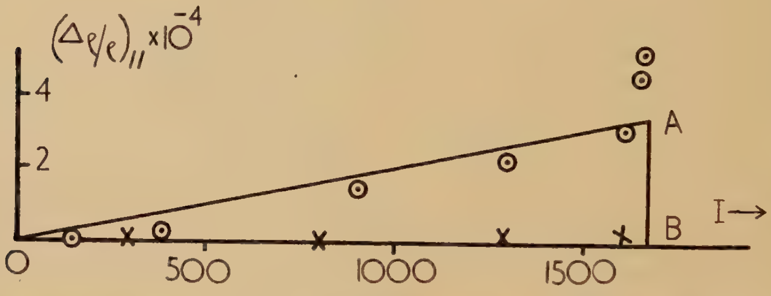

Magnetoresistance of (001) [100] specimen. Line OA consistent with eqn. (9).
Points according to experiment.
⊙ Specimen previously demagnetized by a.c.;
× Specimen previously cooled from Curie point.

4.5. *Specimen plane* ($\bar{1}$10), *long axis* [111]

The directions of easy magnetization for this specimen are all equally inclined to the long axis of the specimen at an angle of $\cos^{-1} 1/\sqrt{3}$. For this reason any reorientation of the domain vectors among the six easy directions leaves the resistivity of the specimen unchanged. Only a rotation of the domain vectors away from the nearest easy directions towards the field direction will be detected electrically. The magnetoresistance coefficients associated with this process will now be calculated.

Considerations of crystal symmetry require that each domain separately is described by direction cosines

$$\alpha_1=\alpha_2=[(1-\cos^2\phi)/2]^{1/2},\ \alpha_3=\cos\phi. \qquad (21)$$

Since $\beta_1=\beta_2=\beta_3=1/\sqrt{3}$, one obtains from (1) and (21) after due simplification:

$$(\Delta\rho/\rho)_{\parallel}=(\tfrac{1}{6}k_2+\tfrac{7}{32}k_3)+\sqrt{2}/3k_2\sin 2\phi-(\tfrac{1}{6}k_2+\tfrac{1}{8}k_3)\cos 2\phi-(\tfrac{3}{32}k_3+\tfrac{1}{24}k_5)\cos 4\phi+(\tfrac{1}{3}\sqrt{2})k_5\sin 2\phi\cos\phi. \qquad (22)$$

The magnetization is given by

$$I = I_s(\cos\phi + \sqrt{2}\sin\phi)/\sqrt{3}. \quad . \quad . \quad . \quad . \quad . \quad . \quad . \quad (23)$$

The values of $(\Delta\rho/\rho)_{\parallel}$ as a function of I have been calculated from eqns. (22) and (23) and are shown in fig. 7, together with the values reported from experiment. It will be noted that very good agreement is obtained. The only conclusion to be drawn from these results is that the reorientation of the domain vectors along the easy directions of magnetization nearest to the applied field is almost complete before rotation away from the easy directions commences.

Fig. 7

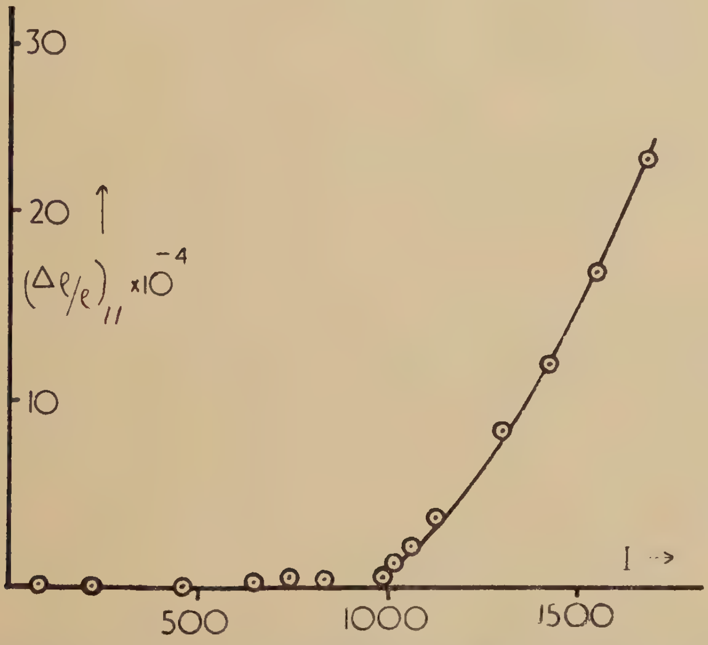

Magnetoresistance of ($\bar{1}$10) [111] specimen. Curve calculated according to eqns. (22) and (23); points according to experiment.

§ 5. CONCLUSION

A detailed analysis of the magnetoresistance data of Kuwahara and Tatsumoto on single crystal strips of iron has been given. It was found that in a number of favourable cases the electrical data yield detailed information concerning the distribution of magnetic domains in the demagnetized state and the nature of the magnetization processes. Good agreement is obtained where this information was already available. In other cases the analysis of magnetoresistance data facilitates the choice between a number of possible alternatives. With one specimen a study of the demagnetized state in relation to the magnetic history was possible.

In the past the principal experimental method available for the study of domain processes has been the powder pattern technique. The magnetoresistance method cannot give the same detailed information concerning the size and shape of surface domains as the Bitter pattern technique since the former only records the integrated effect over the volume of the specimen between the potential probes. On the other hand the electrical method has a number of advantages. Results are not masked by unrepresentative surface effects ; measurements are readily extended to cover a wide range of temperature, applied stress and specimen shape. Thus the two methods provide information about the magnetization processes, which is largely complementary. A combination of electrical and Bitter figure measurements on the same specimen would therefore readily extend our present knowledge of magnetization processes in ferromagnetic single crystals of cubic symmetry.

ACKNOWLEDGMENTS

The author is indebted to Professor E. R. Andrew for a number of helpful suggestions and to the Council of the Royal Society for a grant which has enabled him to undertake this investigation.

REFERENCES

BATES, L. F., 1946, *Proc. Phys. Soc.*, **58,** 153.
BATES, L. F., and MEE, C. D., 1952, *Proc. Phys. Soc.* A, **65,** 129.
BATES, L. F., and NEALE, F. E., 1950, *Proc. Phys. Soc.* A, **63,** 374.
BOZORTH, R. M., 1951, *Ferromagnetism* (New York : D. van Nostrand Inc.), p. 765.
DÖRING, W., 1938, *Ann. Phys.*, **32,** 259.
GONDO, Y., and FUNATOGAWA, Z., 1952, *Proc. Phys. Soc.*, Japan, **7,** 41.
KUWAHARA, K., 1954, *J. Sci. Hiroshima Univ.*, **18,** 87.
KUWAHARA, K., and TATSUMOTO, E., 1955, *J. Sci. Hiroshima Univ.*, **19,** 385.
LEE, E. W., 1953, *Proc. Phys. Soc.* A, **66,** 623.
NÉEL, L., 1944, *J. Phys. Radium*, **5,** 241.
PARKER, R., 1952, *Proc. Phys. Soc.* B, **65,** 616.
SHIRAKAWA, Y., 1940, *Sci. Rep. Tôhoku Imp. Univ.*, **29,** 132.
WEBSTER, L. W., 1926, *Proc. Roy. Soc.* A, **113,** 196 ; 1927, *Ibid.*, **114,** 611.
WILLIAMS, H. J., BOZORTH, R. M., and SHOCKLEY, W., 1949, *Phys. Rev.*, **75,** 155.

CXVI. *Angles Between Partial Magnetizations in Spinel Ferrites Containing Manganese Ions of more than One Valency*

By W. P. Osmond

Mullard Research Laboratories, Salfords, Surrey †

[Received June 15, 1956]

Abstract

In iron-deficient spinel ferrites containing manganese, but no other constituent of variable valency, all the manganese will not be divalent. Mn^{3+} ions tend to form strong directed semicovalent bonds in octahedral (B) sites but not in tetrahedral (A) sites. The reverse is true for Fe^{3+} ions. The antiparallel A–B indirect exchange interaction should thus be weaker when one interacting ion is Mn^{3+} than when both are Fe^{3+}. Any Mn^{3+} ions are likely to be coupled with parallel spins by double exchange with Mn^{2+} or Mn^{4+} ions in the same type of lattice site. The magnetic ions in either sublattice can then be considered as divided into two groups, one based on Mn^{3+} ions, and the other on Fe^{3+} ions, with different degrees of departure from antiparallelism of their net spins to the net magnetization of the other sublattice. The molecular field approximation as applied by other authors to single ions is extended to such groups of ions, with certain provisos as to the correct interpretation to be given to the mathematical symbols used for interaction coefficients and angles between spin directions.

§ 1. Introduction

The chemical formula for a stoichiometric mixed spinel ferrite may be written perfectly generally as $X_p\ Y_q\ Fe_rO_4$ with $p+q+r=3$, X and Y representing metal atoms. For compositions containing the stoichiometric amount of iron (represented by 50% (mol) Fe_2O_3) $r=2$, $p+q=1$. With only ferric iron present, X and Y must then both be divalent (if we exclude ferrites containing monovalent ions such as Li^+). In practice the relative iron content is often made less than this, so as to reduce the risk of lowered resistivity resulting from the easy electron transfer which is known to occur between ferrous and ferric ions in similar lattice sites. In such circumstances one of the other two metal constituents X, Y must appear in other than the solely divalent state, in order that electrostatic neutrality combined with no oxygen deficiency may be maintained. An example of this type of composition is provided by the magnesium manganese ferrites $Mg_pMn_q\ Fe_rO_4$ frequently used for the small cores exhibiting ‘square’ hysteresis loops in magnetic storage units. In this instance manganese is the element appearing with an average valency in excess of 2, and unless Mn^{3+} or Mn^{4+} ions alone are found in similar lattice sites there will be lowered resistivity through electron transfer. However, any resultant disadvantage is usually considered to be offset by the improved sintering found with a higher Mn/Mg ratio than that commonly employed in compositions of this type for use in microwave components, where the dielectric loss caused by electronic conduction is required to be negligible.

---

† Communicated by the Author.

Such ‘square loop’ compositions, with all the loss of oxygen arising from the deficiency of Fe_2O_3 made good by enhanced manganese valency, can be considered as mixtures of $MgFe_2O_4$ and (*a*) $MnFe_2O_4$ and Mn_3O_4 for $r/2>p$, (*b*) Mn_3O_4 and $MgMn_2O_4$ for $1>p>r/2$, (*c*) $MgMn_2O_4$ and Mg_2MnO_4 for $1+q>p>1$. The last two compositions are not known unequivocally to exist, but the formulae provide convenient symbols for representing the required manganese valency (Mn^{III} for the former and Mn^{IV} for the latter). Compositions for which $p>1+q$ must contain some excess MgO, complete oxygen compensation being impossible (if we exclude the possibility of the presence of tetravalent iron). In all this reasoning it is assumed that the manufacturing precautions have been sufficient to prevent the formation of ferrous iron, all this metal then being present as Fe^{3+} ions.

From the known ionic distribution in $MnFe_2O_4$ (Gorter 1954), and from the strong tendency of Mn^{3+} and Mn^{4+} ions respectively to form square (dsp^2) and octahedral (d^2sp^3) semicovalent bonds in octahedral coordination with O^{2-} ions (Goodenough and Loeb 1955, to be referred to hereafter as *G L*), we should expect to find the following types of manganese ions in the octahedral (*B*) sites of the spinel lattice in the above ranges of composition : (*a*) Mn^{2+} and Mn^{3+}, (*b*) Mn^{3+}, (*c*) Mn^{3+} and Mn^{4+}. In each of these ranges the remaining magnetic ions in *B* sites will be Fe^{3+}, and there will also be some of the latter in the tetrahedral (*A*) sites where they have a moderately strong tendency to form stable tetrahedral (sp^3) semicovalent bonds (*G L*). In ranges (*a*) and (*b*) there will also be some Mn^{2+} ions expected in *A* sites, again with a tendency to form ($s\,p^3$) semicovalent bonds, while from the resistivity measurements of Economos (1954) it appears likely that in ranges (*b*) and (*c*), associated with the $MgMn_2O_4$ constituent, there will be some unstable Mn^{3+} ions in these sites as well, probably behaving like $Mn^{2+} \leftrightharpoons 2Mn^{3+} \leftrightharpoons Mn^{4+}$.

Two theories of indirect exchange have an important bearing on the magnetic properties of such ferrites. (i) According to Zener's (1951) theory of double exchange, the Mn^{3+} ions in *B* sites will be ferromagnetically coupled (parallel spins) with up to an equal number of Mn^{2+} or Mn^{4+} ions in ranges (*a*) and (*c*) respectively. The same is also likely to be true in *A* sites in range (*b*), if Mn^{3+} ions really occur there, while the possible unstable manganese ions in these sites in range (*c*) should also be ferromagnetically coupled. (ii) According to the theory of semicovalent exchange (*GL*), the antiparallel (antiferromagnetic) interaction between semicovalently bonded Fe^{3+} (or Mn^{2+}) ions in *A* sites and the Fe^{3+} and any other predominantly ionically bonded magnetic ions in *B* sites is much stronger than that between the magnetic *A* ions and semicovalently bonded Mn^{3+} or Mn^{4+} ions in *B* sites.

Combining these two theoretical postulates, we can expect that the spins of the Mn^{3+} ions in *B* sites, together with those of any other manganese ions ferromagnetically coupled with them by double exchange, are less likely to be antiparallel to the spins of their nearest-neighbour Fe^{3+} ions in *A* sites than are those of the Fe^{3+} ions in *B* sites. There should thus be a reduction of the net moment of the *B* sublattice compared with the value to be expected if Néel's (1948) law for simple ferrites were followed exactly. This reduction can be conveniently expressed mathematically as resulting from an angle between the spin direction of the exchanging manganese ions (or of the Mn^{3+} ions alone in (*b*)) and that of the other magnetic ions. In the same way, if manganese ions other than Mn^{2+} are found in *A* sites in ranges (*b*) and (*c*), the ferromagnetic coupling of double exchange may lead to a difference between the spin direction of the exchanging ions and that of the other magnetic ions in these sites. The consequent reduction in net moment of the *A* sublattice, relative to that expected with all spins parallel, can similarly be expressed as resulting from an angle between these two spin directions.

In the molecular field approximation used by Néel (1948) for his basic theory of the ferrimagnetism of ferrites, invoking antiparallel interactions between magnetic ions through the superexchange mechanism, the existence of *A–A* and *B–B* interactions as well as the more important *A–B* interactions is a necessity. This concept of non-negligible interactions between ions in the same type of site was extended to explain the occurrence of angles in either the *A* or the *B* sublattice by Yafet and Kittel (1952) for the case of a single kind of magnetic ion, and by Niessen (1953, 1954) for the case of two kinds of magnetic ions, one kind appearing only in *B* sites. Although with the semicovalent exchange treatment it can be shown (Osmond 1956 a) that such *A–A* and *B–B* interactions do not occur in the same way, the molecular field approximation remains the only convenient mathematical treatment of the problem. In this paper Niessen's method is first applied to grouped ions in *B* sites, and is later extended to similar pairs of groups in both sublattices, with the following provisos :

(i) The *A–B* interaction coefficients are to be taken as average values over a relatively small range of compositions.

(ii) The *A–A* and *B–B* interaction terms are introduced to account for different spin directions, without necessarily having their usual physical significance.

(iii) The sublattices into which the main spinel sublattices are further divided are to be considered as convenient mathematical concepts, and not necessarily as representing actual inter-penetrating crystal lattices on which the ions are ordered.

§ 2. ANGLES BETWEEN PARTIAL MAGNETIZATIONS IN THE B SUBLATTICE ONLY

In compositions such as those included in range (a) of the last section we expect the spins of the magnetic ions (Fe^{3+} and Mn^{2+}) in A sites to be parallel, as they are in B sites in $MnFe_2O_4$, on account of their identical electronic configuration ($3d^5$) which here enables them both to form stable (sp^3) semicovalent bonds. We denote by $\mathbf{M}_A$ the total saturation magnetization of this group of ions in Bohr magnetons ($\boldsymbol{\beta}$) per formula unit. In the same way we denote by $\mathbf{M}_B$ the total saturation magnetization of the Fe^{3+} ions and any non-exchanging Mn^{2+} ions in B sites, the spins of which will again be expected to be mutually parallel. These two groups are therefore of precisely the same type. Finally we denote by $\mathbf{M}_B'$ the total saturation magnetization of the other magnetic ions in B sites, consisting of the Mn^{3+} ions and up to the same number of Mn^{2+} ions, all spins being parallel through the ferromagnetic coupling of double exchange. There is thus a close analogy between this grouping and the simpler case of single ions treated by Niessen (1953) in a general way and later (1954) in more detail.

Following Niessen, but with the proviso (iii) given at the end of § 1, we now imagine the B sublattice to be further divided into two sublattices B_{I} and B_{II}, with half of each group of ions located in each sublattice in such a way that the two partial magnetizations $\frac{1}{2}\mathbf{M}_B$ make equal angles ϕ with the direction antiparallel to $\mathbf{M}_A$ and the two partial magnetizations $\frac{1}{2}\mathbf{M}_B'$ make equal angles ϕ' with the same direction. This symmetrical arrangement is shown in fig. 1. It is clear that the resultant moment of the B sublattice as a whole is antiparallel to that of the A sublattice, the net moment per formula unit for the ferrite being

$$n_\beta = |M_B \cos\phi + M_B' \cos\phi' - M_A|, \quad . \quad . \quad . \quad . \quad (1)$$

which naturally reduces to the simple Néel (1948) form when $\phi=0=\phi'$.

We next need exchange interaction coefficients for the molecular field approximation. Again following Niessen, subject to the provisos (i) and (ii) given at the end of § 1, we define the following coefficients.

n proportional to the absolute value of the antiparallel (negative) exchange integral between two M ions when one is on an A site and one on a B site,

n' a similar coefficient for use when one of the two ions is an M' ion,

n'' a similar coefficent which would apply if both exchanging ions were M' ions.

γ_1 the absolute value of the ratio of the antiparallel B_{I}–B_{I} or B_{II}–B_{II} interaction to the corresponding A–B interaction for all combination of groups,

γ_2 the similar ratio of the B_{I}–B_{II} interaction to the A–B interaction.

A logical extension of the first set of definitions is the assumption $nn''=n'^2$ or $z=n/n'=n'/n''$. Strictly speaking we should have three different coefficients γ_1 and three different γ_2 to take account of the different possible combinations of interacting ions. However, only one of the γ_1 occurs in molecular field components which involve the angles, so that a single coefficient is alone required here. We follow Niessen in justifying the use of a single γ_2 by the assumption that the physical differences between the different types of ions are sufficiently accounted for by the differences between the values n, n', n''.

According to the molecular field theory the field h_{bI} giving rise to the partial magnetization $\frac{1}{2}\mathbf{M}_{\mathrm{B}}$ in sublattice B_{I} has the direction of this magnetization. The contribution to this field of each of the other partial magnetizations is antiparallel to the particular partial magnetization concerned, and therefore has a component perpendicular to the direction of h_{bI} on account of the angles ϕ, ϕ'. The algebraic sum of these perpendicular components must then vanish. Thus

Fig. 1

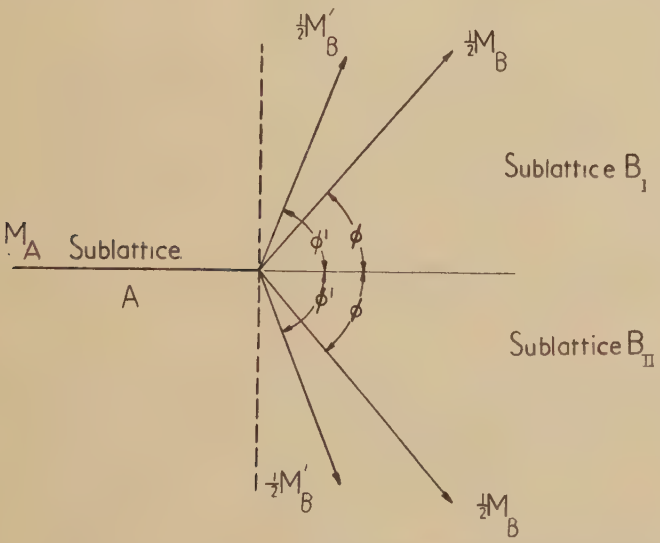

Symmetrical arrangement of partial magnetizations when two different ion groups are found in the B spinel sublattice only.

$$nM_A \sin\phi = \gamma_2 n\tfrac{1}{2}M_B \sin 2\phi + \gamma_2 n'\tfrac{1}{2}M_B' \sin(\phi'+\phi) - \gamma_1 n'\tfrac{1}{2}M_B' \sin(\phi'-\phi).$$

Writing $z = n/n'$ and $y = \sin\phi'/\sin\phi$ this expression reduces to

$$2zM_A = 2z\gamma_2 M_B \cos\phi + (\gamma_2+\gamma_1)M_B' \cos\phi' + y(\gamma_2-\gamma_1)M_B' \cos\phi. \qquad (2)$$

Similarly, from the components of the molecular field h_{bI}' giving rise to the partial magnetization $\frac{1}{2}\mathbf{M}_B'$ in the same sublattice we find the condition

$$n'M_A \sin\phi' = \gamma_1 n'\tfrac{1}{2}M_B \sin(\phi'-\phi) + \gamma_2 n'\tfrac{1}{2}M_B \sin(\phi'+\phi) + \gamma_2 n''\tfrac{1}{2}M_B' \sin 2\phi,$$

which, since $n'/n'' = n/n' = z$, leads to

$$2zM_A = (z/y)(\gamma_2-\gamma_1)M_B \cos\phi' + z(\gamma_2+\gamma_1)M_B \cos\phi + 2\gamma_2 M_B' \cos\phi'. \quad . \quad (3)$$

On account of the symmetry of the arrangement the same two expressions are derived by considering the molecular fields giving rise to the two partial magnetizations in sublattice B_{II}.

Equating expressions (2) and (3) for $2zM_A$ we find

$$y\cos\phi(\gamma_2-\gamma_1)(zM_B+yM_B')=\cos\phi'(\gamma_2-\gamma_1)(zM_B+yM_B'), \quad . \quad . \quad . \quad (4)$$

with possible solutions

(i) $\cos\phi/\cos\phi'=1/y=\sin\phi/\sin\phi'$, hence $\phi=\phi'$,

(ii) $\gamma_2=\gamma_1$.

Niessen (1954) adopts the first solution, thus inherently preserving the physical distinction between the sublattices B_{I} and B_{II} indicated by $\gamma_1\neq\gamma_2$. However, in the resulting simplification of the identical expressions (2) and (3) γ_1 disappears and we find

$$zM_A=\gamma_2(zM_B+M_B')\cos\phi. \quad . \quad . \quad . \quad . \quad . \quad (5\,a)$$

In the present instance of grouped ions, very possibly with different relative reductions of the resolved net moment in the direction antiparallel to the moment of the A sublattice, it seems preferable to adopt the second solution $\phi\neq\phi'$, $\gamma_1=\gamma_2$. This means that the two B sublattices are equivalent as regards average mutual interaction effects, which is a logical deduction from the basic supposition that the subdivision is a convenient mathematical fiction rather than a physical reality. Writing $\gamma=\gamma_1=\gamma_2$, each of expressions (2) and (3) reduces to

$$zM_A=\gamma(zM_B\cos\phi+M_B'\cos\phi'). \quad . \quad . \quad . \quad . \quad . \quad . \quad (5\,b)$$

In the type of ferrite being considered we should expect no angles at all if there were no Mn^{3+} ions present, i.e. when $M_B'=0$. If therefore relation (5 *b*) may be considered as a legitimate formula right down to this limit we find

$$\gamma=M_A/M_B=\lambda/\mu, \quad . \quad . \quad . \quad . \quad . \quad . \quad . \quad . \quad (6)$$

where λ and μ are the relative proportions in A and B sites respectively of the numbers of equivalent ions (Fe^{3+} and Mn^{2+}) subject to the strongest A–B antiparallel interactions. In other words, the degree of departure of the spin directions of either B site group from complete antiparallelism to all the A site spins increases as the proportion of the Fe^{3+} group in B sites decreases relative to that in A sites. Although, on account of the presence of neutral ions such as Mg^{2+}, the relative variation of the three groups will not necessarily be linear, the above statement is equivalent to saying that the departure from antiparallelism should increase with increasing relative proportion of the Mn^{3+} group. The mathematical treatment thus predicts a trend which is physically plausible.

Substituting for γ in eqn. (5 *b*) we find

$$zM_B(1-\cos\phi)=M_B'\cos\phi', \quad . \quad . \quad . \quad . \quad . \quad . \quad . \quad . \quad (7)$$

whence, from (1), the magnetic moment per formula unit is

$$n_\beta=|M_B\{(1-z)\cos\phi+z\}-M_A|. \quad . \quad . \quad . \quad . \quad . \quad . \quad (8)$$

If this net moment is to remain antiparallel to that of the A sublattice even when $M_B < M_A$, $(1-z)\cos\phi > 1-z$, whence $z > 1$, which is the actual situation assumed in this discussion. When this is true we find from (8)

$$(z-1)(1-\cos\phi)=(n_\beta+M_A-M_B)/M_B, \quad \ldots \quad (9\,a)$$

whence, from (7)

$$(1-1/z)\cos\phi'=(n_\beta+M_A-M_B)/M_B'. \quad \ldots \quad (9\,b)$$

In all these formulae the values of M_A, M_B, M_B' and n_β are assumed to be those per formula unit at the particular temperature considered. The temperature variation of the saturation moment of the different ions concerned will not be the same, but at 0°K each group moment will be the sum of the products of concentration, g factor and spin factor for its individual ions. Conveniently the g factor is 2 for Fe^{3+} and Mn^{2+} ions (Gorter 1954) and approximately so (1.99) for Mn^{3+} (Jonker and van Santen 1950), while the spin factor $j/2$ is 5/2 for the two former and 2 for the latter. For comparison of the theory with experiment we should require accurate measurements of the net magnetic moment extrapolated to 0°K, determination of the ionic distribution by X-rays or neutron diffraction, and knowledge of the non-divalent manganese content by chemical analysis.

§ 3. ANGLES BETWEEN PARTIAL MAGNETIZATIONS IN BOTH A AND B SUBLATTICES

It was shown in § 1 that in the composition ranges (b) and (c) there is the possibility of unstable Mn^{3+} ions in A sites, as well as the Fe^{3+}, and in (b) Mn^{2+}, ions expected there, while in both ranges there will be two groups of ions in B sites of the types already considered. In such cases it is equally logical to divide the A ions into two groups, one containing the Mn^{3+} ions, and the other the Fe^{3+} ions, and to consider that the two groups will be subject to A–B interactions of different strengths. We now have two groups of the same two kinds in both A and B sublattices. We can thus extend the formal molecular field treatment to both these sublattices, symbolically dividing each into two further sublattices with the symmetrical geometrical arrangement of partial magnetizations shown in fig 2. The net magnetic moment per formula unit is directed along the axis of symmetry and given by

$$n_\beta=|M_B\cos\phi+M_B'\cos\phi'-(M_A\cos\psi+M_A'\cos\psi')|. \quad . \quad (10)$$

For the mathematical molecular field expressions we retain the interaction coefficients n, n', n'', and γ alone in place of γ_1, γ_2, with the same provisos as before, and we introduce the coefficient α for the absolute value of the ratio of any antiparallel A–A interaction to the corresponding A–B interaction, for all combinations of groups. The single 'average' coefficients α and γ simplify these expressions in spite of the extra terms due to the second group of A ions. The condition that the molecular field $h_{b\mathrm{I}}$ giving rise to the partial magnetization $\frac{1}{2}\mathbf{M}_B$ in sublattice B_{I} should be parallel to this magnetization is now

$$(nM_A \cos\psi + n'M_A' \cos\psi') \sin\phi = n'\gamma M_B' \cos\phi' \sin\phi + n\gamma\tfrac{1}{2}M_B \sin 2\phi,$$

which, with $n/n'=z$ and $\phi\neq 0$, gives

$$zM_A \cos\psi + M_A' \cos\psi' = \gamma(zM_B \cos\phi + M_B' \cos\phi'). \qquad (11)$$

On account of the assumption $n'/n''=n/n'=z$ we find exactly the same quasi-symmetrical relationship by considering the molecular field acting on the partial magnetization $\frac{1}{2}\mathbf{M}_B'$ in the same sublattice, and naturally also, from symmetry, if we consider either of the partial magnetizations in sublattice B_{II}. Applying now the same treatment to the partial magnetizations of the A lattice we arrive by similar steps at the relation

$$zM_B \cos\phi + M_B' \cos\phi' = \alpha(zM_A \cos\psi + M_A' \cos\psi'), \qquad (12)$$

from which in conjunction with (11) we find $\alpha = 1/\gamma$, a result which was only to be expected from the somewhat idealized symmetrical mathematical arrangement. Moreover, since in the limit when $M_A'=0$ we expect $\psi=0$ and we have the case studied in § 2, we find for this more general case

Fig. 2

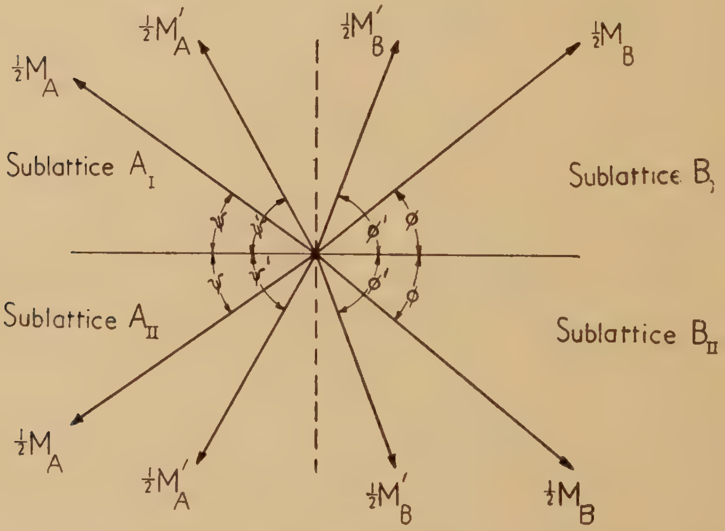

Symmetrical arrangement of partial magnetizations when two different ion groups are found in both A and B spinel sublattices.

$$\alpha = 1/\gamma = M_B/M_A. \qquad (13)$$

As in the last section, the physical interpretation to be given to this mathematical result is that a relative decrease in the number of ions of the Fe^{3+} group in either sublattice, or increase in the number of ions of the Mn^{3+} group in the same sublattice, compared with the number of ions of the former type in the other sublattice, leads to fewer of the spins in the first two groups being antiparallel to the net moment of the second sublattice. This is a trend which it is reasonable to expect over a relatively small range of compositions, and it is only for small ranges that we can assume the value z of the ratios n/n' and n'/n'' to be virtually constant when dealing with grouped ions.

If we now write $r_A = M_A'/M_A$ and $r_B = M_B'/M_B$ in eqn. (12) we find

$$M_B(z \cos \phi + r_B \cos \phi') = \alpha M_A(z \cos \psi + r_A \cos \psi'),$$

whence, from (13)

$$z(\cos \phi - \cos \psi) = r_A \cos \psi' - r_B \cos \psi', \quad . \quad . \quad . \quad . \quad (14)$$

which is the counterpart of relation (7) in § 2. We cannot here combine this result with (10) to obtain such moderately straightforward expressions as (9 a) and (9 b) of that section. However, if through any change in composition the value of z $(\cos \phi - \cos \psi)$ remains virtually unaltered, the relative changes in the values of ψ' and ϕ' must depend very much upon the initial and final values of r_A and r_B.

In any range of compositions for which these simple theoretical results are substantially applicable, relation (13) indicates that for $M_B > M_A$ the reduction in the net A lattice moment may well be greater than that of the net B lattice moment, since $\alpha > 1 > \gamma$ so that ψ would tend to be larger than ϕ, and possibly also ψ' larger than ϕ'. In these circumstances the total net moment might then be greater than the value $M_B + M_B' - (M_A + M_A')$ given by the simple Néel formula. The opposite might be expected for $M_A > M_B$.

§ 4. CONCLUSION

In this paper the molecular field treatment of the magnetization of simple ferrites by indirect exchange has been applied to more complex ferrites having two dissimilar groups of magnetic ions, one of which contains Fe^{3+} ions, in one or both of the spinel sublattices. The particular type considered is that in which the second group is based on Mn^{3+} ions, for which strong nearest neighbour A–B semicovalent exchange interactions (Goodenough and Loeb 1955), depending on oxygen p^3 orbitals directed towards tetrahedral A sites, are expected to be virtually non-existent. The A–A, B–B interaction coefficients and postulated angles are considered as convenient mathematical tools for estimating the results of physical differences rather than as having a physical existence themselves.

There are at present no detailed data available by which to check the accuracy of the magnetization trends to be expected from this theoretical treatment, and for reasons of space we shall not repeat here the results found from the values of maximum flux density at room temperature reported by Economos (1954) for a series of magnesium manganese ferrites in the composition ranges (a) and (b) of § 1. This has been done elsewhere (Osmond 1956 b), using the results only of the present theoretical work, with satisfactory confirmation of the theoretical trends, considering the inaccuracies inherent in the necessary averaging factors and assumed ionic distributions.

ACKNOWLEDGMENTS

I wish to thank Mr. P. E. Trier, Manager of the Mullard Research Laboratories, for permission to publish this paper, and Dr. K. Hoselitz, Head of the Solid State Physics Group, for his interest and encouragement.

REFERENCES

ECONOMOS, G., 1954, Laboratory for Insulation Research, *M.I.T.*, *Technical Report* 78.

GOODENOUGH, J. B., and LOEB, A. L., 1955, *Phys. Rev.*, **98,** 391.

GORTER, E. W., 1954, *Philips Res. Rep.*, **9,** 295–365, 403–443.

JONKER, G. H., and VAN SANTEN, J. H., 1950, *Physica*, **16,** 337.

NÉEL, L., 1948, *Ann. Phys., Paris*, **3,** 137.

NIESSEN, K. F., 1953, *Physica*, **19,** 1035 ; 1954, *Philips Res. Rep.*, **9,** 197.

OSMOND, W. P., 1956 a, offered to I.E.E. for presentation at the Convention on Ferrites, Autumn 1956 ; 1956 b, offered for publication in *Proc. Phys. Soc.* B.

YAFET, Y., and KITTEL, C., 1952, *Phys. Rev.*, **87,** 290.

ZENER, C., 1951, *Phys. Rev.*, **82,** 403.

CXVII. *The Height Variation of Upper Atmospheric Winds*

By J. S. Greenhow and E. L. Neufeld
Jodrell Bank Experimental Station, University of Manchester †

[Received February 29, 1956 and in revised form March 29, 1956]

Abstract

The radio echo meteor technique has been used to investigate the variation of wind velocity with altitude in the 80–100 km region. Phase changes of 5 deg km^{-1} are found in the 12 hour periodic wind and the amplitude of this component also increases by about 1 m sec^{-1} km^{-1} with height. There is also a uniform height gradient of 0·5 m sec^{-1} km^{-1} in the prevailing wind. The variations in the periodic wind are considered in relation to the theory of atmospheric oscillations.

§ 1. Introduction

Two principal methods are available for the systematic observation of winds in the 100 km region above the earth. These are the ionospheric echo fading technique employing three spaced receivers, and the radio echo observation of drifting meteor trails. Because of the properties of ionized meteor trails the second method is especially suited to the investigation of the variation of wind velocity with height. The height of reflection can be determined to within ±1 km, independently of time of day, season, or radio wavelength.

Meteor wind observations have been in progress for a number of years, principally at Jodrell Bank (Greenhow 1952, 1954, Greenhow and Neufeld 1955 a) and Adelaide (Elford and Robertson 1953). Measurements have shown the presence of large periodic and prevailing wind components in the meteor region. Previous results have been restricted to a rather limited height range between 90 and 95 km, although there is evidence for quite large wind gradients even over this height difference. Of particular interest is the height variation of the solar semi-diurnal wind component. Preliminary observations (Greenhow and Neufeld 1955 a) have shown that the amplitude and phase of this component may change considerably with height, and this paper describes an investigation of the variations between 80 and 100 km for the year September 1954–August 1955.

§ 2. Technique

The coherent pulse system used for measuring drift velocities of meteor trails has been described previously (Greenhow 1954). The heights of reflection are estimated from echo duration, using an experimental curve relating echo decay time and altitude (Greenhow and Neufeld 1955 b) In the calibration experiment meteor heights were measured using a split beam technique (Clegg and Davidson 1950). The height of reflection can be determined to within ±3 km from the rate of decay ; which is satisfactory for grouping the observations at 5 km height intervals.

---

† Communicated by Professor A. C. B. Lovell, F.R.S.

Five duration groups are used (where echo duration is measured from maximum to half maximum amplitude) : approximately 0·015–0·03, 0·03–0·07, 0·07–0·15, 0·15–0·30 and 0·30–0·60 sec. These correspond to height ranges 97·5–102·5, 92·5–97·5, 87·5–92·5, 82·5–87·5 and 78·5–82·5 km. Above 102·5 km the echo duration is too short to enable an accurate measure of the wind velocity to be obtained, although echoes are observed up to 110 km. The number of echoes recorded below 80 km is very small, and integration of results obtained over a long period will be necessary in order to determine the wind velocity below this height.

§ 3. PRESENTATION OF RESULTS

(*a*) *Velocity Distributions*

North–South and East–West components of wind velocity are measured by directing a beamed aerial alternately in these directions. In the first years observations all the individual wind measurements from 50–500 meteors observed in each hourly interval were grouped together. The diurnal variations in wind velocity thus referred to a mean height between 90 and 95 km, where most meteors are observed (Greenhow and Neufeld 1955 a).

Between September 1954–August 1955 continuous observations were made on 2–3 days each month. The echoes obtained during each hour have been divided into the height groups listed in § 2. Figure 1 shows an example of the velocity distributions obtained in this way. The N–S wind component is seen to change from 50 m sec^{-1} towards North at a height of 100 km, to 50 m sec^{-1} towards South at 85 km showing the ability of the method to resolve differences in wind velocity at 5 km height intervals.

Because of the low echo rate in the afternoon and evening, subdivision of the results into groups such as in fig. 1 is not always possible. Thus while hour by hour wind variations in the 90 and 95 km height groups can usually be made throughout the day, at 85 and 100 km an accurate wind determination can often be made only between midnight and midday. The echo rate in the 80 km height group is not sufficiently high to enable the mean wind speed in any hour to be determined from a single days observations.

The diurnal variations in wind velocity will now be considered in detail

(*b*) *Component Plots*

Following previous practice NS and EW components of wind velocity are plotted at hourly intervals. Examples of the results obtained for four heights are given in figs. 2 and 3. Figure 2 shows the observations for November 18–19, 1955 when it was only possible to measure the wind in all four height regions during the night. In the N–S direction 12-hour oscillations in the wind are present at all heights. The amplitude of the oscillation decreases with decreasing height, falling from approximately 60 m $\sec^{-1}$ at 100 km, to 20 m $\sec^{-1}$ at 85 km.

Fig. 1

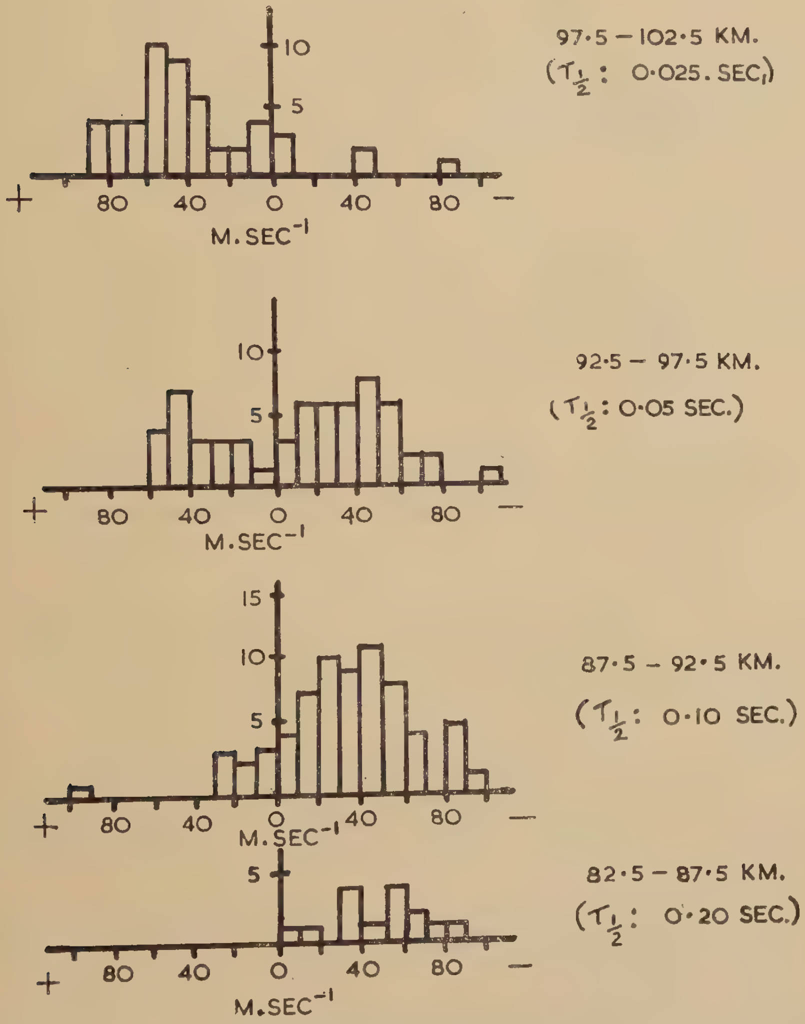

North–South components of wind velocity 0300–0500 hr. Jan. 12–13, 1955. (Movements towards North +ve.) Histograms showing distributions of individual meteor drift velocities at heights between 82·5 and 102·5 km.

Equally well marked is the height variation in phase of this semi-diurnal wind component. Maximum velocity towards North occurs near 0500 hr at 100 km, 0700 at 95 km, 0900 at 90 km, and 1200 at 85 km.

This is a mean phase change of approximately 12° km^{-1}, the oscillation leading at greater heights.

Similar results are obtained in the EW direction, but with a phase lag of 90° behind the NS component. Thus maximum East velocity always occurs 3 hours later than maximum North velocity, corresponding to a complete rotation of the wind vector in 12 hours. The mean wind shear is again 3 m sec^{-1} km^{-1}, and the change in phase approximately 12° km^{-1}.

Fig. 2

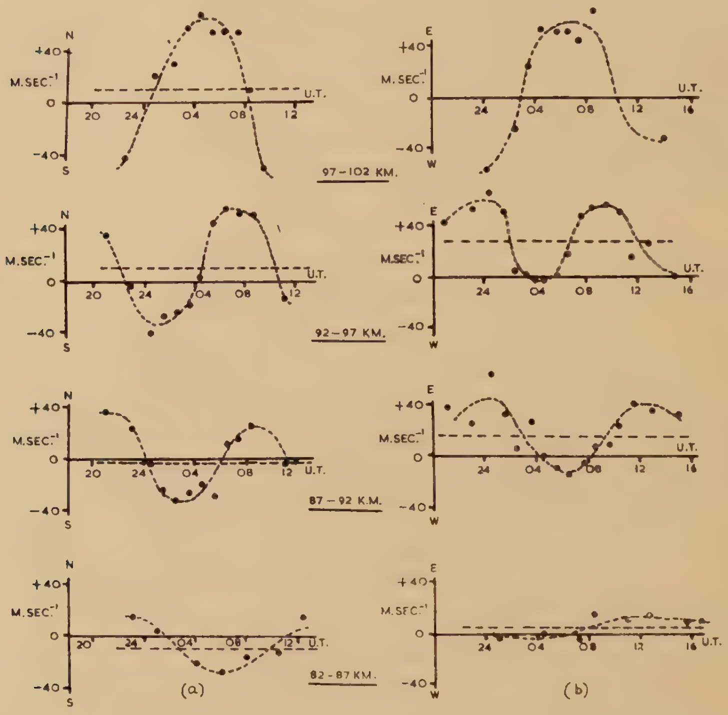

Variation of wind velocity with height.

(*a*) North–South components of wind velocity Nov. 18–19, 1954. (Movements towards North $+^{\mathrm{ve}}$.)

(*b*) East–West components of wind velocity. Nov. 18–19, 1954. (Movements towards East $+^{\mathrm{ve}}$.)

Similar phase and amplitude variations are observed in the complete September day shown in fig. 3, although the changes are smaller in magnitude. The September observations are discussed in § 4, when the method of analysis is described.

§ 4. HARMONIC ANALYSIS OF DAILY OBSERVATIONS

(*a*) *Method of Analysis*

Twenty-four hour component plots of the type illustrated in fig. 3 are analysed to give the first three terms of the Fourier series,

$$V_{NS}=A_1+B_1 \sin \pi/12(T+t_1')+C_1 \sin \pi/6\,(T+t_1'') \quad . \quad (1)$$

$$V_{EW}=A_2+B_2 \sin \pi/12\,(T+t_2')+C_2 \sin \pi/6\,(T+t_2''). \quad . \quad (2)$$

In the NS direction, for example, A_1 is the mean wind speed during 24 hours, and gives the prevailing wind component. B_1 is the amplitude of the 24 hr periodic wind component, and t_1' its phase. Similarly C_1 and t_1'' are the amplitude and phase of the 12 hr periodic component.

Fig. 3

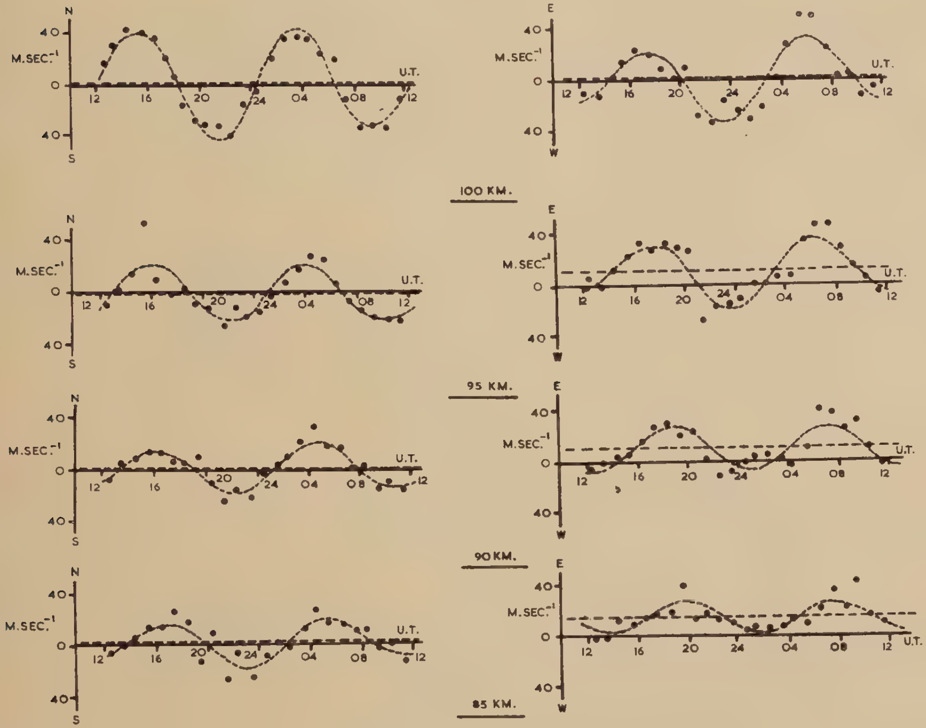

September 16–17, 1954. Height variation of North–South and East–West wind components. The constant and sum of the first two periodic terms of the Fourier series are shown as broken curves.

100 km $V_{NS}=+\ 1{\cdot}4+\ 6{\cdot}6 \sin \pi/12\,(t-2{\cdot}3)+40{\cdot}0 \sin \pi/6\,(t-0{\cdot}4)$
$V_{EW}=+\ 2{\cdot}2+12{\cdot}5 \sin \pi/12\,(t-3{\cdot}4)+26{\cdot}5 \sin \pi/6\,(t-3{\cdot}0)$
95 km $V_{NS}=-\ 2{\cdot}6+\ 2{\cdot}8 \sin \pi/12\,(t-3{\cdot}6)+23{\cdot}0 \sin \pi/6\,(t-1{\cdot}1)$
$V_{EW}=+10{\cdot}7+10{\cdot}9 \sin \pi/12\,(t-4{\cdot}9)+23{\cdot}0 \sin \pi/6\,(t-3{\cdot}2)$
90 km $V_{NS}=+\ 0{\cdot}2+\ 5{\cdot}1 \sin \pi/12\,(t-0{\cdot}4)+18{\cdot}1 \sin \pi/6\,(t-1{\cdot}5)$
$V_{EW}=+\ 8{\cdot}9+\ 1{\cdot}9 \sin \pi/12\,(t-3{\cdot}0)+16{\cdot}9 \sin \pi/6\,(t-4{\cdot}3)$
85 km $V_{NS}=+\ 1{\cdot}8+\ 4{\cdot}7 \sin \pi/12\,(t-3{\cdot}8)+15{\cdot}8 \sin \pi/6\,(t-2{\cdot}2)$
$V_{EW}=+13{\cdot}8+\ 1{\cdot}6 \sin \pi/12\,(t-3{\cdot}8)+12{\cdot}0 \sin \pi/6\,(t-5{\cdot}0)$

T is the time in hours measured from 0000 hr. Phase is defined such that maximum velocity towards North (or East) occurs when $T+t=06$ hr for the 1st harmonic and 03 hr for the 2nd harmonic. When observations are available for only half a day, the diurnal term is omitted.

The results for a complete day in September 1954 are given in fig. 3. The smooth curves represent the first three terms of the Fourier series V_{NS}, V_{EW} (eqns. (1), (2)). There is good agreement between the experimental and theoretical points, showing that harmonics higher than the second are negligible. The amplitudes and phases of the NS and EW semi-diurnal wind components shown in fig. 3 are represented on harmonic dials in figs. 4 (*a*) (*b*). The individual points show the time of maximum velocity towards North (or East). The changes in amplitude and phase with height are very clear, the variations in both directions being similar except for the constant phase difference of 3 hours.

The 24-hour harmonics are shown on a single harmonic dial in fig. 4 (*c*). There are no regular variations in either amplitude or phase with height, and no significant difference between the phases in NS and EW directions. A true diurnal rotating vector would, of course, show a 6 hour phase difference between maximum North and maximum East velocity. The mean diurnal wind has a magnitude of only 5 m sec⁻¹, and is probably due to irregularities in the prevailing and semi-diurnal wind components. For this reason the 24-hour harmonic may be neglected when determining the prevailing wind from only 12-hours observations.

Fig. 4

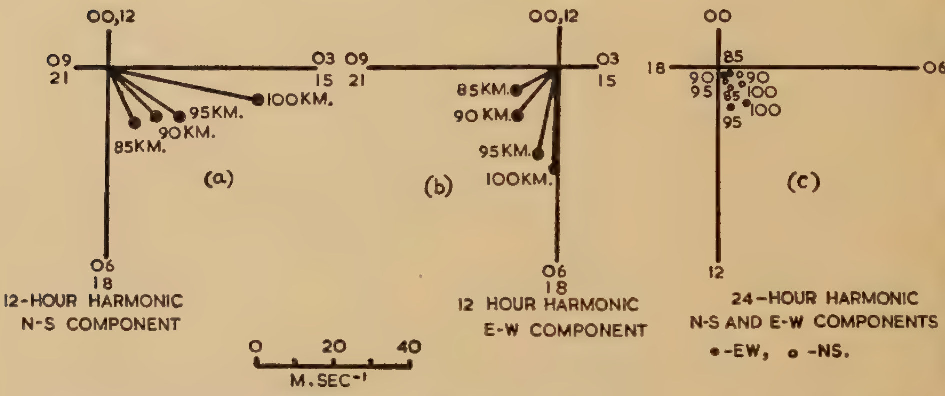

Harmonic dials showing height variation of semi-diurnal and diurnal wind components, Sept. 16–17, 1954.

(*b*) 12-*hour Harmonic Dials*

The height variations of the semi-diurnal wind component for the year September 1954–August 1955 are summarized by the series of harmonic dials in fig. 5. Separate dials are used for each height group, and for both NS and EW components. Inspection of any individual harmonic dial shows that large seasonal variations in the amplitude and phase of the 12-hour wind component occur. Smooth lines have been drawn through the points for individual months or groups of months. An attempt has been made to draw similar curves for each harmonic dial, so that the trend of the variations at different heights and in both directions may be compared at a glance. Between September and

Fig. 5

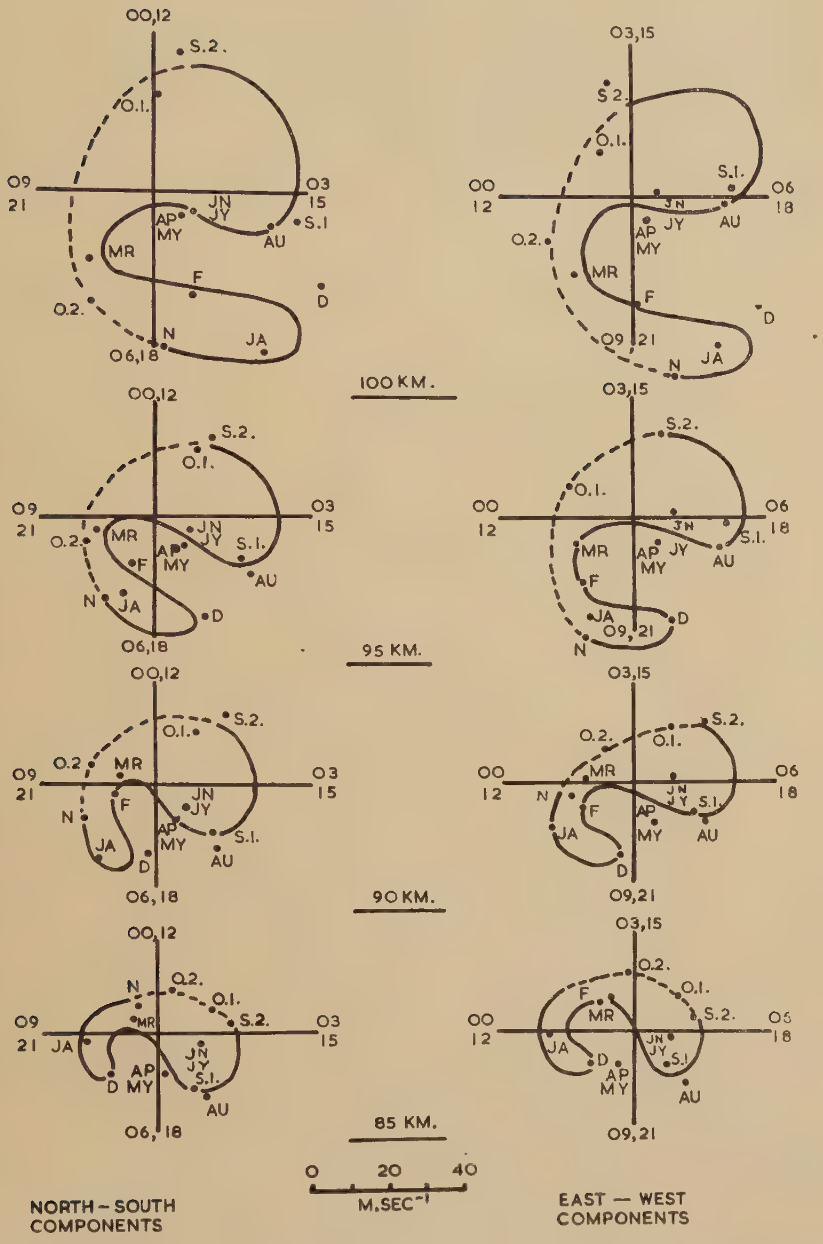

12-hour harmonic dials. North–South and East–West components at heights of 85, 90, 95 and 100 km.

November when the phase of the 12-hour harmonic undergoes a reversal the curve has been discontinued. This variation which has repeated itself during 3 successive years is extremely complex, and will be discussed in a later paper. North–South components for four height groups are shown in the left hand vertical column. Inspection of the smooth curves shows that the whole pattern decreases in size at lower heights, because of the decrease in amplitude of the wind component. Further, in successive harmonic dials the pattern slowly rotates, showing a phase change of approximately 90° between the 100 km and 85 km height groups.

Fig. 6

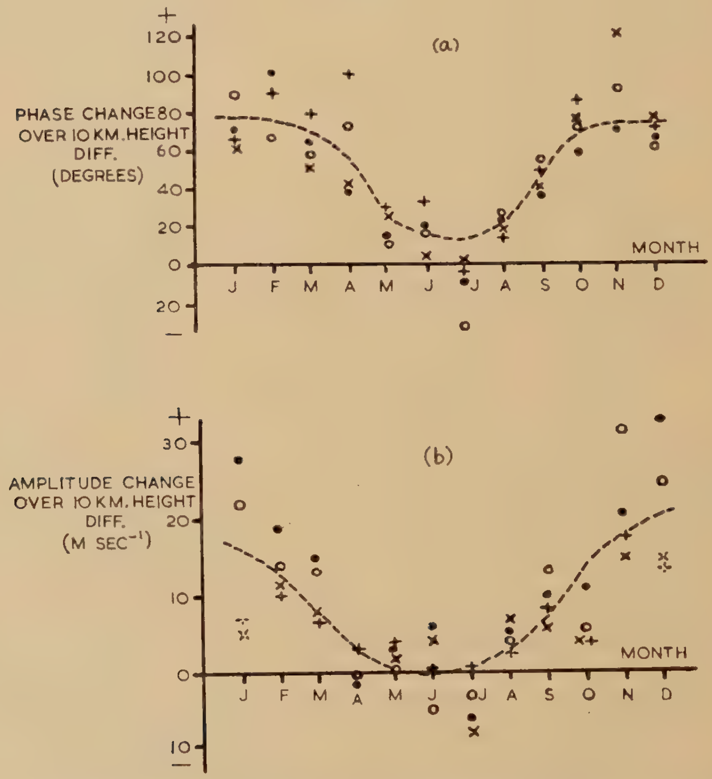

(*a*) Change in phase of semi-diurnal wind component over a height difference of 10 km. +ve change is phase lead at greater heights.

(*b*) Change in amplitude of semi-diurnal wind component over a height difference of 10 km.

90–100 km : ●N–S comp. ; ○E–W comp.
85–95 km : ×N–S comp. ; +E–W comp.

Harmonic dials for EW components are shown in the right hand column, and similar variations in amplitude and phase are observed at all heights. The EW dials have been rotated through 90°, to take account of the 3-hour period required for the wind vector to rotate from North to East As the NS and EW components of wind velocity determined by the present method give two independent measurements of the 12-hour harmonic, the similarities between the two series of harmonic dials gives good confirmation of the observed changes in amplitude and phase.

(*c*) *Variation of Phase of* 12-*hour Component with Height*

The rate of change of phase with height is found to vary with season. In fig. 6 (*a*) the phase change for a 10 km height difference is plotted for each month of the year in order to illustrate this seasonal effect. To make full use of the observations the difference in phase between 100–90 km, and 95–85 km are measured, for both NS and EW components. This method gives four determinations of the phase change over a height range of 10 km for each month. In fig. 6 (*a*) a positive change corresponds to a phase lead at greatest heights. A smooth line drawn through the points shows that the phase difference per km undergoes a marked seasonal change, varying from a mean value of 7° km^{-1} in winter to 3° km^{-1} in summer. The average annual value is approximately 5° km^{-1}.

(*d*) *Variation in Amplitude of the* 12-*hour Component with Height*

The rate of change in amplitude of the semi-diurnal wind component with height also varies with season. In fig. 6 (*b*) the amplitude change for a 10 km height difference is plotted for each month of the year. Once again the differences between 100–90 km, and 95–85 km are measured for both N–S and E–W components. In winter the magnitude of the wind gradient is approximately $1{\cdot}5\ \text{m sec}^{-1}\ \text{km}^{-1}$, falling to only $0{\cdot}4\ \text{m sec}^{-1}\ \text{km}^{-1}$ in summer. Thus in summer-time the amplitude of the semi-diurnal wind component is almost constant, increasing from only 10 to 15 m sec^{-1} over the observed height range, while in winter the amplitude is approximately 10 m sec^{-1} at 85 km increasing to over 30 m sec^{-1} at 100 km.

If the winter gradient of $1{\cdot}5\ \text{m sec}^{-1}\ \text{km}^{-1}$ is extrapolated to lower heights, it would suggest that the amplitude of the periodic wind falls to zero at 75 km. However, the mean gradient over the 90–100 km height range is twice as great as that over the 85–95 km region, the respective values being $2{\cdot}0$ and $1{\cdot}0\ \text{m sec}^{-1}\ \text{km}^{-1}$. This suggests that the wind gradient is reduced at lower heights, and that the amplitude of the semi-diurnal wind component falls off less rapidly below 85 km. This view is supported by the summer observations which show an almost constant small amplitude at all heights.

It is interesting to note the similarities between the smooth curves showing the seasonal variations in amplitude and phase of the 12-hour harmonic. These suggest that small amplitude changes are associated with small changes in phase, while large phase changes are accompanied by correspondingly bigger amplitude variations.

(*e*) *Height Variation of Prevailing Wind*

(i) *East–West Component*

Because of the difficulty of presenting the four variables, time, speed, direction and height on a single diagram, the prevailing wind vector has also been resolved into NS and EW components. As an example, the variations in amplitude of the EW component throughout the year at heights of 85 and 100 km are shown in fig. 7 (*a*). It is interesting to observe that although the wind is towards East in summer and winter and towards West in spring and autumn at 100 km, at 85 km the wind remains towards East in autumn. There is thus a negative wind gradient

Fig. 7

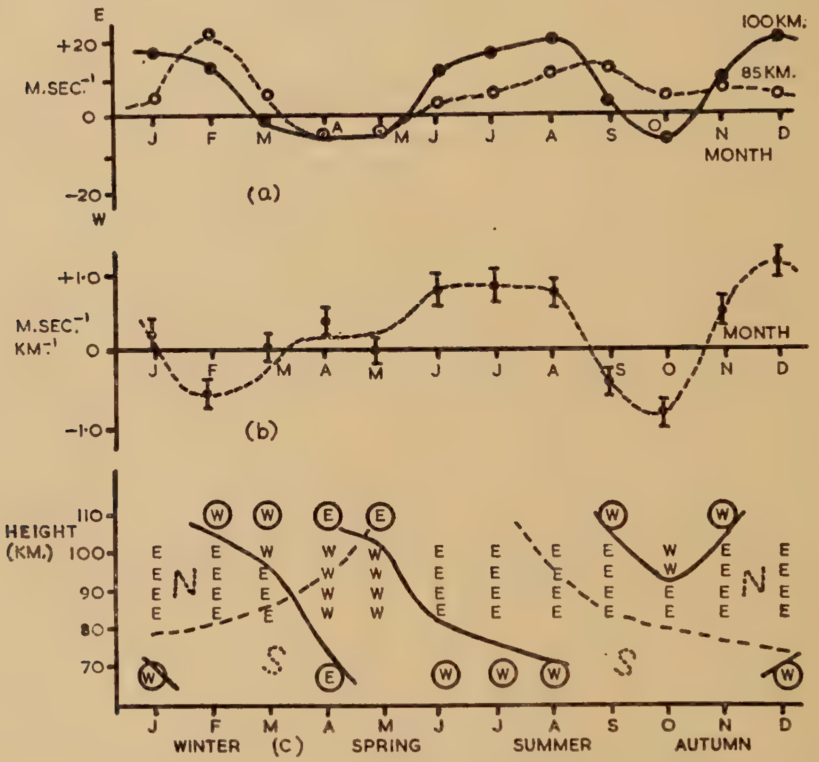

(*a*) Seasonal variation of East–West component of prevailing wind at heights of 85 and 100 km.

(*b*) Gradient of E–W component of prevailing wind. +ve gradient: increase in east or decrease in west velocity with height.

(*c*) Composite diagram showing sign of E–W and N–S components of prevailing wind between 70 and 110 km. (Wind blows towards direction shown.)

at this time. The wind gradient is shown in greater detail in fig. 7 (*b*). As we are dealing with one component of a vector it has been necessary to define a positive wind gradient as one in which the EW wind component increases towards East, or decreases towards West. The point for each month has been determined by measuring the difference in wind velocity over the two 10 km height ranges 85–95 km and 90–100 km. Gradients up to 1 m sec^{-1} km^{-1} are observed during most of the year with negative gradients in February–March and September–October.

Figures 7 (*a*), (*b*) have been combined in 7 (*c*) to show qualitatively the measured wind directions at 85, 90, 95 and 100 km; together with extrapolated values at 110, 70 km. These estimated directions have been deduced in the following manner. In September, for example, the wind blows towards East and the amplitude decreases with height by 0·5 m sec^{-1} km^{-1}, falling to only 2 m sec^{-1} at 100 km. Thus the mean gradient observed over a height range of 15 km has only to continue for another 4 km, and the wind component will reverse sign to West. This view is supported by the October observations, when the reversal actually takes place within the observed height range. Additional evidence for changes in wind direction at levels outside those directly observed is given by inspection of the results for individual days. Thus although from June to August the mean wind is towards East at all heights, on some days the wind becomes West in the lower height groups. Taken in conjunction with the observed mean decrease of velocity of 1 m sec^{-1} km^{-1}, this suggests reversal near 75 km.

Fig. 8

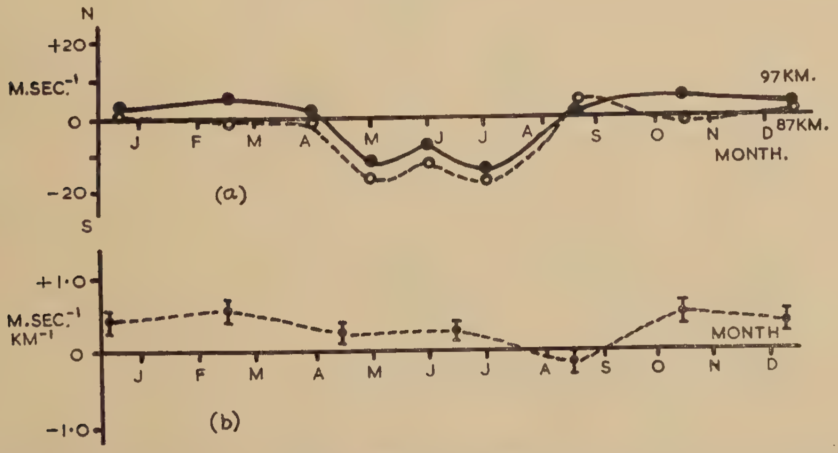

(*a*) Seasonal variation of North–South component of prevailing wind at heights of 85 and 97 km.

(*b*) Gradient of N–S component of prevailing wind.

(ii) *North–South Component*

The seasonal variations of the N–S component of prevailing wind, at heights of 87·5 km and 97·5 km are shown in fig. 8 (*a*). The curves were obtained by integrating the two upper and two lower height groups. At 87·5 km the NS component is approximately zero except from May to August, when large South components are observed. The positive wind gradients of 0·3 m sec^{-1} km^{-1} shown in 8 (*b*) reduce the amplitude of these South components during summer, and produce small North components at other times. The direction of the NS component has been superimposed on the EW components in fig. 7 (*c*). Thus in July, for example, the composite diagram shows that the overall wind vector is towards South–East above 85 km.

It is important to note that the wind gradients displayed in figs. 7 (*b*) and 8 (*b*) not only indicate changes in amplitude of the wind vector, but can arise from a change in wind direction. Because of the small amplitude of the NS component during most of the year, the variations in the overall wind gradient are very similar to those of the EW component.

§ 5. SUMMARY AND DISCUSSION

(*a*) *Comparison with Theory*

(i) *Amplitude of 12-hour Harmonic*

The semi-diurnal wind component is caused by a 12-hour pressure oscillation of the earth's atmosphere, as a result of thermal and tidal effects of the sun. At ground level the amplitude of the oscillation is only 0·001 of atmospheric pressure, and the associated wind system has a theoretical amplitude of only 0·4 m sec^{-1}. This periodic component is obscured by much larger irregular tropospheric winds. At greater

Fig. 9

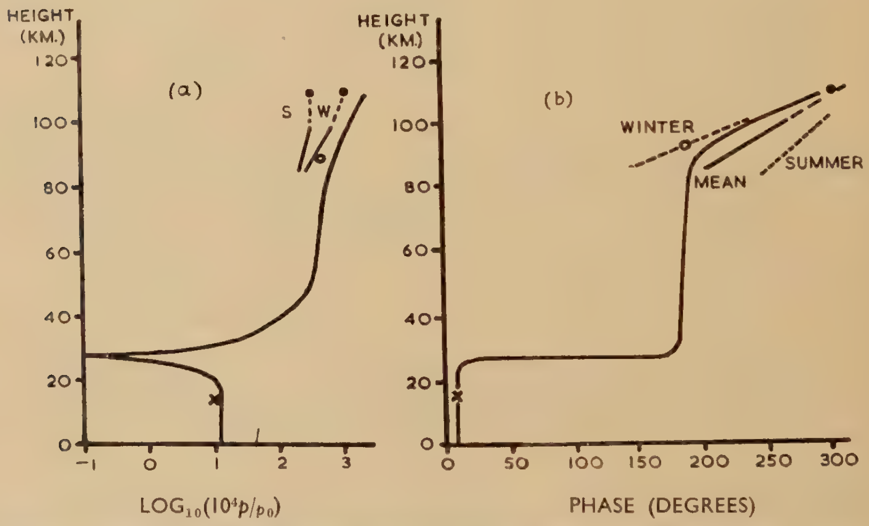

Variation of amplitude and phase of semi-diurnal pressure oscillation with height. Experimental observations are compared with theoretical curves (after Wilkes).

(*a*) Amplitude variation, p_0 is atmospheric pressure, p the amplitude of the 12 hr oscillation.

(*b*) Phase variation.

● Briggs and Spencer. ○ Elford and Robertson (Southern hemisphere summer), × Johnson.

heights, however, the amplitude of the pressure oscillation p is increased many times by resonance (Taylor 1936, Pekeris 1937). Figure 9 shows the predicted variation in amplitude and phase of the semi-diurnal pressure oscillation with height (Wilkes 1949). p_0 is mean atmospheric pressure. The ratio p/p_0 increases from 0·001 at the earth's surface to 0·1 at a height of 100 km with a node at 30 km. The ratio p/p_0 deduced from the observed magnitude of the 12-hour wind component between 85 and 100 km is also shown in fig. 9 (*a*). The magnification of the semi-diurnal pressure oscillation at 100 km varies between 20 and 80, agreeing within a factor of 2 with theory. The observed increase in amplitude of the wind component with height shows reasonable agreement with the theoretical predictions. The mean gradient of 1 m sec^{-1} km^{-1} is very nearly that required by the change in ratio of p/p_0, due to the increase in resonant magnification with height.

(ii) *Phase of* 12-*hour Harmonic*

The predicted variations in phase of the 12-hour pressure oscillations are shown in fig. 9 (*b*). Maximum pressure at the earth's surface occurs at 1000 and 2200 hr local time, and this corresponds to +10° on the arbitrary scale. The pressure oscillation undergoes a phase reversal at the 30 km node, and above this height maximum pressure is at 0400 and 1600 hr. A slow variation in phase of 5° km^{-1} occurs above 80 km the oscillation leading at greater heights.

The wind system associated with the semi-diurnal pressure wave in the northern hemisphere is such that the wind vector is directed towards West when the pressure is a maximum. Thus the observed times of maximum North or West wind components enable the phase of the pressure oscillation to be determined. Experimental curves for the winter and summer, and the annual mean, are shown in fig. 9 (*b*). The theoretical curve agrees well with the mean experimental observations, maximum pressure occurring near 0400 and 1600 hr at 80 km. The observed phase change of 5° km^{-1} is also in agreement with theory.

As in the case of the amplitude variation, seasonal variations in phase are observed at a given height. The exact form of the theoretical curves in fig. 9 depends critically upon the temperature distribution in the upper atmosphere. Thus, seasonal changes in temperature in the high atmosphere could cause variations of the type observed.

(*b*) *Comparison with Other Observations*

Mean wind gradients of +2·3 m sec^{-1} and 3·6 m sec^{-1} throughout the meteor region have been found by the authors (Greenhow 1954) and by Elford and Roberston (1953). It is not clear whether these measurements refer to the periodic components or prevailing wind, although in the case of the measurements of Greenhow some sort of average value was measured. Briggs and Spencer (1954), using the ionospheric echo technique, find that the semi-diurnal wind vector is directed towards

North at 0300 hr. in the northern hemisphere. Assuming a mean height of 110 km for their observations, this result fits in well with the measurements described in the present paper, and suggests that the phase change of 5° km^{-1} continues throughout the E region. The prevailing winds measured by these workers are also approximately twice as fast as those observed in the meteor region, showing a continuation of the steady wind gradient to greater altitudes.

Observations of the semi-diurnal wind system have been made between altitudes of 15–20 km using normal meteorological methods (Johnson 1955). At this height the amplitude of the wind vector is only 0·3 m sec^{-1}, and its phase is that required by a pressure oscillation which is in phase with the pressure oscillation at the earth's surface. These observations are also included in fig. 9, and agree with the theoretical curves below the node at 30 km.

(*c*) *Relation to Sq Variations*

The variation in phase of the semi-diurnal wind component with height is of great interest in consideration of the earth's Sq variations, and the situation of the dynamo region. The quiet day variations in the earth's magnetic field can be explained by an ionospheric wind system of the type discussed if the wind vector is directed towards North at approximately 1100 and 2300 hr. Thus, it is evident that on the basis of existing theory the dynamo region does not lie between 85–110 km. However, evidence is now available that between these heights there is a progressive change in phase of the semi-diurnal wind component; time of North velocity advancing from 0730 to 0300 hr. Extrapolation to a height where maximum velocity to North occurs at 2300 hr. indicates that the dynamo region is at a height of approximately 135 km in temperate latitudes. This is within the range suggested by Baker and Martyn (1952) but considerably above the height of 105 km observed during rocket flights near the magnetic equator (Singer *et al.* 1952).

§ 6. ACKNOWLEDGMENTS

The upper atmosphere wind measurements have been carried out at the Jodrell Bank Experimental Station, University of Manchester. We wish to thank Professor A. C. B. Lovell, Director of the Station, for his interest in the investigation. One of the authors (J. S. G.) is indebted to Messrs. I.C.I. for a research fellowship.

REFERENCES

Baker, W. G., and Martyn, D. F., 1952, *Nature, Lond.*, **170,** 1090.
Briggs, B. H., and Spencer, M., 1954, *Phys. Soc. Rep. Prog. Phys.*, **17,** 245.
Clegg, J. A., and Davidson, I. A., 1950, *Phil. Mag.*, **41,** 77.
Elford, W. G., and Robertson, D. S., 1953, *J. Atmos. Terr. Phys.*, **4,** 271.
Greenhow, J. S., 1952, *J. Atmos. Terr. Phys.*, **2,** 282; 1954, *Phil. Mag.*, **45,** 471.
Greenhow, J. S., and Neufeld, E. L., 1955 a, *Phil. Mag.*, **46,** 549; 1955 b, *J. Atmos. Terr. Phys.*, **6,** 133.

JOHNSON, D. H., 1955, *Quart. J. Roy. Met. Soc.*, **81,** 1.
PEKERIS, C. L., 1937, *Proc. Roy. Soc.* A, **158,** 650.
SINGER, S. F., MAPLE, E., and BOWEN, W. A., 1952, *Nature, Lond.*, **170,** 1093.
TAYLOR, G. I., 1936, *Proc. Roy. Soc.* A, **156,** 318.
WILKES, M. V., 1949, *Oscillations of the Earth's Atmosphere* (Cambridge: University Press).

EDITORIAL NOTE

The Editors have received a letter from Professor Dorfman of the Leningradsky Gidrometeorologischesky Institut pointing out in regard to the paper by D. F. Evans published in the Philosophical Magazine (1956, **1,** 370), that the principles used by Mr. Evans for measuring nuclear magnetism had been already suggested by him in papers published earlier. Professor Dorfman gives references to a paper (in Russian): *Doklady, Akad. Nauk. S.S.S.R.*, 1947, **57,** 769, and to several monographs.

[*The Editors do not hold themsevles responsible for the views expressed by their correspondents.*]

INDEX TO VOL. I.

ABSORPTION of sound in liquid helium below 1°K (Newell and Wilks), 588.

Almond (Mary), Clegg (J. A.) and Jaeger (J. C.), remanent magnetism of some dolerites etc., 771.

Amelinckx (S.), direct observation of dislocation nets in rock salt, 269.

Angular correlation measurements on ^{88}Sr (Coleman), 166.

Annealing rate of vacancies, effect of prior extension (Pearson and Bradshaw), 880.

Attree (R. W.) and Plaskett (J. S.), self- and interaction energy of stacking faults in metals, 885.

Baldock (G. R.), lattice vibrations and specific heat of graphite, 789.

Barker (F. C.), collective effects of nuclei of mass 18 and 19, 329.

Beattie (I. R.) and Davies (D. R.), solution of diffusion equation for isotopic exchange between solid and solution, 874.

Beghian (L. E.), Hicks (D.) and Milman (B.), inelastic scattering of 2·5 Mev neutrons by Cr, Mn and Va, 261.

Bell (J. S.) and Skyrme (T. H. R.), nuclear spin–orbit coupling, 1055.

Bellamy (E. H.) and Hogg (W. R.), columnar recombination in nitrogen, 722.

Bennett (J. E.) and Ingram (D. J. E.), paramagnetic resonance spectrum of chlorine dioxide, 109.

Bennett (J. E.) and Ingram (D. J. E.), long range nuclear interaction in paramagnetic resonance, 970.

β-decay of ^{12}B (Tanner), 47.

Bitler (W. R.), *see* Coles, 477.

Bombardment of osmium by nitrogen ions (Greenlees and Kuo), 973.

Books, new :—Adams, basic statistical concepts, 978 ; astronomical optics and related subjects, 1081 ; Andrew, nuclear magnetic resonance, 692 ; annual review of nuclear sciences, Vol 5, 977 ; Bauer, champs de vecteurs et de tenseurs, 691 ; Bronsted, principles and problems in energetics, 691 ; Campbell, theorie generale de l'equation de Mathieu, 689 ; Cartmell and Fowles, valency and molecular structure, 1082 ; Determination of organic structures by physical methods, 221 ; Fischer, fundamentals of electroacoustics, 978 ; Guild, interference systems of crossed diffraction gratings, 1078 ; Heitler, elementary wave mechanics, 1081 ; Higman, applied group-theoretic and matrix methods, 112 ; Hildebrand, introduction to numerical analysis, 980 ; Ingram, spectroscopy at radio and microfrequencies, 377 ; International conference of theoretical physics, Kyoto and Tokyo, 221 ; Jeffreys and Swirles, methods of mathematical physics, 692 ; Kopal, numerical analysis, 487 ; La résonance paramagnetique nucléaire, 1080 ; Linfoot, recent advances in optics, 977 ; Littler and Raffle, reactor physics, 788 ; Lovell, meteor astronomy, 690 ; Mesons and Fields, Vols. I and II, 1079 ; Meteors, 375 ; Mirsky, introduction to linear algebra, 690 ; Pawsey and Bracewell, radioastronomy, 112 ; Pierls, laws of nature, 222 ; Physics and chemistry of the earth, Vol. I, 979 ; Progress in metal physics, Vol. 6, 980 ; Progress in nuclear energy, series I, vol. I, 979 ; Progress in semiconductors, 1080 ; Radiation dosimetry, 1082 ; Richtmyer, Kennard and Lauritsen, introduction to modern physics, 487 ; Scarborough, numerical mathematical analysis, 980 ; Schiff, quantum mechanics, 221 ; Science and applications of photography, 689 ; Schrödinger, expanding universes, 1078 ; Smith, electric dipole moments, 788 ; Smith, electromagnetically enriched isotopes, 691 ; Solid state physics, 488, 1082 ; Sommerfeld, thermodynamics and statistical mechanics, 691 ; Sturrock, static and dynamic electron optics, 375 ; Surveys in mechanics (G. I. Taylor, volume), 1081 ; Thermodynamics and physics of matter, Vol. I, 376 ; Vistas in astronomy, Vol. I, 487 ; von Engel, ionized gases, 978 ; Book notices, 222 ; 488 ; 692 ; 1083.

Bradley (E. F.), *see* West, 97.

Bradshaw (F. J.) and Pearson (S.) quenching vacancies in platinum, 812.

Bradshaw (F. J.), *see* Pearson, 880.

Brenner (Sheila), calculation of μ-mesic energy levels in heavy atoms, 432.

Brewer (D. F.), Edwards (D. O.) and Mendelssohn (K.), onset of friction in helium II, 1130.

Brisbout (F. A.), Dahanayake (C.), Engler (A.), Fujimoto (Y.) and Perkins (D. H.), nature of particles produced by extremely energetic nucelar collisions, 605.

Bull (T. H.), tensile strengths of liquids under dynamic loading, 153.

Burge (E. J.), Fujimoto (Y.) and Hossain (A.), optical model applied to elastic scattering of nucleons, 19.

Burge (E. J.) and Prowse (D. J.), proton-excited energy levels in ^{14}N, 912.

Cabrera (N.) and Levine (M. M.), dislocation theory of evaporation of crystals, 450.

Chambers (R. G.), cyclotron resonance under anomalous skin effect conditions, 459.

Chisholm (J. S. R.), S-matrix for neutral PS–PV meson–nucleon interaction, 338.

Christian (J. W.) and Spreadborough (J.), stacking faults in cold-worked Co–Ni alloys, 1069.

Clarebrough (L. M.), Hargreaves (M. E.) and West (G. W.), density changes during annealing of deformed nickel, 528.

Clegg (A. B.), radiative capture of protons of less than 1 MEV in Be,

Clegg (A. B.), *see* Wilkinson, 291.

Clegg (J. A.), Deutsch (E. R.) and Griffiths (D. H.), rock magnetism in India, 419.

Clegg (J. A.), *see* Almond, 771.

Cold work during fatigue of copper (McCammon and Rosenberg), 964.

Cold worked copper, internal friction at low temperatures (Niblett and Wilks), 415.

Coleman (C. F.), angular correlation measurements on ^{88}Sr, 166.

Coles (B. R.) and Bitler (W. R.), saturation moments and d-band configurations in iron and its alloys, 477.

Collective effects of nuclei of mass 18 and 19 (Barker), 329.

Collective oscillations and characteristic electron-energy losses, 1.

Columnar recombination in nitrogen (Bellamy and Hogg), 722.

Cosmic rays, daily variation, sunspot minimum (Possener and van Heerden), 253.

Cottrell (A. H.), *see* Roberts, 711.

Coupling between two cavities (Gould and Cunliffe, 1126.

Creep in metal crystals at very low temperatures (Mott), 568.

Creep of α uranium during irradiation (Roberts and Cottrell), 711.

Creep of cadmium crystals at liquid helium temperatures (Glen), 400.

Cross (L. E.), thermodynamic treatment of ferroelectricity and antiferroelectricity in pseudo-cubic dielectrics, 76.

Cu_3Au, vacancies and interstitials (Dugdale), 537.

Cunliffe (A.), *see* Gould, 1126.

Cyclotron resonance (Chambers), 459.

Dahanayake (C.), *see* Brisbout, 605.

Das (N. C.), *see* Sinha, 785.

Das Gupta (M. K.), *see* Jennison, 55, 65.

Davey (A. R.), *see* Thewlis, 409.

Davies (D. R.), *see* Beattie, 874.

Davies (R. D.), *see* Williams (D. R. W.), 622.

Dearnaley (G.), elastic scattering of protons by light elements, 821.

Decay of ^{58}Co and ^{57}Co (Grace, Jones and Newton), 363.
Decay of ^{40}K (McNair, Glover and Wilson), 199.
Deformed nickel, changes during annealing (Michell), 584.
Dekeyser (W.), *see* Van der Vorst, 882.
Density changes during annealing of deformed nickel (Clarebrough, Hargreaves and West), 528.
Density changes, irradiated quartz (Klemens), 938.
Deutsch (E. R.), *see* Clegg, 419.
Diffusion in crystals, correlation effects (LeClaire and Lidiard), 518.
Diffusion of Cl ion in NaCl (Patterson, Rose and Morrison), 393.
Dislocations, arrangement and motion (Hirsch, Horne and Whelan), 677.
Dislocation densities (Williamson and Smallman), 34.
Dislocation nets in rock salt (Amelinckx), 269.
Dislocation theory of evaporation of crystals (Cabrera and Levine), 450.
Drever (R. W. P.), Moljk (A.) and Scobie (J.), ratio of K-capture of positron emission in ^{18}F, 942.
Drude dispersion formula (Krishnan and Roy), 926.
Ductile fracture of polycrystalline α-iron (Petch), 186.
Dugdale (R. A.), some properties of vacancies and interstitials in Cu_3Au, 537.
Edwards (D. O.), *see* Brewer, 1130.
Effect of free electrons on lattice conduction (Ziman), 191.
Elastic scattering of neutrons by nuclei (van Zyl, Voss and Wilson), 1003.
Elastic scattering of nucleons by light nuclei (Burge, Fujimoto and Hossain), 19.
Elastic scattering of protons by light elements (Dearnaley), 821.
Elasticity and antiferromagnetism of Cr_2O_3 (Street and Lewis), 663.
Electrical and thermo magnetoresistance, sodium (White and Woods), 846.
Elliot (H.) and Rothwell (P.), solar daily variation of cosmic ray intensity, 669.
Elliott (J. R.), long β-lifetime of ^{14}C and the ^{14}N spectrum, 503.
Elliott (R. J.), vibrations of a perturbed lattice, 298.
Energy distribution, cosmic ray particles (Fowler and Waddington), 637.
Energy levels of ^{40}A (van Heerden and Prowse), 967.
Engler (A.), *see* Brisbout, 605.
Etchpits and dislocations in zinc single crystals (Méléka), 803.
Evans (D. F.), direct observation of static nuclear susceptibilities at room temperature, 370.
Extremely energetic nuclear collisions (Brisbout *et al.*), 605.
Fatigue fracture in copper, origin (Thompson, Wadsworth and Louat), 113.
Ferro and anti-ferroelectricity in dielectrics (Cross), 76.
Figgins (B. F.), Jones (G. O.) and Riley (D. P.), thermal expansion of Al at low temperatures, 747.
Fowler (P. H.) and Waddington (C. J.), energy distribution of cosmic ray particles over northern Italy, 637.
Francis (J. R. D.), wave motions on a free oil surface, 685.
Frank (F. C.) and Keller (A.), periodicity in ice-flowers, 975 and errata, 1084.
Franks (A.) and McLean (D.), polygonization in copper, 101.
Freeman (Joan M.), levels of ^{19}F, from inelastic neutron scattering 591.
Fujimoto (Y.), *see* Brisbout, 605.
Fujimoto (Y.), *see* Burge, 19.
Gabor (D.), collective oscillations and characteristic electron-energy losses, 1.
Gale (B.) and Trotter (J.), soft x-ray spectroscopy of solid solutions of Al and Mg, 759.
γ-radiation from ^{238}Pu, ^{242}Cm and ^{243}Cm (Newton, Rose and Milsted), 981.
γ-rays from inelastic neutron scattering in sodium and iodine (Wolf), 102.

γ-ray pair from decay of K-meson (Sinha and Das), 785.
Glen (J. W.), creep of cadmium crystals at liquid helium temperatures, 400.
Glover (R. N.), *see* McNair, 199.
Gould (R. N.) and Cunliffe (A.), coupling between two cavities, 1126.
Grace (M. A.), Jones (G. A.) and Newton (J. O.), decay of ^{58}Co and ^{57}Co, 363.
Grane (A.), neutrons from $^{10}\beta$(d, n) ^{11}C at 1·08 MEV, 1027.
Greenhow (J. S.) and Neufeld (E. L.), height variation of upper atmospheric winds, 1157.
Greenlees (G. W.) and Kuo (L. G.), bombardment of osmium by nitrogen ions, 973.
Griffiths (D. H.), *see* Clegg, 419.
Hargreaves (M. E.), *see* Clarebrough, 528.
Heat capacities of chromium and nickel (Rayne and Kemp), 918.
Height variation of upper atmospheric winds (Greenhow and Neufeld), 1157.
Henry (W. G.) and Rogers (J. L.), magnetic susceptibilities of copper, silver and gold, 223.
Henry (W. G.) and Rogers (J. L.), magnetic susceptibilities of some diamagnetic alloys, 237.
Heslop (J.) and Petch (N. J.), stress to move a free dislocation in alpha iron, 866.
Heymann (F. F.) and Williams (W. F.), multiple scattering of electrons and positrons in nuclear emulsions, 212.
Hicks (D.), *see* Beghian, 261.
Hirsch (P. B.), Horne (R. W.) and Whelan (M. J.), direct observations of the arrangement and motion of dislocations in aluminium, 677.
Hogg (W. R.) and Sinclair (D.), photoproduction of charged mesons from calcium, 466.
Hogg (W. R.), *see* Bellamy, 722.
Horne (R. W.), *see* Hirsch, 677.
Hossain (A.), *see* Burge, 19.
Inelastic scattering of 2·5 MEV neutrons by Cr, Mn and Va (Beghian, Hicks and Milman), 261.
Ingram (D. J. E.), *see* Bennett, 109, 970.
Intense radio sources, angular diameter (Jennison and Das Gupta), 55, 65.
Interactions of cosmic ray alpha-particles (Waddington), 105.
Isotopic exchange between solid and solution, equation (Beattie and Davies), 874.
Isotopic spin selection rules, VI (Wilkinson and Clegg), 291.
Isotopic spin selection rules, VII and VIII (Wilkinson), 379, 1031.
Jaegar (J. C.), *see* Almond, 771.
James (D. B.), Jones (G. A.) and Wilkinson (D. H.), reaction ^{9}Be(α, n)^{12}C, 949.
Jennison (R. C.) and Das Gupta (M. K.), measurement of angular diameter of two intense radio sources, I and II, 55, 65.
Johnson (C. M. P.), lifetime of 200 kev excited state of ^{19}F, 573.
Jones (G. A.), *see* Grace, 363.
Jones (G. A.), *see* James, 949.
Jones (G. A.), *see* Phillips, 576.
Jones (G. O.), *see* Figgins, 747.
Kehoe (R. B.), Newman (R. C.) and Pashley (D. W.), migration of copper atoms on the surface of silver, 783.
Keller (A.), *see* Frank, 975, and errata, 1084.
Kelly (A.), mechanism of work softening in Al, 835.
Kemp (W. R. G.), *see* Rayne, 918.
Klemens (P. G.), density changes in neutron irradiated quartz, 938.
Kolsky (H.), propagation of stress pulses in viscoelastic solids, 693.
Kothari (L. S.), Singwi (K. S.) and Visvanathan (S.), scattering of cold neutrons in liquid metals and the entropy of disorder, 560.
Krishnan (Sir K. S.) and Roy (S. K.), Drude dispersion formula, 926.
Kuo (L. G.), *see* Greenlees, 973.
Lamden (R. J.) and Lovell (A. C. B.), Cygnus and Cassiopeia radio sources, low frequency spectrum, 725.
Lattice vibrations and specific heat of graphite (Baldock), 789.

LeClaire (A. D.) and Lidiard (A. B.), correlation effects in diffusion in crystals, 518.
Levels of ^{19}F from inelastic neutron scattering (Freeman), 591.
Levine (M. M.), *see* Cabrera, 450.
Lewis (B.), *see* Street, 663.
Lidiard (A. B.), *see* LeClaire, 518.
Lifetime of 200 kev excited state of ^{19}F (Johnson), 573.
^{8}Lithium emission from proton induced disintegrations (Munir), 355.
Lloyd (J. L.) and Wolfendale (A. W.), an unusual double V-event at sea level, 93.
Lomer-Cottrell sessile dislocations, strength (Stroh), 489.
Long β-lifetime of ^{14}C and ^{14}N spectrum (Elliott), 503.
Louat (N.), *see* Thompson, 113.
Lovell (A. C. B.), *see* Lamden, 725.
Low temperature internal friction peak in metals (Seeger), 651.
Lowering of fracture-stress due to surface adsorption (Petch), 331.
Luminescence of decorated dislocations (van der Vorst and Dekeyser), 882.
McCammon (R. D.) and Rosenberg (H. M.), cold work introduced during fatigue of Copper, 964.
McLean (D.), *see* Franks, 101.
McNair (A.), Glover (R. N.) and Wilson (H. W.), decay of ^{40}K, 199.
McNeill (K. G.), *see* Prentice (J. D.), 373.
Magnetic moment, excited ^{19}F (Phillips and Jones), 576.
Magnetic susceptibilities of copper, silver and gold (Henry and Rogers). 223.
Magnetic susceptibilities of some diamagnetic alloys (Henry and Rogers), 237.
Magnetization processes in iron single crystals (Parker), 1133.
Measurement of distance of radio sources (Williams and Davies), 622.
Méléka (A. H. A.), etchpits and dislocations in zinc single crystals, 803.
Mendelssohn (K.) and Montgomery (H.), scattering of phonons and electrons by imperfections in metal, 718.
Mendelssohn (K.), *see* Brewer, 1130.
Michaelis (E. G.) and Powell (B. W.), cloud chamber observations of negative heavy mesons, 441.
Michell (D.), release of stored energy and changes in line shape during annealing of nickel, 584.
Migration of copper atoms on the surface of silver (Kehoe, Newman and Pashley), 783.
Milman (B.), *see* Beghian, 261.
Milsted (J.), *see* Newton, 981.
Mitchell (E. W. J.) and Paige (E. G. S.), optical effects of radiation induced atomic damage in quartz, 1085.
Moljk (A.), *see* Drever, 942.
Montgomery (H.), *see* Mendelssohn, 718.
Morrison (J. A.), *see* Patterson, 393.
Mott (N. F.), creep in metal crystals at very low temperatures, 568.
Multiple scattering in nuclear emulsions (Heymann and Williams), 212.
μ-mesic levels in heavy atoms, calculation (Brenner), 432.
Munir (B. A.), ^{8}Li emission from proton induced disintegrations at 950 MEV, 355.
Negative heavy mesons (Michaelis and Powell), 441.
Neufeld (E. L.), *see* Greenhow, 1157.
Neutrons from ^{10}B(d, n)^{11}C at 1·08 MEV (Graue), 1027.
Newell (J. A.) and Wilks (J.), absorption of sound in liquid helium below 1°K, 588.
Newman (R. C.), *see* Kehoe, 783.
Newton (J. O.), Rose (B.) and Milsted (J.), γ-radiation from decay of ^{238}Pu, ^{242}Cm and ^{243}Cm, 981.
Newton (J. O.), *see* Grace, 363.
Niblet (D. H.) and Wilks (J.), internal friction of cold worked copper at low temperatures, 415.
Nuclear radius and potential from neutron diffraction scattering (Wilson), 1013.
Nuclear spin–orbit coupling (Bell and Skyrme), 1055.
Nuclear surface (Skyrme), 1043.
Nutter (P. B.), spin and magnetic moment of ^{116*}In, 587.

Onset of friction in helium II (Brewer, Edwards and Mendelssohn), 1130.

Optical effects of radiation induced damage (Mitchell and Paige), 1085.

Osborne (D. V.), propagation of heat in liquid helium below 0·6°K, 301.

Osmond (W. P.), angles between partial magnetizations in spinel ferrites containing manganese ions, 1147.

Paige (E. G. S.), *see* Mitchell, 1085.

Paramagnetic resonance, long range nuclear interaction (Bennett and Ingram), 970.

Paramagnetic resonance spectrum of chlorine dioxide (Bennett and Ingram), 109.

Parker (R.), magnetization processes in iron single crystals, analysis by an electrical method, 1133.

Pashley (D. W.), *see* Kehoe, 783.

Patterson (D.), Rose (G. S.) and Morrison (J. A.), diffusion of Cl ion in NaCl, 393.

Pearson (S.) and Bradshaw (F. J.), effect of prior extension on annealing rate of vacancies in platinum, 880.

Pearson (S.), *see* Bradshaw, 812.

Periodicity in ice-flowers (Frank and Keller), 975, and errata, 1084.

Perkins (D. H.), *see* Brisbout, 605.

Petch (N. J.), ductile fracture of polycrystalline α-iron, 186.

Petch (N. J.), lowering of fracture-stress due to surface adsorption, 331.

Petch (N. J.), *see* Heslop, 866.

Phillips (W. R.) and Jones (G. A.), magnetic moment of 200 kev excited state of ^{19}F, 576.

Photoneutron yields from ^{208}Pb (Prentice and McNeill), 373.

Photoproduction of charged mesons from calcium (Sinclair and Hogg), 466.

π-mesonic x-rays from Be (West and Bradley), 97.

Pippard (A. B.), thermodynamic relations applicable near a lambda-transition, 473.

Plaskett (J. S.), *see* Attree, 885.

Polygonization in copper (Franks and McLean), 101.

Possener (M.) and van Heerden (I. J.), daily variation of cosmic rays near sunspot minimum, 253.

Powell (B. W.), *see* Michaelis, 441.

Prentice (J. D.) and McNeill (K. G.), photoneutron yields from ^{208}Pb, 373.

Propagation of heat in liquid helium below 0·6°K (Osborne), 301.

Proton-excited energy levels in ^{14}N (Burge and Prowse), 912.

Prowse (D. J.), *see* Burge, 912.

Prowse (D. J.), *see* van Heerden, 967.

Quenching vacancies in platinum (Bradshaw and Pearson), 812.

Radiative capture of protons in Be (Clegg), 1116.

Radiative transitions in light elements: II (Wilkinson), 127.

Radio sources, Cygnus and Cassiopeia (Lamden and Lovell), 725.

Ratio of K-capture of positron emission in ^{18}F (Drever, Moljk and Scobie), 942.

Rayne (J. A.) and Kemp (W. R. G.), heat capacities of chromium and nickel, 918.

Reaction ^{9}Be(α, n)^{12}C (James, Jones and Wilkinson), 949.

Remanent magnetism of rocks from Tasmania (Almond, Clegg and Jaeger), 771.

Riley (D. P.), *see* Figgins, 747.

Roberts (A. C.) and Cottrell (A. H.), creep of α uranium during irradiation with neutrons, 711.

Rock magnetism in India (Clegg, Deutsch and Griffiths), 419.

Rogers (J. L.), *see* Henry, 223, 237.

Rose (B.), *see* Newton, 981.

Rose (G. S.), *see* Patterson, 393.

Rosenberg (H. M.), thermal and electrical conductivity of lithium at low temperatures, 738.

Rosenberg (H. M.), *see* McCammon, 964.

Rothwell (P.), *see* Elliot, 669.

Roy (S. K.), *see* Krishnan, 926.

Runciman (W. A.), Stark-splitting in crystals, 1075.

Saturation moments and d-band configurations in iron and its alloys (Coles and Bitler), 477.

Scattering of cold neutrons in liquid metals (Kothari, Singwi and Visvanathan), 560.

Scattering of high energy neutrons by Coulomb field (Voss and Wilson), 175.

Scattering of phonons and electrons by metal imperfections (Mendelssohn and Montgomery), 718.

Scobie (J.), *see* Drever, 942.

Seeger (A.), theory of low-temperature internal friction peak in metals, 651.

Sinclair (D.), *see* Hogg, 466.

Singwi (K. S.), *see* Kothari, 560.

Sinha (M. S.) and Das (N. C.), pair of γ-rays from the point of decay of a K-meson, 785.

Skyrme (T. H. R.), the nuclear surface, 1043.

Skyrme (T. H. R.), *see* Bell, 1055.

Smallman (R. E.), *see* Williamson, 34.

S-matrix for neutral PS–PV meson–nucleon interaction (Chisholm), 338.

Smith (P. L.) and Wolcott (N. M.), specific heats of cadmium and mercury, 854.

Solar daily variation of cosmic ray intensity (Elliot and Rothwell), 669.

Solid state of argon (Stansfield), 934.

Specific heats of cadmium and mercury (Smith and Wolcott), 854.

Spin and magnetic moment of ^{116*}In (Nutter), 587.

Spinel ferrites, angles between partial magnetizations (Osmond), 1147.

Spreadborough (J.), *see* Christian, 1069.

Stacking faults in cold-worked Co–Ni alloys (Christian and Spreadborough), 1069.

Stacking faults in metals (Attree and Plaskett), 885.

Stansfield (D.), solid state of argon, 934.

Stark-splitting in crystals (Runciman), 1075.

Static nuclear susceptibilities (Evans), 370.

Steady flow past sphere at high Reynolds number (Stewartson), 345.

Stewartson (K.), steady flow past sphere at high Reynolds number using Oseen's approximation, 345.

Street (R.) and Lewis (B.), elasticity and anti-ferromagnetism of Cr_2O_3, 663.

Stress to move a free dislocation in alpha iron (Heslop and Petch), 866.

Stroh (A. N.), strength of Lomer–Cottrell sessile dislocations, 489.

Tanner (N. W.), coincidence measurements on the β-decay of ^{12}B, 47.

Tensile strengths of liquids under dynamic loading (Bull), 153.

Thermal and electrical conductivity of lithium at low temperatures (Rosenberg), 738.

Thermal expansion of Al at low temperatures (Figgins, Jones and Riley), 747.

Thermal expansion of diamond (Thewlis and Davey), 409.

Thermodynamic relations applicable near a lambda-transition (Pippard), 473.

Thewlis (J.) and Davey (A. R.), thermal expansion of diamond, 409.

Thompson (N.), Wadsworth (N.) and Louat (N.), origin of fatigue fracture in copper, 113.

Trotter (J.), *see* Gale, 759.

Unusual V-event (Lloyd and Wolfendale), 93.

Van der Vorst (W.) and Dekeyser (W.), luminescence of decorated dislocations, 882.

van Heerden (I. J.) and Prowse (D. J.), energy levels in ^{40}A, 967.

van Heerden, *see* Possener, 253.

van Zyl (C. P.), Voss (R. G. P.) and Wilson (R.), elastic scattering of 136 MeV neutrons by nuclei, 1003.

Vibrations of a perturbed lattice (Elliott), 298.

Viscoelastic solids, stress pulses (Kolsky), 693.

Visvanathan (S.), *see* Kothari, 560.

Voss (R. G. P.) and Wilson (R.), scattering of high energy neutrons by a coulomb field, 175.

Voss (R. G. P.), *see* van Zyl, 1003.

Waddington (C. J.), interactions of cosmic ray alpha-particles, 105.

Waddington (C. J.), *see* Fowler, 637.
Wadsworth (N.), *see* Thompson, 113.
Wave motions on a free oil surface (Francis), 685.
West (D.) and Bradley (E. F.), π-mesonic X-rays from Be, 97.
West (G. W.), *see* Clarebrough, 528.
Whelan (M. J.), *see* Hirsch, 677.
White (G. K.) and Woods (S. B.), electrical and thermal magnetoresistance in thin rods of pure sodium, 846.
Wilkinson (D. H.), isotopic spin selection rules, VII and VIII, 379, 1031.
Wilkinson (D. H.), radiative transitions in light elements: II, 127.
Wilkinson (D. H.), *see* James, 949.
Wilkinson (D. H.) and Clegg (A. B.), the 6·88 MeV state of ^{10}B: Isotopic spin selection rules, VI, 291.
Wilks (J.), *see* Newell, 588.
Wilks (J.), *see* Niblett, 415.
Williams (D. R. W.) and Davies (R. D.), measurement of distance of radio sources by interstellar neutral hydrogen absorption, 622.
Williams (W. F.), *see* Heymann, 212.
Williamson (G. K.) and Smallman (R. E.), dislocation densities in annealed and cold-worked metals, 34.
Wilson (H. W.), *see* McNair, 199.
Wilson (R.), nuclear radius and potential from neutron diffraction scattering, 1013.
Wilson (R.), *see* van Zyl, 1003.
Wilson (R), *see* Voss, 175.
Wolcott (N. M.), *see* Smith, 854.
Wolf (Elizabeth A.), γ rays from inelastic neutron scattering in sodium and iodine, 102.
Wolfendale (A. W.), *see* Lloyd, 93.
Woods (S. B.), *see* White, 846.
Work softening in Al, mechanism (Kelly), 835.
X-ray spectroscopy, Al and Mg solid solutions (Gale and Trotter), 759.
Ziman (J. M.), effect of free electrons on lattice conduction, 191.

END OF THE FIRST VOLUME

Printed by Taylor & Francis, Ltd.
Red Lion Court, Fleet Street, London, E.C.4

U. of Haw.